

**Universität
Rostock**



Traditio et Innovatio

**Photocatalytic remediation of water from the new
emerging low concentrated pharmaceutical
contaminations**

Dissertation

zur

Erlangung des akademischen Grades

doctor rerum naturalium (Dr. rer. nat.)

der Mathematisch-Naturwissenschaftlichen Fakultät

der Universität Rostock

vorgelegt von Julia Choina

Rostock, 14.07.2014

Die vorliegende Arbeit wurde in der Zeit von Juli 2009 bis Juni 2012 am Institut für Chemie der Universität Rostock am Lehrstuhl für Anorganische Chemie in der Arbeitsgruppe von Prof. Dr. Axel Schulz angefertigt.

1. Gutachter: Prof. Dr. Axel Schulz
2. Gutachter:
3. Gutachter:

Erklärung

Ich versichere hiermit an Eides statt, dass ich die vorliegende Arbeit selbstständig angefertigt und ohne fremde Hilfe verfasst habe. Dazu habe ich keine außer den von mir angegebenen Hilfsmitteln und Quellen verwendet und die den benutzten Werken inhaltlich und wörtlich entnommenen Stellen habe ich als solche kenntlich gemacht.

Rostock, den 14.07.2014

Julia Choina

Dedication

To my family, who offered me endless support.

Acknowledgments

Foremost, I would like to thank and express my deepest gratitude to my supervisor Prof. Axel Schulz for his guidance and assistance during my Ph.D study. Especially, for supporting me through these past four years, for his kindness, many insightful discussions and suggestions and for giving me the freedom to realize various ideas in the field of photocatalysis.

Secondly, I would like to thank very much my advisor, Dr. Hendrik Kosslick for his unlimited time, advice and for many motivating discussions. The many improvements in my knowledge and in my writing and presentation skills can be attributed to his extensive guidance.

Thanks to Prof. Gerd-Uwe Flechsig and Dr. Heiko Duwenske (voltammetric analysis) for the efficient cooperation, possibility providing me a great work environment in his lab and for help and scientific hints.

I will forever be thankful to my first college research advisor Prof. Antoni Waldemar Morawski for his motivation and guidance, who has made a great impact on my education.

I acknowledge the members and co-workers of the Vietnamese Academy of Science and Technology in Hanoi in Vietnam (VAST) and of the King Abdulaziz City for Science and Technology (KACST) in Riyadh in Saudi Arabia for the providing some titania and ZnO photocatalysts.

I am grateful to Dipl. Ing. Gerhard Fulda and Dr. Marcus Frank (Electron Microscopic Center of Medical Faculty, Rostock, Germany) for the discussion and the assistance provided during the TEM measurements. I am appreciating the analytical department of the Leibniz Institute for Catalysis (LIKAT Rostock), especially Dr. Christine Fischer, Mrs. Susann Buchholz and Mr. Andreas Koch for excellent analytical work. I warmly acknowledge also Dr. Ursula Bentrup (UV-Vis), Mrs. Angela Weihs (FTIR), Dr. Jörg Radnik (XPS), Mr. Reinhard Eckelt (N₂ sorption), Dr. Matthias Schneider and Dr. Farooq Ibad (XRD) for the characterization of the photocatalytic materials.

I want to thank present and past members of the AK Schulz research group, as well as analytical staff from the Institute of Inorganic Chemistry.

I acknowledge the DAAD (German Academic Exchange Service) for the financial support of studies at the University of Rostock.

I am very grateful for meeting my polish friends Marta, Kasia, Magda and Julita, for their friendship, company and the most amazing time spend in Rostock. Finally, I thank to my parents, my sister Gosia and the special person in my life Marcin for their support, care, faith and love.

List of content

List of symbols and abbreviations	1
List of units and constants.....	3
Abstract	4
1. Goals and objectives	5
2. Introduction	7
2.1. Semiconductor photocatalysis	12
Photocatalysis	12
Mechanism of photocatalysis.....	12
Doping of semiconductors.....	16
2.2. State-of -the -Art of the degradation of pharmaceuticals.....	19
3. Results and discussion	22
3.1. Photocatalytic abatement of ibuprofen and tetracycline over titania 25 photocatalyst.....	22
Photocatalytic activity	23
Influence of pH solution.....	28
Formation of ibuprofen and tetracycline intermediates	33
Re-use experiments	36
Summary.....	37
3.2. Photocatalytic abatement of ibuprofen and tetracycline over zirconium doped titania (Zr-TiO ₂) photocatalyst.....	38
Photocatalytic activity	38
Influence of pH solution.....	43
Formation of ibuprofen intermediates.....	45
Formation of tetracycline intermediates.....	52
Re-use experiments	57

Summary.....	60
3.3. Photocatalytic abatement of low concentrated (ppb-low ppm) tetracycline over novel titania based photocatalysts	61
Photocatalytic abatement of tetracycline over titania and titania doped materials (Zr-TiO ₂ , Fe-TiO ₂ and N-TiO ₂)	61
Photocatalytic abatement of tetracycline over new porous titania-based photocatalysts.....	66
Summary.....	71
3.4. Photocatalytic abatement of ibuprofen and tetracycline over two types of nanosized ZnO photocatalyst.....	72
Photocatalytic activity	72
Influence of pH solution.....	82
Formation of ibuprofen and tetracycline intermediates	86
Re-use experiments	93
Summary.....	96
3.5. Final conclusions.....	97
List of appendixes.....	103
A 1. Experimental details	104
A 1.1 Photocatalytic materials preparation and characterization.....	104
Titanium dioxide (TiO ₂)	104
Doped titania photocatalysts.....	108
Titania nanotubes (TNs).....	111
Titania/MIL-101 composite and MIL-125 photocatalyst.....	116
Zinc oxide nanoparticles (ZnO)	122
A 1.2 Photocatalytic testing and experimental procedure	125
Materials	125

Photocatalytic performances.....	127
Reaction intermediates	128
ESI-TOF-MS/HPLC.....	130
A 1.3 Voltammetry.....	130
A 2. References	137
A 3. Academic achievements.....	148

List of symbols and abbreviations

A	Anatase
abs. A	Absolute abatement
AdSV	Adsorptive stripping voltammetry
AOP	Advanced oxidation process
BDC	1,4-benzendicarboxylate (terephthalic acid)
BET	Brunauer–Emmett–Teller, specific surface area
BJH	Barrett, Joyner & Halenda measurement
cat	Photocatalyst, catalyst
CB	Conduction band
CHA	Cyclohexylammonium nitrate
CMC	Critical micelle formation concentration
CVD	Chemical vapor deposition
e^-	Generated electron on the photocatalyst
E	Redox potential
EDCs	Endocrine disrupting compounds
E_g	Band gap
ESI-TOF-MS	Electrospray ionisation time of flight mass spectrometry
EtOH	Ethanol
Fe-TiO ₂	Iron doped titania
h^+ (h_{VB}^+)	Generated electron hole on the photocatalyst
HO ₂ \cdot	Hydroperoxyl radicals
HMDE	Hanging mercury drop electrode
HPLC	High performance liquid chromatography
IBP	Ibuprofen sodium salt (C ₁₃ H ₁₇ O ₂ Na)
LOD	Limit of detection
MIL	Materials of Institute Lavoisier
MOF	Metal organic framework
NSAIDs	Non-steroidal anti-inflammatory drugs
N-TiO ₂	Nitrogen doped titania
O ₂ \cdot^-	Superoxide radicals

OH ⁻	Hydroxide ion
·OH	Hydroxyl radical
p/p ₀	Relative pressure
P25	Titania (Degussa)
pK _a	Logarithmic acid dissociation constant
P _{zc}	Point of zero charge
PPCPs	Pharmaceuticals and personal care products
r	Effective mean first order reaction rates
R	Rutile
R ²	Correlation coefficient
rel. A	Relative abatement
ST	Tetrahedron building unit
sub	Substrate (ibuprofen or tetracycline)
SWV	Square wave voltammetry
TBOT	Tetrabutyl orthotitanate
TEM	Transmission electron microscopy
TC	Tetracycline hydrochloride (C ₂₂ H ₂₄ N ₂ O ₈ •HCl)
TNs	Titania nanotubes
TOC	Total organic carbon
UV-A	400-315 nm ultra-violet wavelength
UV-B	315-280 nm ultra-violet wavelength
UV-C	280-100 nm ultra-violet wavelength
VB	Valence band
wt%.	Weight percentage
XPS	X-Ray photoelectron spectroscopy
XRD	X-Ray diffraction
Zr-TiO ₂	Zirconium doped titania
λ	Wavelength [nm]

List of units and constants

Å	Angstrom
°C	Celsius
eV	Electronvolt
h	Hour
h	Planck's constant
M	Molarity
min	Minute
mL	Mililiter
nm	Nanometer
ppb	Parts per billion ($\mu\text{g/L}$)
ppm	Parts per million (mg/L)
ppt	Parts per trillion (ng/L)
t	Time min
V	Volt
W	Watt

Abstract

Nowadays, hazardous organic compounds like pharmaceuticals and personal care products (PPCPs) are frequently found in water, especially in low concentration, down to ppb-ppt scale. After use, these compounds are delivered into the aquatic environment. These low concentrated pollutions by pharmaceuticals found in drinking, waste and surface water are a new, emerging problem. Therefore, advanced oxidation processes (AOPs) have achieved increasing attention for the water remediation such as disinfection, hazardous drug and endocrine disruptive compounds (EDCs) degradation. Among AOPs, heterogeneous photocatalysis is of special interest, because it does not require additional chemicals and allows to recover the solid photocatalysts from the treated water. In this work five types of titania and zinc oxide based photocatalysts with different particle size, texture and morphology have been prepared, characterized and comparatively tested in the photocatalytic decomposition of model drugs: tetracycline and ibuprofen. These are in detail: titania doped photocatalysts (Zr-TiO₂, Fe-TiO₂ and N-TiO₂), titania nanotubes, new porous titania/MIL-101 composites, metal organic framework MIL-125 and two types of nanosized ZnO. The present knowledge of the photocatalytic performances at low photocatalyst and pollutant concentrations, the influence of the photocatalyst-to-substrate mass ratio as well as appearing reaction intermediates is very limited. Therefore, this work is dedicated to these above mentioned subjects, in order to clarify whether heterogenous photocatalytic degradation of organics is useful for the decontamination of hazardous low concentrated pollutions in water. The formation of reaction intermediates of tetracycline and ibuprofen during photocatalytic treatment has been investigated by electrospray ionization time-of-flight mass spectroscopy (ESI-TOF-MS). An improved procedure for the detection of tetracycline in the ppb to ppt range by voltammetry has been developed. In the first time, it has been shown, that the photocatalysis with titania and zinc oxide photocatalysts is a very effective method for the degradation of pharmaceuticals even at very low concentration (ng/L), which is one million times lower than, so far considered in the literature.

1. Goals and objectives

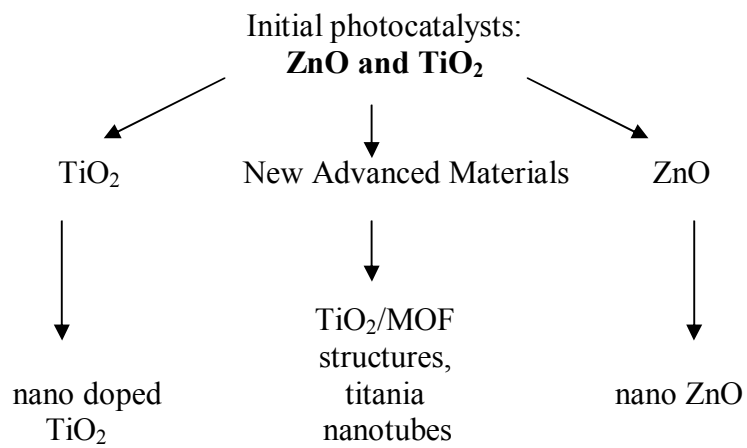
The main objectives of this work concern:

- Evaluation of the potential of titania and ZnO based photocatalysts for the photocatalytic abatement of low concentrated pharmaceutical solutions tetracycline and ibuprofen under reliable conditions, i.e. in the presence of low concentrated pollutants and photocatalyst amount.
- Novel titania based photocatalytic materials (doped titania, titania nanotubes and titania/MOF composites) are synthesized, tested and compared with commercial titania P25 photocatalyst.
- Development of an advanced procedure of the electroanalytical (voltammetry) method allowing for the determination of very low concentrated tetracycline solution down to the low ppb and ppt ranges.

In details this work aims to:

- Establish and redefine the State-of-the-Art.
- Study of the photocatalytic performances beyond “the proof of principle”, down to the low ppb scale.
- Compare of novel titania and ZnO based materials with “standard used“ titania P25 photocatalyst.
- Use of the certain photocatalytic conditions as low pollutant and photocatalyst concentrations, low catalyst-to-substrate mass ratios and a solar - light equivalent irradiation (by spectral range and light intensity in the UV-A range) for photocatalysis.
- Develop the analytical procedure of voltammetry by optimization of the experimental parameters like: buffer, pH value of solution, the deposition time and potential and different measurement modes. These variation parameters allowed to measure the tetracycline concentration at very low ppb - ppt range.
- Investigate reaction intermediates of pharmaceuticals formed during the course of photocatalytic abatement, by using soft electrospray ionization (ESI-TOF-MS) method.

- Prepare novel photocatalysts with improved specific surface area, porosity, distinguished titania species and morphology i.e. isolated titania rings in MOF, amorphous titanate sheets in nanotubes or titania/MOF nanocomposites:



2. Introduction

Nowadays, water contaminations like pharmaceuticals, hormones and pesticides are very serious problem for human health and clean water supply.^[1-4] The emerging problems occurring in the aquatic environment, concern markedly increase of type, amount and concentration of hazardous, pharmaceutical pollutants. Pharmaceuticals are extremely dangerous because they are able to perform biological effects on living organisms, sometimes in a non - predicable way.^[5-9] After use, these compounds are delivered into the aquatic environment. Indeed, more than 4000 compounds are used as different human and animal drugs.^[10] Recent investigations have shown that a number of biological compounds are not completely eliminated by wastewater treatment and are also not biodegraded in the environment. Many pollutants occur at very low concentrations within the lower ppb - ppt scale^[11-13] and have been recently detected in drinking water resources (Tab. 1).

Table 1. Concentration of pharmaceuticals found in drinking water in European countries.^[14]

Pharmaceuticals	Country	Application	Max. conc (ng/L)
Bezafibrate	Germany	Lipid regulator	27
Bleomycin	UK	Anti-neoplastic	13
Carbamazepine	Canada	Anti-epileptic	24
	USA		258
Diazepam	UK	Psychiatric drug	10
	Italy		23.5
Diclofenac	Germany	Analgesic and anti-pyretic	6
Gemfibrozil	Canada	Lipid regulator	70
Ibuprofen	Germany	Analgesic and anti-pyretic	3
Phenazone	Germany	Analgesic and anti-pyretic	400
Propylphenazone	Germany	Analgesic and anti-pyretic	120

Moreover, some active compounds possess an extremely high biological potential down to the $\mu\text{g/day}$ doses. Therefore, concentrations which are low as 1 ng/L can be

very dangerous. These biological active substances have been found in lakes, rivers and oceans.^[15-17] There are several possible sources and routes for the occurrence of pharmaceutical compounds in the aquatic environment and wildlife (Fig. 1).^[18-22] Many human pharmaceuticals like non - and some prescription drugs are taken up in households, while other prescription pharmaceuticals are consumed in healthcare facilities such as hospitals and clinics.^[23,24] Emerging environmental contaminants occurring in the aquatic environment and wildlife,^[25-27] mainly come from industrial factories,^[28,29] households,^[30,31] animal^[32-35] and fish farms.^[36-38]

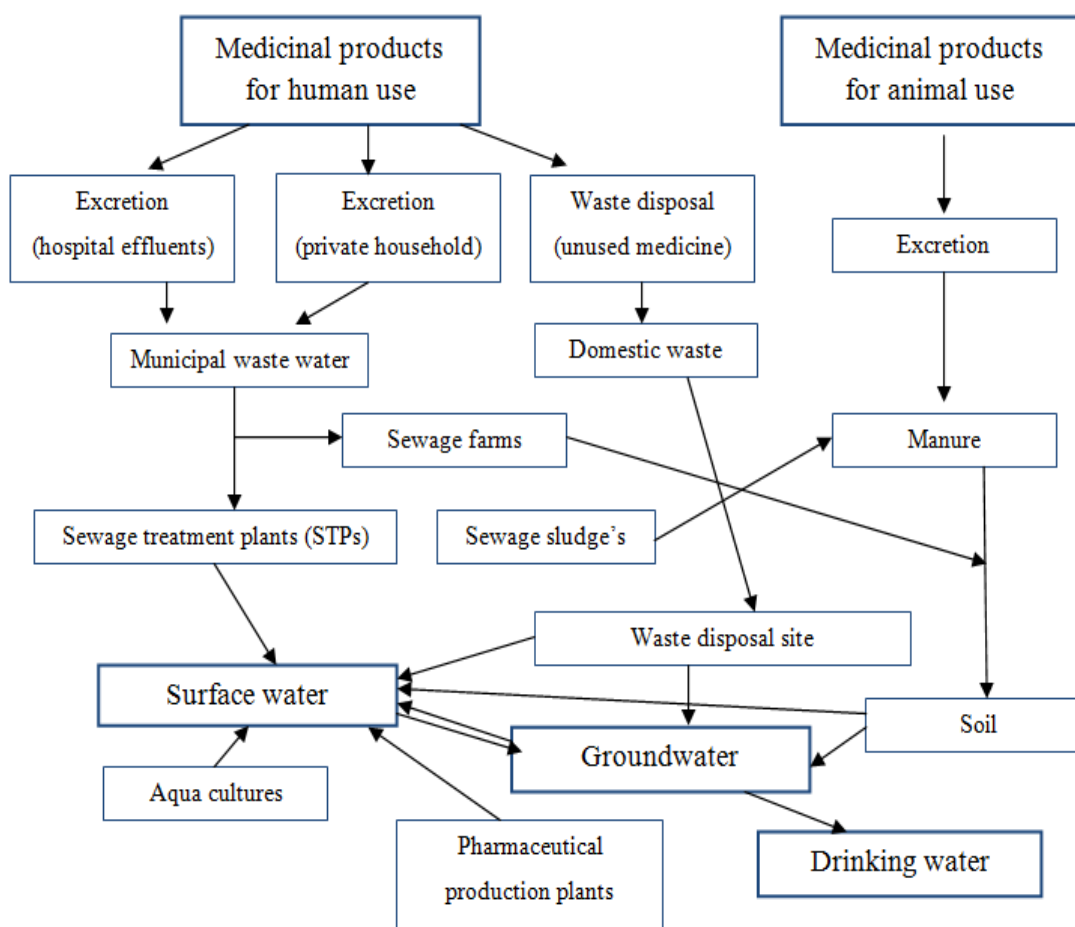


Figure 1. Fate and occurrence of pharmaceuticals in the environment.^[39]

Therefore, increasing attention is paid to these compounds as a new group of very risky, environmental, recalcitrant water pollutants.^[40,41] Figure 2 shows that the number of papers dealing with the degradation of these toxic pharmaceuticals increases. This increase is not as large as could be expected from the reports of many

international organizations which raise alarm over pharmaceutical fates in rivers, lakes and oceans, nevertheless the problem cannot be neglected.^[42,43] The degradation of pharmaceuticals, personal care products (PPCPs) as well as endocrine disrupting chemicals (EDCs) is now a very actual, important and demanding task.

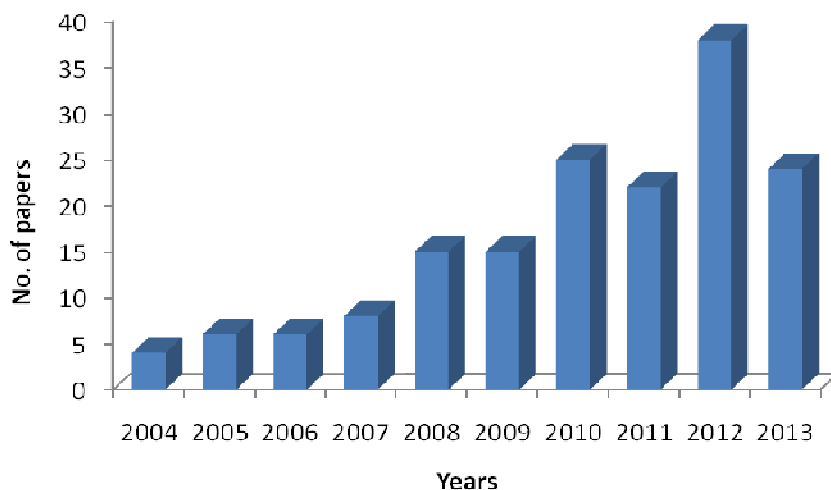


Figure 2. Number of publications concerning photocatalytic degradation of pharmaceuticals over the years 2004-2013 (till May), based on the Science Direct database; keywords: “photocatalytic degradation, abatement, pharmaceutical, drug, antibiotic, decomposition, photocatalysis, TiO₂, ZnO, photocatalyst”; this work.

The number of drugs and their concentrations found in wastewaters constantly increases each year. The steroids, common drugs (pain killers) and antibiotics occurring in the surface waters in Germany are listed in Table 2.^[44]

Their concentrations may finally achieve the high ppb to low ppm range. Among them, nonsteroidal anti-inflammatory drugs (NSAIDs) ibuprofen and naproxen are common best known prescribe drugs (due to *Consumer Reports: Best Buy Drugs*^[45]) and recently call as the emerging water pollutants.^[46-48] The surface water contaminants are highly problematic, because they are detected in water streams and resources used for drinking water production.^[49-52]

For the effective and efficient degradation of toxic pharmaceuticals, the advanced oxidation processes (AOPs) are high of interest.^[53-56] In addition, the heterogeneous photocatalysis might present an interesting option for pharmaceuticals removal from water.^[57-63]

Table 2. Environmental occurrence of the commonly used drugs in Germany.^[44]

Pharmaceuticals	Usage	Environmental occurrence		
		Loading of drug [g/day]	Maximal concentration of drug in effluents [ppb]	Maximal concentration of drug in surface waters [ppb]
Ibuprofen	analgesic, anti-inflammatory	200	3.4	0.53
Diclofenac	analgesic, anti-inflammatory	100	2.1	1.2
Carbamazepine	Analgesic, antiepileptic	100	6.3	1.1
Naproxen	analgesic, anti-inflammatory	50	0.52	0.39
Aminophenazone (or aminopyrine)	analgesic, anti-inflammatory	50	1.0	0.34
Gemfibrozil	blood lipid and cholesterol-regulator medicine	50	1.5	0.3
Indomethacin	analgesic, anti-inflammatory	10	0.6	0.2

In the water remediation processes also some other oxidative methods such as ozonation,^[64,65] chlorination^[66,67] and oxidation with H₂O₂^[68-70] are commercially available. Unfortunately, they often require expensive chemicals (Cl, H₂O₂, O₃), soluble homogeneous catalysts and mixed treatments like O₃/H₂O₂,^[71] TiO₂/UV/H₂O₂,^[72] Fe²⁺/UV/H₂O₂,^[73] TiO₂/UV/O₃.^[74] Therefore, these methods tend to be more sophisticated in water remediation than popular photocatalysis. It is proved that among advanced oxidation processes (AOPs), heterogeneous photocatalysis with semiconductors allows for successfully cleaning water from hazardous pharmaceuticals. The heterogeneous TiO₂ photocatalyst is still the most often used in water purification systems (Fig. 3). Titania is a non - hazardous and eco - friendly compound, which offers the possibility to be recovered and re-used. In principle, it can be widely applied in water remediation because of its special high photocatalytic activity and oxidation power. TiO₂ is also of high benefit due to its availability and reasonable low costs. Moreover, as is observed in Figure 3, doping of titania is also

taken into account in the photocatalytic decomposition of drug from water.^[75-80] Various semiconductors like ZnO and mixture of TiO₂ and SiO₂ are also more often applied in the photocatalysis due to its improved photocatalytic and adsorption properties.^[81,82] The Science Direct database shows that among 164 papers, titania seems to be the most attractive material. Contrary to titania, only 8 of papers the zinc oxide is used in the photocatalytic degradation of pharmaceuticals and antibiotics. However, non - reliable experimental conditions, different from that occurring in the aquatic environment, show that the photocatalytic degradation of dangerous drugs at high ppm concentrations (between 10 - 100 mg/L) also require high amount of ZnO photocatalyst (0.1-2 g/L).^[83-90]

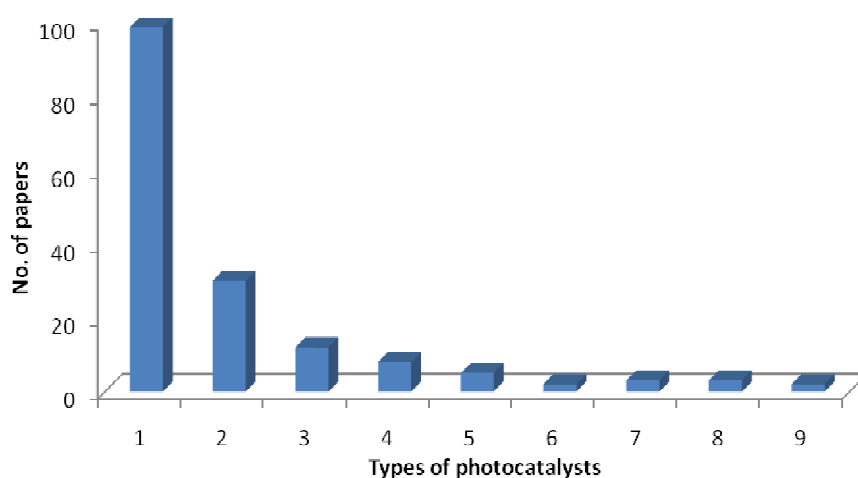


Figure 3. Number of publications concerning the photocatalytic degradation of pharmaceuticals with different available photocatalysts: 1. TiO₂, 2. metal and non-metal doped TiO₂, 3. photo-fenton catalyst, 4. ZnO, 5. TiO₂-SiO₂, 6. mixed metal oxides, 7. Titanate nanofibers, 8. graphene-TiO₂ composites, 9. TiO₂/fly-ash cenospheres over years 2004-2013 (till May), based on the Science Direct database; keywords: “photocatalytic degradation, ZnO, antibiotic, pharmaceutical, drug, decomposition, photocatalysis”; this work.

Some advanced titania type structures presented in Figure 3, like TiO₂ nanowires,^[91] titanate nanofibers,^[92] nanocarbon TiO₂,^[93] graphene - TiO₂ composites,^[94] beta - cyclodextrin/TiO₂,^[95] porphyrin/TiO₂ composite^[96] and TiO₂/fly - ash cenospheres^[97] have found application as photocatalysts.

2.1. Semiconductor photocatalysis

Photocatalysis

Photocatalysis is one of the most promising technologies for elimination of organic pollutants by using heterogeneous photocatalyst (semiconductor) activated by photon of proper light energy.^[98-101] For this purpose mainly commercially available titania (TiO₂) photocatalyst is used. The photocatalyst absorbs ultraviolet irradiation from sunlight or other artificial light source producing pairs of highly reactive electron hole (e⁻ - p⁺) pairs by excitation of valence band (VB) electrons to the conducting band (CB).^[102,103] Depending on the excitation energy (band gap) of the photocatalysts three different ranges of UV radiation can be used: UV-A (400 - 315 nm), UV-B (315 - 280 nm) or UV-C (280 - 100 nm). The electron-hole pairs are produced in the bulk of the semiconductor and migrate to the catalyst surface for photocatalytic use. The photocatalytic oxidation of the organic species often proceeds via adsorption of the pollutant on the surface of the catalyst, followed by direct subtraction of the pollutant's electrons by positively charged holes (direct photocatalytic oxidation). Another possible way is oxidation with hydroxyl radicals ([•]OH) at or in the vicinity of photocatalyst. The hydroxyl radicals are generated from water by oxidation with surface holes or via reduction of dissolved oxygen with CB surface electrons. The energy difference between the valence and the conduction band is known as the 'band gap' (*E_g*). The wavelength of the light necessary for photo - excitation for TiO₂ is: $1240 \text{ (Planck's constant, } h) / 3.2 \text{ eV (band gap energy)} = 388 \text{ nm}$.^[104] Generally, the difference in the absorption of two modification phases of TiO₂ are noticed.^[105] The reflectance curves located near the UV part point to the absorption band for anatase at wavelength of $\lambda = 377 \text{ nm}$ and for rutile at wavelength of $\lambda = 397 \text{ nm}$.

Mechanism of photocatalysis

Figure 4 shows the stages in the photocatalytic decomposition of organic pollutants over titania (top) and time scales of these occurring reactions (bottom). The primary reactions indicate the critical role of charge carriers (electron - hole pairs) generation and trapping. These processes are very fast. Additionally, two competitive processes occur. Firstly, there is a competition between the charge - carrier trapping and the

recombination. The trapping of holes (h^+) occur very fast (nanoseconds), then the somewhat slower recombination proceeds. The same situation is observed with electrons (e^-). After trapping the electron, the recombination also proceeds. These processes are very fast (picoseconds). At the same time, recombination of trapped carrier competes with interfacial charge transfer. These stages are slower (microseconds to milliseconds). Therefore, the enhancement of charge carrier separation (h^+ and e^-) is of high importance for the photocatalytic activity. To delay the recombination and accelerate the charge transfer to the surface different attempts (like preparation methods) are taken up. It is assumed that the formed surface bound hydroxyl radicals (i.e. trapped holes at the photocatalyst surface) oxidized the pollutants.^[106]

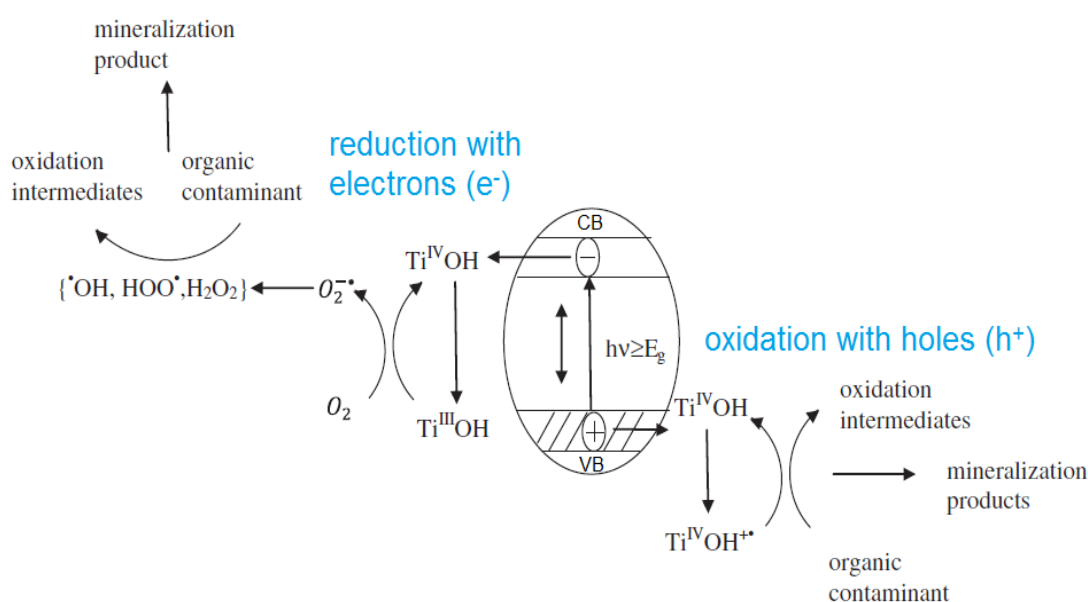
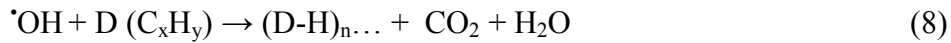


Figure 4. Schematic representation of states occurring on the surface of semiconductors; used abbreviations: CB: conduction band, VB: valence band, e^- : photogenerated electron, h^+ : photogenerated hole, $h\nu$: photon of light, E_g : band gap.^[107-111]

A photocatalytic degradation usually involves highly reactive radicals or intermediate species such as hydroxyl radicals ($\cdot\text{OH}$), photogenerated holes (h^+), superoxide radicals ($\text{O}_2^{\cdot-}$), and hydroperoxyl radicals (HO_2^{\cdot}), which oxidize a large variety of organic compounds.^[112,113] The hydroxyl radicals are formed on the titania surface by the reaction of holes (h^+) with adsorbed water, hydroxide, etc. The photogenerated electrons (e^-) react with oxygen to generate $\text{O}_2^{\cdot-}$. The formation of hydrogen peroxide

(H₂O₂) requires two electrons for reduction of the adsorbed oxygen.^[114] VB holes are more needed, because they have higher oxidation power and are direct sources for the hydroxyl radical production (Eq. 2). The formation pathway via of CB electrons requires three electrons to produced [•]OH radicals (Eq. 3, 5 and 6).^[115]



In summary, an organic compound (D) can be completely degraded to carbon dioxide and water (Eq. 8). The equation 1 represents the charge carrier separation, where $\{\text{TiO}_2\}^+$ species are equivalent to generated holes (h^+_{VB}). The equation 9 shows the final recombination of holes and electrons on the $\{\text{TiO}_2\}$ of bulk material.

It is generally accepted that the [•]OH are considered to be the major species responsible for the photocatalytic degradation of organic pollutants in wastewater.^[116-119] The oxidative ability of [•]OH is 2.05 times higher than that of Cl₂, 1.58 times higher than that of H₂O₂, and 1.35 times higher than that of O₃ (Tab. 3).^[120]

Table 3. Oxidation potential (*E*) of the reactive oxidants.^[121,122]

Oxidant	Oxidation potencial [V]
[•] OH	2.8
O ₃	2.07
H ₂ O ₂	1.77
ClO ₂	1.49
Cl ₂	1.35
O ₂	1.2

The band gaps and the band edge positions of various semiconductors are given in Figure 5. Several metal oxides (TiO₂, ZnO, ZrO₂, WO₃, SnO₂, SrTiO₃) can be used as photocatalysts.^[123-127] However, according to the thermodynamic requirement, the VB and CB of the semiconductors should be located in such a way that:

The oxidation potential of the hydroxyl radicals

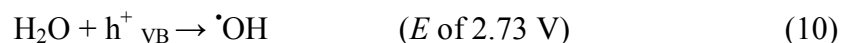
$$(E(\text{H}_2\text{O}/\cdot\text{OH}) = 2.8 \text{ V vs NHE})$$

and the reduction potential of superoxide radicals

$$(E(\text{O}_2/\text{O}_2^{\cdot-}) = -0.28 \text{ V vs NHE})$$

should fit the band gap region of semiconductors.

The redox potential of the VB holes must be sufficiently positive to generate hydroxyl radicals and that of the CB electrons must be sufficiently negative to generate superoxide radicals. TiO₂, ZnO, SrTiO₃ and ZrO₂ photocatalysts exhibit favourable band gap positions compared to the other materials. The effective degradation of organic compounds is possible when the redox potential of H₂O/ \cdot OH must be within the band gap of the semiconductors. The Equation 10 presents the oxidation reaction, where the reactive VB hole has an oxidizing potential of *ca.* 2.73 V vs. normal hydrogen electrode (NHE) and can oxidize water molecule to hydroxyl radicals. In this condition, semiconductor is able to produce more reactive radicals and easy decompose the pollutant molecule.



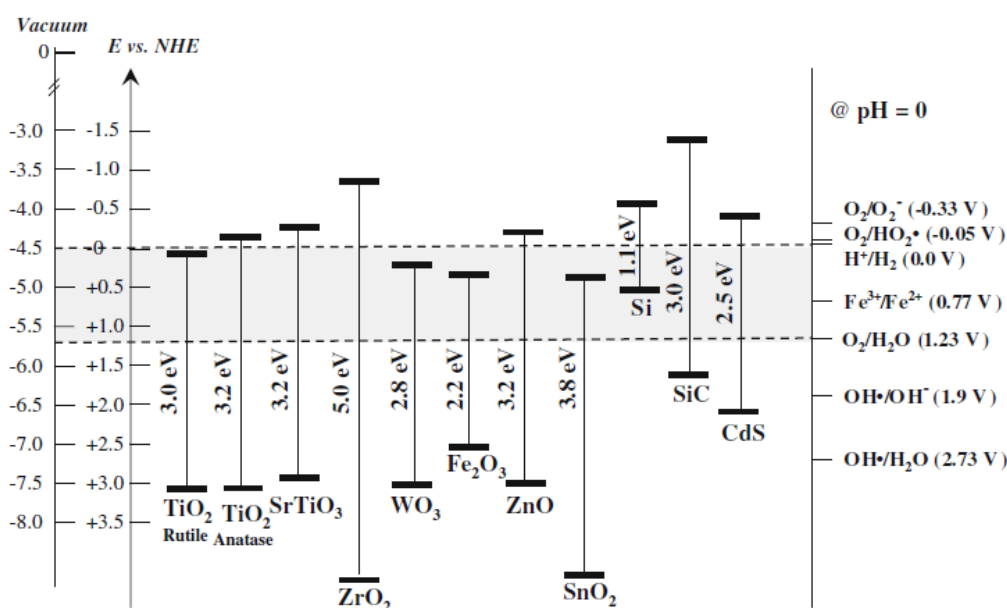


Figure 5. Energy-level diagram of the conduction (CB) and valence (VB) bands of different semiconductors at pH 0 along with selected redox potentials (E). The energy scales are referred to vacuum level and the normal hydrogen electrode (NHE).^[128,129]

Doping of semiconductors

The improvement of photocatalytic activity of heterogeneous semiconductors can be done by either morphological modifications such as increasing surface area and porosity or by chemical modifications as doping or by incorporation of additional components into the photocatalysts structure.^[130,131] The chemical modification includes the doping of semiconductors by metal or non - metal elements. The doping is a processes where an ion of the lattice of a pure semiconductor is substituted by metal or non - metal ion or is located interstitial. Also impurities can act as dopants (e.g. carbon). The main expected advantages of doping are:

- increasing activity in the decomposition of hazardous contaminations,
- band gap narrowing for efficient use of visible light,
- band gap shifting (into visible part of light),
- lower electron - hole recombination, better charge carrier separation.^[132-137]

Efficiency of photocatalysis is limited, because only 2 to 5% of the solar spectrum^[138] (UV fraction of the solar light) can be absorb by commercial TiO₂. The improved efficiency might be done by charge carrier separation and band gap shifting into

visible part of light. It has been demonstrated, that the visible light absorption and photocatalytic activity of TiO_2 can be effectively improved by modification of the chemical structure involves introduction of metals (Cr, Pt, V, Nb, Fe, Ru)^[139-142] and non - metals (N, C, S, B).^[143-146]

The doping of titania is effective when the positions of conduction and valence bands are between a value of 2.8 V (the oxidation potential of the hydroxyl radicals ($\text{H}_2\text{O}/\text{OH}^\cdot$)) and - 0.28 V (the reduction potential of superoxide radicals ($\text{O}_2/\text{O}_2^{\cdot-}$)). The difference of both bands (VB and CB) is corresponding to semiconductor which possess the bang gap of *ca.* 2.8 eV. In these conditions the minimum requirements for the doping is achieved. The production of highly active holes (h^+) and electrons (e^-) is maintained. The band gap narrowing (down to *ca.* 2.8 eV) is a necessary condition for the excitation of semiconductor by solar light.

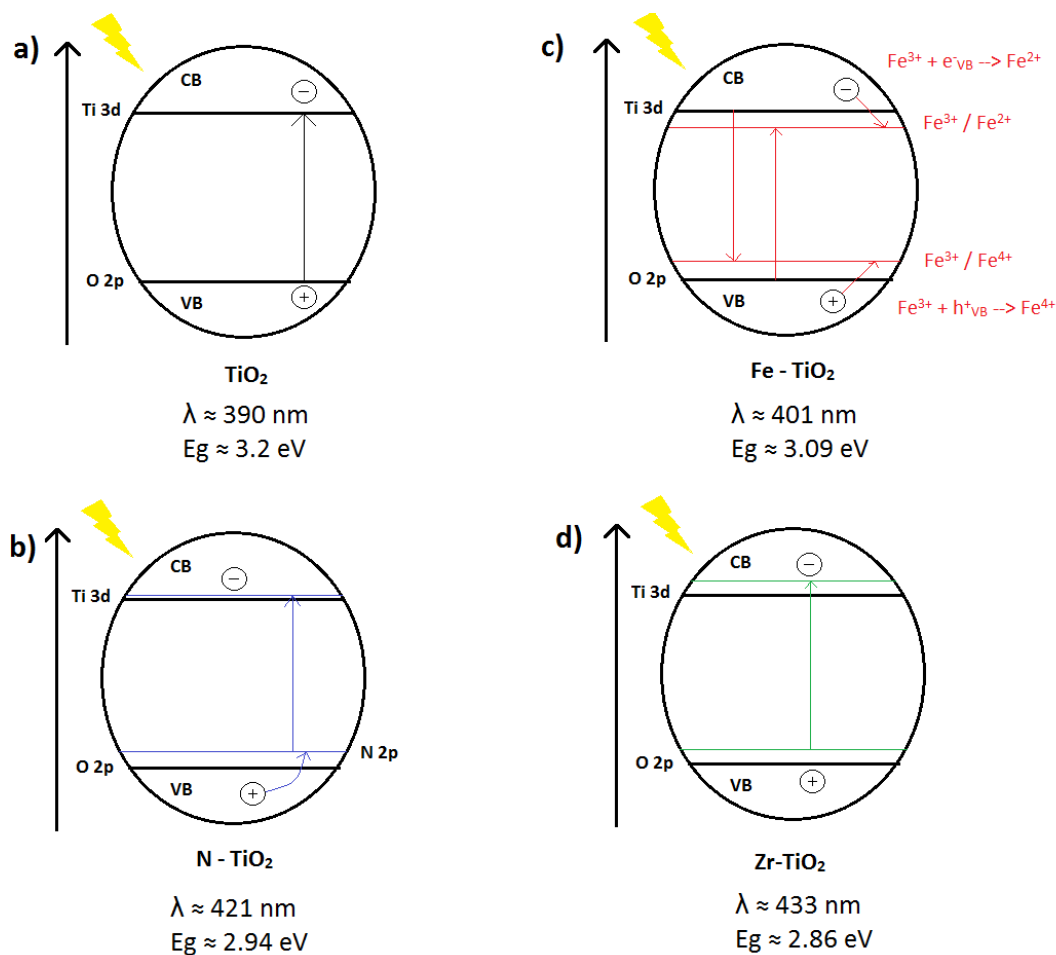
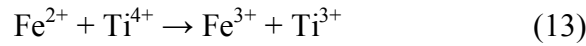
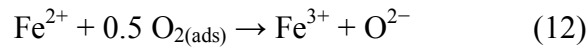


Figure 6. Schematic representation of the doped titania particles: a) titania without doping, b) nitrogen doped titania, c) iron doped titania and d) zirconium doped titania.

Asahi et al. demonstrated that the doping of nitrogen into TiO₂ render the formation of visible light sensitive TiO₂ more easier due to the narrowing of the band gap (Fig. 6 b).^[147] Band gap narrowing is explained by forming the new N_{2p} state with O_{2p} states in titania doped with nitrogen. The introduction of nitrogen form a new *occupied* (*i.e.* electron rich) orbital. It is located between the valence band (which are comprised primarily of O_{2p} orbitals) and conduction band (which are comprised primarily of Ti_{3d} orbitals).^[148,149] Their energies are very close, and thus the band gap of N-doped titania is narrowed and able to absorb visible light, extending from a sharp cut off at about 390 nm to a broad cut off at above 500 nm. Recently, it was proposed that ion doped titania increases the photocatalytic activity.^[150-152]

It is clear that iron (III) ion fits easily into the titanium dioxide lattice, due to a ionic radius of 0.69 Å, which is nearly equal to the ionic radius of titanium (IV) (0.745 Å).^[153] This increase of photocatalytic activity can be explained by dual role of iron doping, the Fe³⁺ can trap, both the photoinduced CB electrons and VB holes (Fig. 6 c) (Eq. 11-14).^[154]



Additionally, iron atoms in the titania can act the recombination centres for electron - hole pairs preventing its recombination (Eq. 15 and 16).



However, within the literature review, some reports related doping of titania with iron are contradictory. Some authors claimed that iron doping decreases the photocatalytic activity.^[155,156]

The titania doping with zirconium shows that the spectral range is extended to 433 nm giving a new value of bang gap of *ca.* 2.8 eV (Fig. 6 d). Although, in many reports the

mechanisms of doped TiO₂ are not well understood^[157] at this point the minimum requirements for the doping is maintained and the obtained Zr-doped titania might show enhanced photocatalytic activity.

2.2. State-of-the-Art of the degradation of pharmaceuticals

The study of the State-of-the-Art clearly shows that the decomposition of hazardous organic compound is realized in such a way:

Titania is still the most popular photocatalyst used in the photocatalytic decomposition of organic pollutants from water. Photocatalytic tests are done with very high pollutant and photocatalyst concentrations, by means working at photocatalyst excess. Dyes and phenol contaminations are still used as model molecules. Less is known about mechanisms of decomposition of pharmaceutical, antibiotics and endocrine disruptive compounds. Real and reliable water conditions, i.e. low concentrated pharmaceutical pollutants (ppt - ppb range) are not investigated, so far.

In order to simulate polluted sewage water conditions (real water matrix), many studies are mainly dedicated to the treatment of highly contaminated wastewater with dyes and phenols. Instead of real environmental conditions, where hazardous pollutants are present in low ppb - ppt range; very high concentration of model contaminations in the mg/L to g/L scale are often investigated. Use of commercially available titania in the degradation of dyes is still a main task.^[158-161] Contrary to, hazardous contaminations like pharmaceuticals, pesticides and hormones are rarely considered. Among a huge number of papers considering heterogeneous photocatalysis, available in the "Science direct" database, only a limited number of them pointed out photocatalytic degradation of drugs (i.e. pharmaceuticals and antibiotics) (Fig. 7). It is shown that the most attractive drugs used in photocatalysis are carbamazepine, diclofenac, paracetamol, sulfamethoxazole, clofibric acid and ibuprofen, while among antibiotics: mainly amoxicillin and tetracycline are chosen for photocatalytic tests. These drugs differ in the chemical structure, action and chemical properties and were

investigated due to their popularity, most frequent intake by humans or animals or by chance.

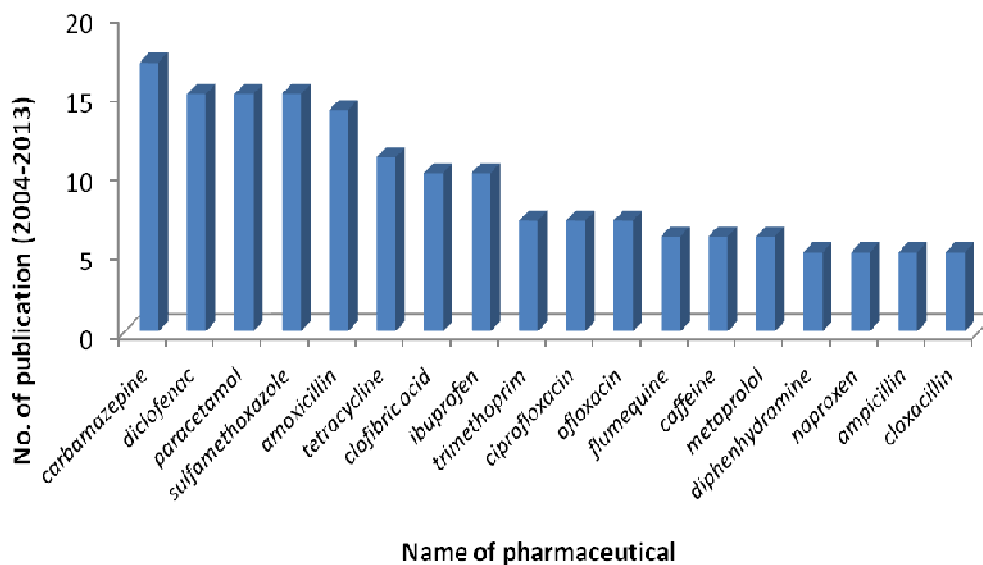


Figure 7. Types and number of pharmaceuticals used in photocatalytic abatement found in the research papers over years 2004-2013 (till May), based on the Science Direct database; keywords: “photocatalytic degradation, photocatalyst, TiO₂, ZnO, doped TiO₂, antibiotic, pharmaceutical, drug, decomposition, photocatalysis”, this work.

Mboula et al. used 30 mg/L of TiO₂ P25 photocatalyst for the decomposition of tetracycline (67 ppm) under 700 W medium mercury lamps.^[162] That means, for the increasing of the photocatalytic efficiency, huge amount of photocatalytic materials as well as high power of lamps are used during the course of treatment. For instance, for the photocatalytic decomposition of pharmaceuticals tamoxifen and gemfibrozil of concentration varied from 2.5 to 48 and 10 ppm, the concentrations of photocatalysts were 0.4 g/L^[163] and from 0.1 - 1 g/L^[164] of course at high photocatalyst excess and by using medium pressure mercury lamps (125 W), respectively. Moreover, the photocatalytic degradation of pharmaceuticals at very low concentrations (ppt - ppb) is nearly unknown. Only some papers highlighted the mixtures of few drugs, which simulated real pollutant matrix of sewage water plants (in ppb scale). In these experiments µg/L concentrated water mixtures were investigated.^[165-168] In summary, the fundamental analysis of the State-of-the-Art shows that almost all studies still deal with high photocatalyst amounts, ranged between 0.1 and 2 g/L.

This work is dedicated to the photocatalytic decomposition of low concentrated tetracycline and ibuprofen over novel based titania photocatalysts and ZnO nanoparticles under simulated solar light. The photocatalytic performance is studied under reliable conditions, by means, at low substrate and photocatalyst concentrations, low photocatalyst-to-substrate mass ratios and under low power of lamps (60 W). An own improved electroanalytical method is used to determine the very low tetracycline concentration in water. Different experimental conditions (photocatalytic activity, adsorption, influence of pH value, re - usability) were investigated in details.

3. Results and discussion

3.1. Photocatalytic abatement of ibuprofen and tetracycline over titania 25 photocatalyst

The photocatalytic properties of common available titania 25 photocatalyst (Degussa, Germany) have been checked during abatement of two model drugs: ibuprofen and tetracycline under simulated visible light. In order to redefine and establish the State-of-the-Art, the influence of the important factors like: photocatalytic activity, pH of solution, re-use properties of photocatalyst and formation of reaction by-products have been investigated. In order to achieve more reliable results (data) only reasonable conditions of photocatalytic treatment have been applied. The low photocatalyst and pollutant concentrations, low photocatalyst-to-substrate mass ratios (abbreviated: cat-to-sub ratios) of 1 to 4, as well as, low power of solarium lamp (60 W) supplying *ca.* 20 % of irradiation (in the part of visible light) have been used. These, above given conditions replaced the less reliable ones, widely reported in the literature, i.e. very high cat-to-sub ratios (mainly: 20, 50, 100 and etc) and high electric power of lamps (mainly > 300 W of pressure Xenon lamps) used as a source of light in photocatalysis.

Photocatalytic activity

The photocatalytic performance of the titania photocatalyst has been checked in the abatement of ibuprofen and tetracycline from aqueous solution. The cat-to-sub ratios were varied by changing the photocatalyst concentrations (from 10 to 40 mg/L) at constant IBP and TC (10 ppm) concentration.

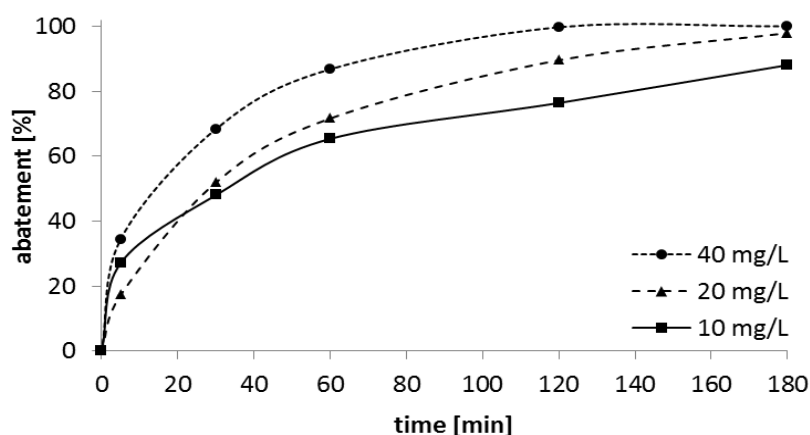


Figure 8. Photocatalytic abatement of ibuprofen in aqueous solution over titania 25 photocatalyst under UV-Vis irradiation; IBP conc.: 10 ppm, cat conc.: 10, 20 and 40 mg/L.

Figure 8 shows the relative abatements of **ibuprofen** vs. time for different photocatalyst concentrations ranging from 10 to 40 mg/L at constant pollutant concentration of 10 ppm. In the first 5 min of photocatalytic treatment, over 10 mg/L of titania photocatalyst, high relative amounts of IBP have been already decomposed (27 %). With prolonged treatment time (after 60 min) the photocatalytic abatement proceeds slower. This diminishment of abatement points to a deactivation of the photocatalyst during the course of reaction. *Ca.* 65 to 88 % of IBP is removed after 60 and 180 min of the treatment, respectively. With increasing photocatalyst concentration, slightly higher abatement is observed in the order: 10 mg/L < 20 mg/L < 40 mg/L. Even the photocatalyst amount is doubled or multiplied the increase in the abatement especially in the first step of treatment (first 60 min) is comparatively low. Two reasons can be discussed, a decreased light penetration and photocatalyst poisoning by formed reaction intermediates. Excess dosage of the photocatalyst decreases the light penetration *via* “screening” effect of the suspended particles^[169] and hence reduces the efficiency of photodegradation. The effective reaction rates

diminish (Tab. 4). This can be explained by the excessive turbidity of the aqueous solution (due to high particle dispersion in the solution) and reduction of photons, which are scattered by the TiO₂ particles. However, the screening effect was reported to occur at higher photocatalyst concentration of > 100 mg/L of titania.^[170,171] The photocatalyst deactivation is in line with the found fast formation of intermediates at the onset of reaction (Fig. 9), which could be connected with the deactivation. Formation of oxidized by reactive radicals aromatic intermediates and some polymerization of intermediates occurring at the photocatalyst surface might block the most active electron - hole species.

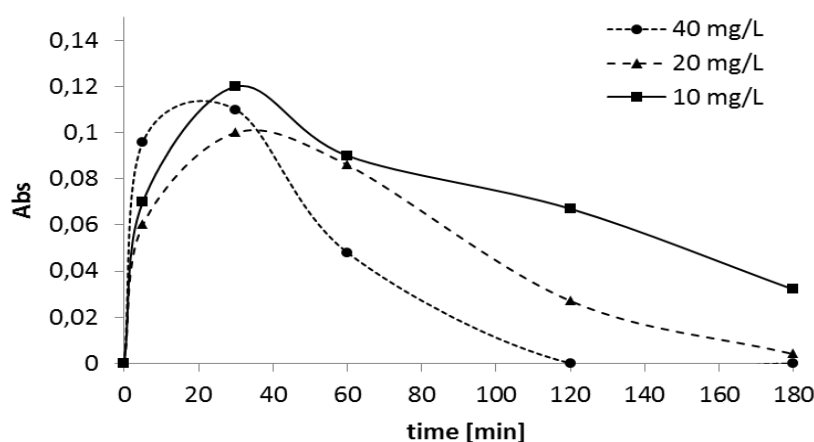


Figure 9. Formation of the temporary intermediates of ibuprofen in aqueous solution during photocatalytic treatment over titania 25 photocatalyst based on UV-Vis absorbance at λ_{\max} 262 nm for different cat conc.: 10, 20 and 40 mg/L, IBP conc.: 10 ppm.

Figure 9 shows the formation of temporary intermediates of ibuprofen during photocatalytic abatement detected by the absorbance at 262 nm in the UV-Vis spectra. Interestingly, the appearance and disappearance of temporary reaction products is closely related to the abatement curves (Fig. 8). The photocatalytic abatement of IBP is very fast at the first onset of reaction leading to rapid formation of intermediates. Decreasing abatement beyond 30 min of reaction is accompanied by an enhanced decomposition of temporary products. They disappear at the same time as IBP is completely abated. This finding additionally confirms that the 262 nm absorbance belongs to reaction intermediates.

The relative and absolute photocatalytic abatements (A) of ibuprofen and corresponding effective first order reaction rates (r) are summarized in Table 4. The effective reaction rates of IBP abatement over titania were estimated from experimental data. Although the photocatalytic abatements increase with reaction time (from 30 to 180 min) the effective reaction rates of photocatalysts decrease. Similar tendency is observed with increasing the photocatalyst amount. With higher amount of titania, absolutely increase of abatement is observed. E.g. after 180 min of treatment the abatements increase in the order 88, 97 and 100 % for 10, 20 and 40 mg/L of photocatalyst, respectively.

Table 4. Data of the photocatalytic abatement of ibuprofen (10 ppm) in water during photocatalytic treatment over titania 25 photocatalyst (cat conc.: 10, 20 and 40 mg/L). Relative and absolute abatements (A) and corresponding experimental effective mean first order reaction rates (r) calculated after 30, 120 and 180 min of treatment.

irradiation time of IBP [min]	rel. A	abs. A	r	rel. A	abs. A	r	rel. A	abs. A	r
	[%]	[mg/L]	[min ⁻¹]	[%]	[mg/L]	[min ⁻¹]	[%]	[mg/L]	[min ⁻¹]
	10 mg/L			20 mg/L			40 mg/L		
5	17	1.7	0.0340	27	2.7	0.027	34	3.4	0.0170
30	48	4.8	0.0160	51	5.1	0.0085	68	6.8	0.0057
120	76	7.6	0.0063	89	8.9	0.0037	99	9.9	0.0021
180	88	8.8	0.0048	97	9.7	0.0027	100	10	0.0014

Figure 10 shows the specific abatement (mg substrate per mg photocatalyst) of ibuprofen over titania vs. the cat-to-sub (IBP) ratios achieved after different times of photocatalytic treatment. As expected, observed specific abatement (mg of IBP per mg of photocatalyst) increases with longer reaction time, especially at low cat-to-sub ratios, ranging from 1 to 0.16, i.e. at low photocatalyst amount.

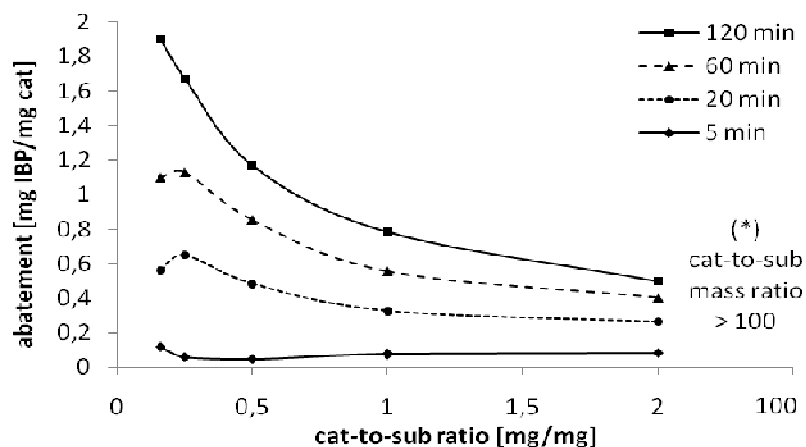


Figure 10. Specific abatement [mg IBP/ mg cat] of ibuprofen in aqueous solution over titania 25 photocatalyst vs. the cat-to-sub ratios of 1:6≈0,16, 1:4=0,25, 1:2=0,5, 1:1=1 and 1:0.5=2), after treatment times of 5, 20, 60 and 120 min, at constant cat conc.: of 10 mg/L. An asterisk (*) corresponding to the mostly used in the literature concentration ranges > 100; e.g. cat-to-sub ratio of 100; for the 10 ppm of pollutants and the 1 g/L of photocatalyst.

Additionally, the photocatalytic abatement of **tetracycline** over titania has been studied at the different photocatalyst concentrations (Fig. 11). Again, the course of abatement over titania photocatalyst shows two steps, a fast step of TC abatement at the onset of reaction (until 30 min) and then after 60 min a slower ones indicated by the lower slope of the abatement curve.

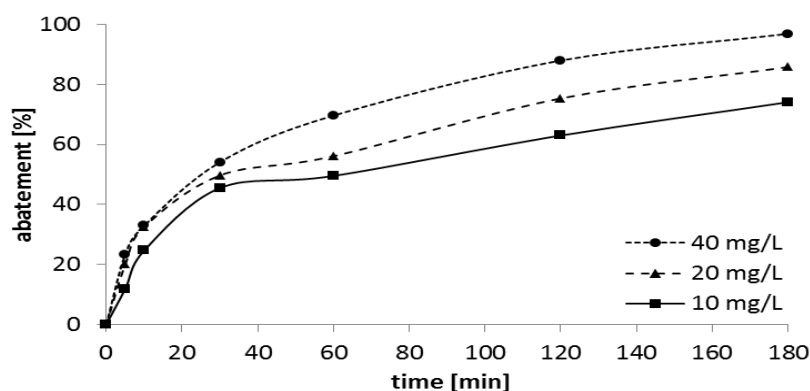


Figure 11. Photocatalytic abatement of tetracycline in aqueous solution over titania 25 photocatalyst under UV-Vis irradiation; TC conc.: 10 ppm, cat conc.: 10, 20 and 40 mg/L.

Compared to the abatement of IBP, the degradation of TC over titania is lower (compare Fig. 8). Generally, the courses of abatement of IBP and TC are similar. With growing photocatalyst amounts meaning excess of photocatalyst by mass, the abatement increases in the order: 10 mg/L < 20 mg/L < 40 mg/L, but again less than expected by the high excess of photocatalyst. At the onset of treatment, after 30 min of treatment, the obtained abatements of TC are similar for the different photocatalyst concentrations. This points to a photocatalyst poisoning (blocking) of most active sites, at the surface created by electron - hole pairs, e.g. by formed polymeric species. This leads likely to a decrease of the effective reaction rates with time (Tab. 5) and with increasing photocatalyst amount.

Table 5. Data of the photocatalytic abatement of tetracycline (10 ppm) in water during photocatalytic treatment over titania P25 photocatalyst (cat conc.: 10, 20 and 40 mg/L). Relative and absolute abatements (A) and corresponding experimental effective mean first order reaction rates (r) calculated after 30, 120 and 180 min of treatment.

irradiation time of TC [min]	rel. A	abs. A	r	rel. A	abs. A	r	rel. A	abs. A	r
	[%]	[mg/L]	[min ⁻¹]	[%]	[mg/L]	[min ⁻¹]	[%]	[mg/L]	[min ⁻¹]
	10 mg/L			20 mg/L			40 mg/L		
5	11	1.1	0.0220	23	2.3	0.0230	22	2.2	0.0110
30	45	4.5	0.0150	49	4.9	0.0081	54	5.4	0.0045
120	62	6.2	0.0051	75	7.5	0.0031	87	8.7	0.0018
180	74	7.4	0.0041	85	8.5	0.0024	96	9.6	0.0013

The determination and investigation of TC intermediates formed during treatment by UV - Vis spectroscopy is not possible, due to overlap any possible bands assigned to intermediates with TC absorption bands. I.e. no other bands arise during photocatalytic treatment. This tend to following the TC intermediates formed during the course of abatement only by ESI-TOF-MS measurements.

In summary, the effective reaction rates for IBP and TC are only slightly higher for IBP compared to TC. However, the onset abatement within the first 5 min of treatment is substantially higher for IBP with 25 % compared to 10 % for TC for 10 mg/L of photocatalyst at 10 ppm of substrate. Both factors lead to higher final abatement of IBP, compared to TC.

Influence of pH solution

The pH value is an important reaction parameter. It influences the formation of reactive oxygen species e.g. $\cdot\text{OH}$ radicals and the improves photocatalyst - substrate interactions (adsorption) by changing the surface charge of the photocatalyst and the substrate molecule. The influence of the pH value on the abatement of ibuprofen and tetracycline over titania (cat-to-sub ratio of 2:1) has been tested under acidic (pH=3), neutral (pH=7) and alkaline (pH=9) conditions.

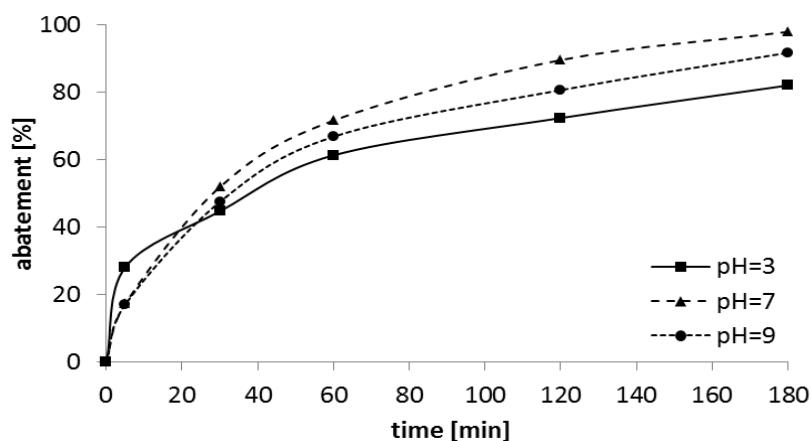
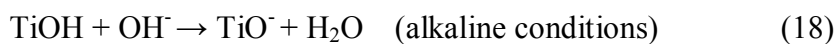
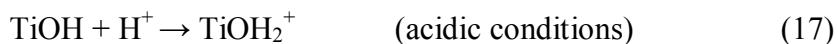


Figure 12. Influence of pH value of the reaction solution on the photocatalytic abatement of ibuprofen in aqueous solution over titania 25 photocatalyst under UV-Vis irradiation; IBP conc.: 10 ppm, cat conc.: 20 mg/L.

Figure 12 shows that the course of **ibuprofen** abatement over titania at different pH solutions is almost similar and does not differ markedly. Rapid abatement of IBP in the first stage of reaction (within 60 min) is observed in all cases. Then with prolonged treatment time from 60 to 180 min the abatement proceeds distinctly slower. The final abatement decreases in the order: neutral > alkaline > acidic and finally reaches *ca.* 97, 91 and 82 %, respectively. Under both, acidic and alkaline conditions the abatement is decreased probably by enhanced electrostatic repulsion between the substrate and the photocatalyst surface. This finding can be explained in the following way. The point of zero surface charge (P_{zc}) of TiO_2 is close to pH of 6.8.^[172]

The surface of titania is positively charged in acidic solution ($\text{pH} < 6.8$) while negatively charged in alkaline ones ($\text{pH} > 6.8$). The following Equations (17 and 18) illustrate this acid - base chemistry of TiO_2 surface.



where: TiOH_2^+ , TiOH , and TiO^- are the positive, neutral, and negative surface hydroxyl groups on the TiO_2 surface, respectively.^[173,174] Lower pH (acidic conditions) will lead to the protonation of titania surface with proton (H^+) from acid (solution adjusted with HCl) as well as of the carboxyl sodium group ($-\text{COONa}$) of ibuprofen. Whereas, at higher pH (solution adjusted with NaOH) the titania surface becomes negatively charged due to deprotonation (with hydroxide ions OH^-) leading to a repulsion of the IBP anions. As a result, adsorption of the substrate at the photocatalyst surface is diminished, leading to a decrease of the reaction rates and finally decrease of the photocatalytic activity. Therefore, under both, acidic and alkaline condition the abatement of ibuprofen is diminished, compared to the neutral solution. Additionally, a slightly higher activity of titania under alkaline conditions may be attributed to the increased formation of reactive $\cdot\text{OH}$ radicals by photocatalytic oxidation of hydroxide ions (OH^-) on TiO_2 surface.^[175]

In Figure 13 the formation of temporary intermediates of ibuprofen at different pH values was again followed by UV-Vis spectroscopy at IBP and photocatalyst concentrations of 10 ppm and 20 mg/L, respectively. The formation of by-products is attributed by the appearance of the band at 262 nm. During the course of reaction, the characteristic IBP absorbance at 222 nm is diminished, whereas the new band at 262 nm is simultaneously arising. These intermediates appear immediately with photocatalytic treatment due to high abatement observed at the very beginning. Moreover, highest formation of temporary products at the onset of reaction is observed under neutral conditions.

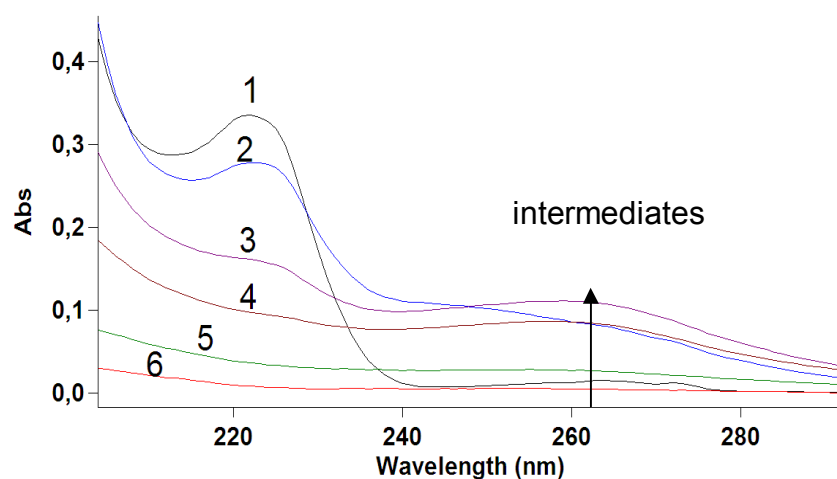


Figure 13. UV-Vis spectra of an aqueous ibuprofen solution after photocatalytic treatment over titania 25 photocatalyst under UV-Vis irradiation: (1) starting IBP solution (10 ppm) and after (2) 5 min, (3) 30 min, (4) 60 min, (5) 120 min, (6) 180 minutes of photocatalytic treatment. Concentration of ibuprofen determined based on the absorbance at 222 nm. Experimental conditions: IBP conc.: 10 ppm, cat conc.: 20 mg/L, pH=7.

In addition to, the formation of intermediates is markedly lower under acidic or base conditions (Fig. 14). The concentration of intermediates decreases again after reaching maximum at 30 min of reaction. The disappearance of temporary reaction products is closely related to the achieved abatement in this period of time (Fig. 12).

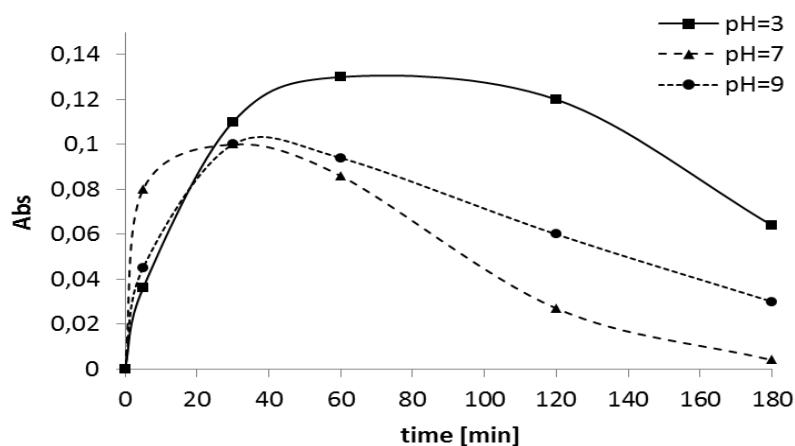


Figure 14. Formation of temporary intermediates of ibuprofen in aqueous solution during photocatalytic treatment over titania 25 photocatalyst based on UV-Vis absorbance at λ_{\max} 262 nm for different pH solutions of 3, 7 and 9; IBP conc.: 10 ppm, cat conc.: 20 mg/L.

Their decrease depends on the pH value of the reaction solution in the given order:

$$\text{pH } 7 > \text{pH } 9 > \text{pH } 3.$$

The photocatalytic abatement of **tetracycline** over titania photocatalyst at different pH values of solution has been also investigated. The decrease of the TC absorbances, at wavelength by 358 nm in the UV - Vis spectra of photocatalytic treated solutions is shown in Figure 15.

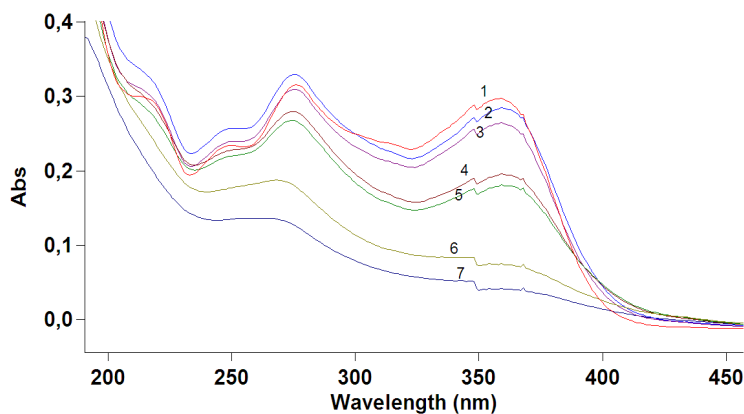


Figure 15. UV-Vis spectra of an aqueous tetracycline solution after photocatalytic treatment over titania 25 photocatalyst under UV-Vis irradiation: (1) starting TC solution (10 ppm) and after (2) 5 min, (3) 10 min, (4) 30 min, (5) 60 min, (6) 120 and (7) 180 minutes of photocatalytic treatment. Concentration of tetracycline determined based on the absorbance at 358 nm. Experimental conditions: TC conc.: 10 ppm, cat conc.: 20 mg/L, pH=7.

As it can be seen, in the derived abatement curves, the tetracycline removal is high and markedly influenced by the pH value especially under acidic conditions. Figure 16 shows the photocatalytic abatement of tetracycline at pH of 3, 7 and 9. It is observed that the impact of pH value on the abatement of TC is much more pronounced at the onset of reaction. Significant increased abatement of tetracycline is observed in the first stage of reaction (up to 60 min) and then further followed by a slower abatement between 120 and 180 min (low slope of degradation curve). In principle, the course of abatement becomes similar at the end of the photocatalytic performance.

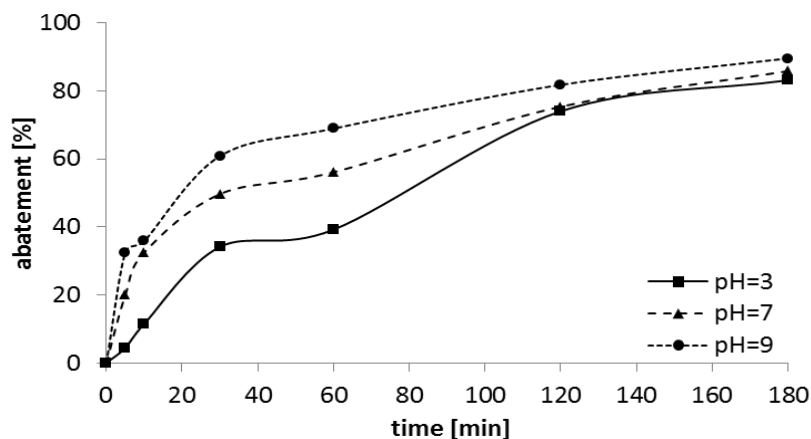


Figure 16. Influence of pH value of the reaction solution on the photocatalytic abatement of tetracycline in aqueous solution over titania 25 photocatalyst under UV-Vis irradiation; IBP conc.: 10 ppm, cat conc.: 20 mg/L.

The comparatively low abatement of TC at the very onset of treatment at low pH reflects the impact of TC zwitterionic nature of tetracycline (Fig. 17).

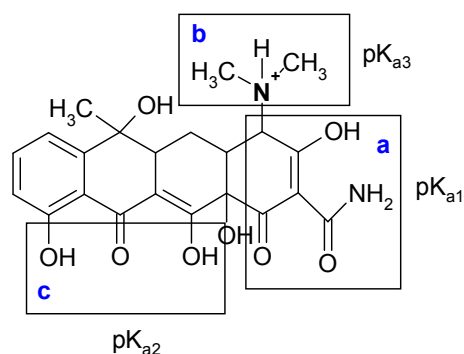
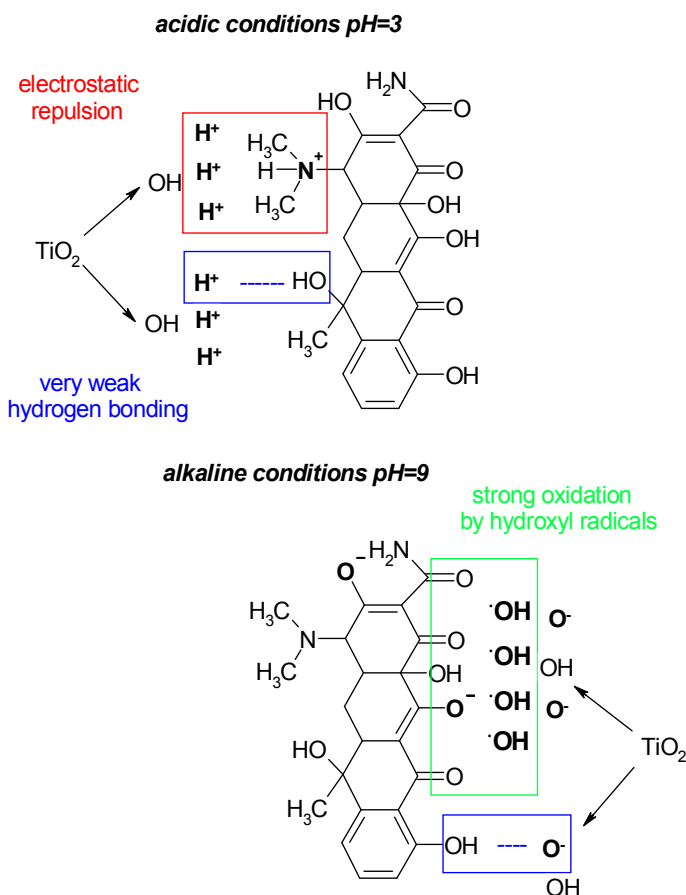


Figure 17. Acid-base equilibria and ionization (speciation) states of tetracycline (a) $pK_{a1}=3.3$ (ab^+c), (b) $pK_{a2}=7.5$ (a^-b^+c), (c) $pK_{a3}=9.4$ ($a^-b^+c^-$ or a^-bc^-).^[176]

At this point, at acidic conditions, cations of TC (mostly protonated states (ab^+c)) are formed which increase the repulsion with positive charged titania surface. The low onset abatement results in a different shaped abatement curves. Later, with prolonged reaction time, other factors could interfere with abatement and change the nature of TC molecule, e.g. the enhanced formation of TC by-products. Finally, the observed abatements after 180 min are similar under alkaline (pH=3), neutral (pH=7) and acidic (pH=9) conditions, resulting the abatement with *ca.* 78 and 84 %, respectively. Increase activity of titania under alkaline conditions may be again attributed by increase amount of reactive $\cdot OH$ radicals on TiO_2 surface (Scheme 1). This finding is in agreement with Zhu et al. who showed that the decomposition of tetracycline from

the aqueous solution succeed better in alkaline solution than in acidic one. After 10 min of irradiation over titania (cat conc.: 1g/L and TC conc.: 40 ppm) *ca.* 70, 75 and 88 % of TC have been removed at pH 3.0, 7.0, and 9.0, respectively.^[177]



Scheme 1. Schematic representation of the interactions between titania hydroxylated surface and tetracycline molecule at acidic and alkaline solutions.

Formation of ibuprofen and tetracycline intermediates

The identification of temporary ibuprofen and tetracycline intermediates, formed during photocatalytic treatment, has been checked by electrospray ionization mass spectroscopy (ESI-TOF-MS). The negative ESI-TOF-MS spectra of the ibuprofen and tetracycline exhibit molecular ion peaks $[M-H]^-$, which are sorted according to the mass-to-charge peaks (m/z). The $[M-H]^-$ peaks of the IBP and TC anions appear at m/z 205 and 443, respectively (Fig. 18 and 19).

After 30 min of photocatalytic treatment of **ibuprofen**, besides the IBP anion peak at m/z 205 $[M-H]^-$, peaks at m/z 221, 251, 277, 305, 319 and others appear abundantly.

Obviously, these higher molecular mass peaks belong to oxidation by-products of IBP and further reaction products of intermediates (Fig. 18). For instance, the m/z 221 and 251 peaks belong to side - chain oxidation products. Deeply discussion will be given below (compare Chapter 3.2). Lower molecular ion $[M-H]^-$ peaks arising at m/z 175, 146, 133, 129 and lower likely belong to deeper oxidized degradation products like aromatic ketones, carboxylic acids or phenols. The appearance of these molecular peaks is in line with the UV-Vis measurements. The absorbance at 262 nm in the UV-Vis spectrum related to intermediates reaches maximum intensity after 30 min of reaction and finally disappears after 180 min (compare Fig. 9). After 240 min of photocatalytic treatment a couple of peaks almost totally disappear (data not shown), indicating nearly fully degradation with prolonged treatment time.

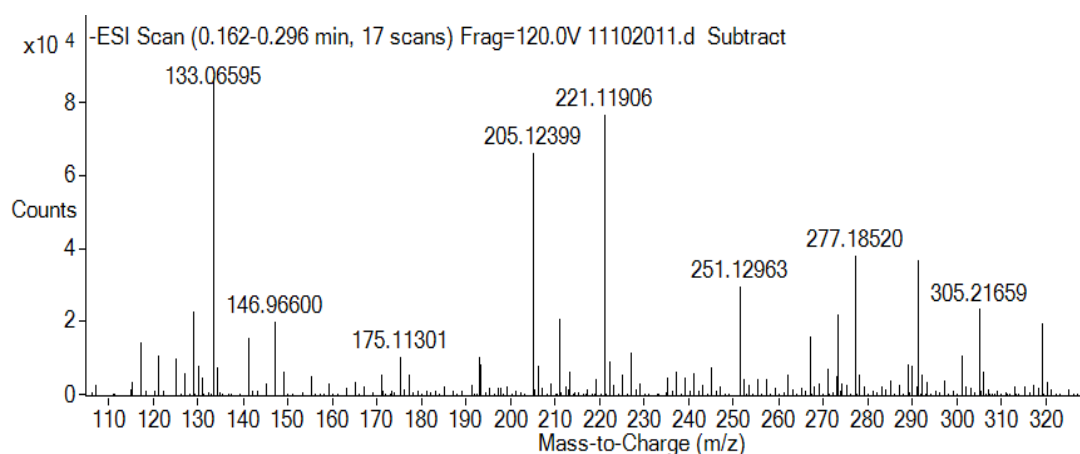


Figure 18. Negative ESI-TOF-MS spectrum of the aqueous ibuprofen solution after 30 min of photocatalytic treatment over titania P25 photocatalyst under UV-VIS irradiation; IBP conc.: 20 ppm, cat. conc.: 20 mg/L.

As was earlier mentioned the determination of by-products of **tetracycline** by UV-Vis spectroscopy was not possible.

The negative ESI-TOF-MS spectrum obtained after 240 min of photocatalytic treatment shows a couple of tetracycline by-products, which still remain in the solution (Fig. 19).

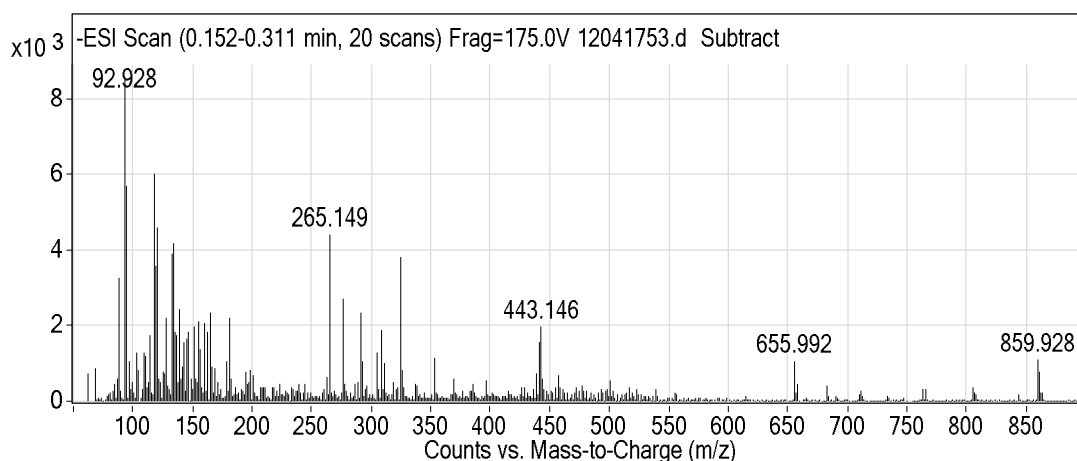


Figure 19. Negative ESI-TOF-MS spectrum of the aqueous tetracycline solution after 240 min of photocatalytic treatment over titania P25 photocatalyst under UV-VIS irradiation; TC conc.: 20 ppm, cat. conc.: 20 mg/L.

Until now, only single studies proposed the possible degradation tetracycline pathways, including TC intermediates formation in the presence of additional oxidation agents as ozone or hydrogen peroxide.^[178-180] Besides the tetracycline molecular peak $[M-H]^-$ at m/z 443, a lot of new peaks, in the lower m/z range between *ca.* 92 and 200 appear. They belong to degradation products of the tetracycline like phenols, ketones, aldehydes or organic acids and impurities.^[181] Additionally, new peaks arise in the range between m/z 265 and 325. These differences in m/z mass peaks strongly imply that signals differ in masses, in following order: 12, 14, 18, and 16 belonging to some ring opening substituents. The given masses are familiar to open ring products of TC (between 265 and 325), especially, from intermediate anthraquinone derivates and/or from phenol substituents. The ring opening products are further decomposed to organic acids (lower masses, between m/z at 90 and 180) like aliphatic acids, alcohols or ethers. The decrease of the TC concentration after long time of treatment is accompanied by the further increase of reaction intermediates, which can poison the surface of titania photocatalyst.

As was former discussed, the TC abatement is lower than for IBP over titania photocatalyst and was assigned to a partial blocking of the photocatalyst by larger amount of TC intermediates found with ESI-TOF-MS measurements.

Re-use experiments

The photocatalyst lifetime (re-use experiments) has been checked in the photocatalytic abatements of ibuprofen and tetracycline during 3 cycles (runs) of treatment. The cat-to-sub ratio was 1:1 (cat. conc. 10 mg/L and drug conc. 10 ppm). Figure 20 shows cycling experiments with **ibuprofen** over titania. *Ca.* 87 % of ibuprofen has been removed in the first cycle of experiment by applying a low cat-to-sub ratio of 1.1. Already, in the second cycle, a substantial decrease of the photocatalyst activity is observed. The abatement of IBP reaches 74 % after 180 min of photocatalytic treatment. Finally, in the 3rd cycle the abatement reached only 48 %.

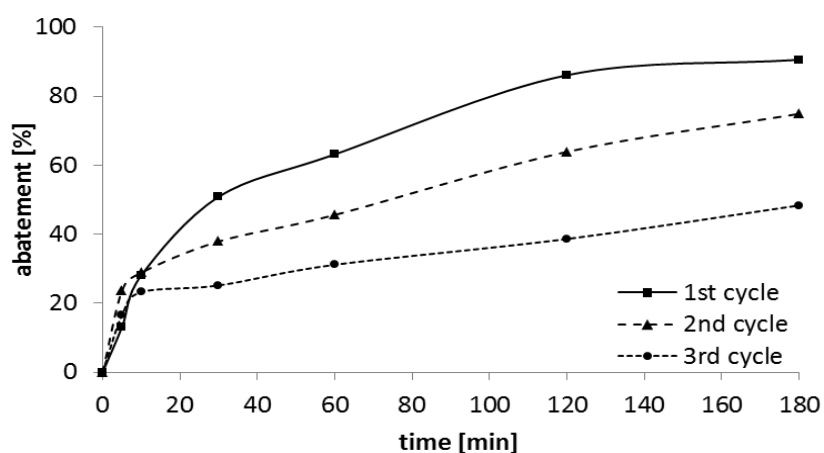


Figure 20. Photocatalytic abatement of ibuprofen in aqueous solution over titania 25 photocatalyst under UV-Vis irradiation after 3 runs of treatment; IBP conc.: 10 ppm, cat conc.: 10 mg/L.

Decreasing photocatalyst activity is also reflected in the formation of IBP intermediates. The concentration of temporary products immediately increases after starting the photocatalytic treatment. Thereafter, concentration of intermediates is slightly decreased with treatment time (graph not shown). Diminishing of the activity in the cycling experiments is accompanied by accumulation of IBP by-products in the treated solution and corresponding poisoning of the photocatalyst surface. ESI-TOF-MS data confirm the oligomeric species from reaction intermediates.

Therefore, it is suggested that growing intermediate formation during cycling experiments leads to poisoning of the photocatalyst (reactive surface sites) by formed oligomers. This process is accelerated with cycling due to growing formation and

presence of temporary intermediates. Reaction by-products are then hardly decomposed.

The re-use experiments have been also carried with **tetracycline**. As is observed in Figure 21, the first run of photocatalytic treatment of TC the photocatalyst shows comparatively high activity in the abatement (*ca.* 74 %). This efficiency in the 1st run is *ca.* 13 % lower than in case of abatement of ibuprofen, where abatement reached *ca.* 87 % (compare Fig. 20). In the 2nd and 3rd run a significant loss of activity is observed. This finding reflects poisoning of the titania surface by TC intermediates.

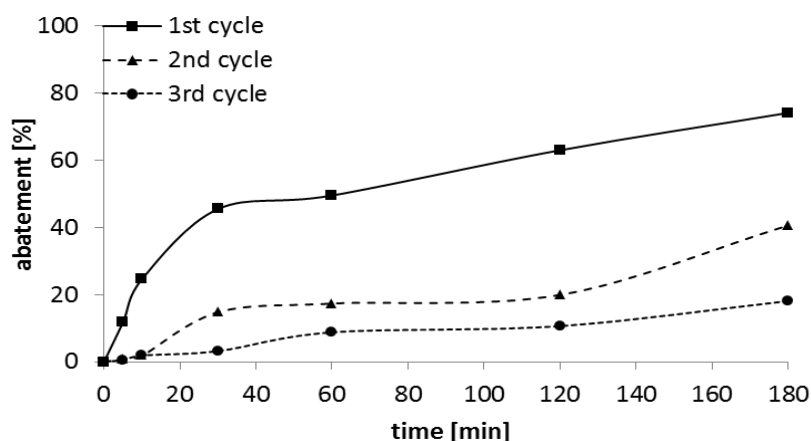


Figure 21. Photocatalytic abatement of tetracycline in aqueous solution over titania 25 photocatalyst under UV-Vis irradiation after 3 runs of treatment; TC conc.: 10 ppm, cat conc.: 10 mg/L.

Summary

- Photocatalytic treatment of ibuprofen and tetracycline over commercial titania was investigated in detail. Beyond the State-of-the-Art and “the proof of principle” (given in most papers) more precise and reliable experimental conditions have been showed.
- Titania photocatalyst is an effective photocatalytic material. *Ca.* 97 % of IBP and 85 % of TC have been effectively abated from solution (cat-to-sub ratio of 2, 180 min of photocatalytic treatment, simulated sun light of solarium lamps). Titania shows very high onset activity.
- The abatement of IBP is somewhat higher compare to TC. The increase of abatement in the onset of reaction (within first 30 min) is similar for both pharmaceuticals. At this point the reaction rates (*r*) are higher and reach of *ca.*

0.016 and 0.015 for IBP and TC, respectively. Further, with prolonged treatment time from 30 to 180 the markedly decrease activity is observed. However, this decrease in the abatement of IBP is lower ($r=0.0033$), compare to TC ($r=0.0024$). This finding is in line with fast deactivation of catalyst.

- Influence of pH solution during abatement of IBP over titania is marginally and is not as much influenced than in case of TC abatement. The change of pH value has impact on the TC abatement because of changing zwitterionic nature of TC molecule, as well. The pH of 7 is optimum for the decomposition of IBP. This value is close to real (environmental) water condition.
- The formation of reaction intermediates is related to the course of abatement. At the beginning of treatment lower formation of by-products is observed. At the first stage, the formation of TC and IBP intermediates proceeds rapidly (consistent with high abatement). With prolonged treatment time both pharmaceuticals are transforming to by-products (abatement is lower due to the deactivation). Then, finally intermediates are decomposed, what is indicated by low intensities of ESI-TOF-MS spectra.

3.2. Photocatalytic abatement of ibuprofen and tetracycline over zirconium doped titania (Zr-TiO₂) photocatalyst

Zr-doped titania of anatase structure have been prepared by a combined sol-gel and chemical vapour deposition (CVD) process. The photocatalytic performance has been studied by varying the photocatalyst concentration (from 10 to 40 mg/L), e.g. at different cat-to-sub ratios. The changing of the pH solution, the re-use and adsorption experiments have been deeply investigated. Additionally, formation of reaction intermediates during the oxidative decomposition of the pharmaceuticals: ibuprofen and tetracycline has been studied and compared with commercial titania.

Photocatalytic activity

The photocatalytic performance of Zr-doped titania has been investigated in the degradation of ibuprofen and tetracycline. The cat-to-sub ratios were varied by changing the photocatalyst concentrations (from 10 to 40 mg/L) at constant pollutant

concentration (10 ppm) of both pharmaceuticals. The course of abatements of **ibuprofen** is shown in Figure 22.

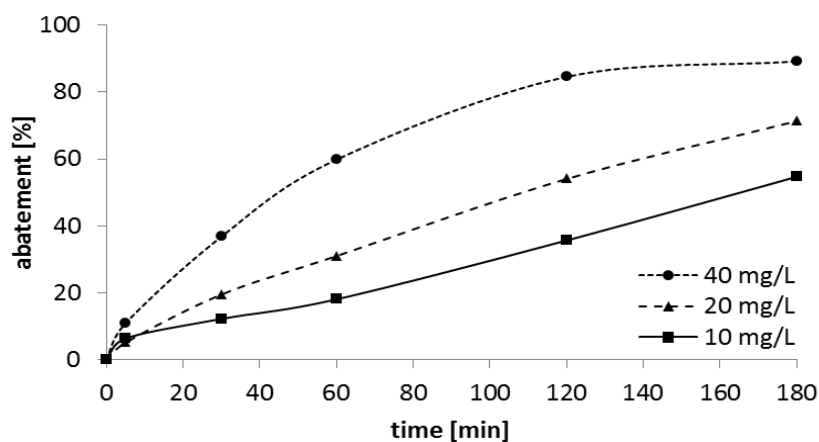


Figure 22. Photocatalytic abatement of ibuprofen in aqueous solution over Zr-TiO₂ photocatalyst under UV-Vis irradiation; IBP conc.: 10 ppm, cat conc.: 10, 20 and 40 mg/L.

After a small initial increase after 5 min of photocatalytic treatment, the abatement proceeds continuously with time. The faster initial abatement at the onset is probably due to the photocatalytic oxidation of IBP at highly reactive electron holes at the surface and in part by adsorption. The electron holes have a higher oxidation potential compared to electrons (compare Tab. 3). Increased cat-to-sub ratio from 1:1 to 4:1 enhances the abatement of ibuprofen of up to *ca.* 90 % due to the presence of more active sites, by means, the surface electrons and holes.

At the same time, formation of intermediates is also increased (Fig. 23). Only with high cat-to-sub ratios (photocatalyst in excess) the concentration of intermediates decrease after prolonged photocatalytic treatment. However, intermediates did not fully disappear even after 180 min (Fig. 23). Although high a percentage of IBP is photocatalytic abated over Zr-doped titania, the achieved photocatalytic abatement is somewhat lower than observed with titania photocatalysts even the specific surface area is markedly increased up to 100 m²/g (compare A 1, Tab. 1). The latter is also reflected in the less effective degradation of formed intermediates.

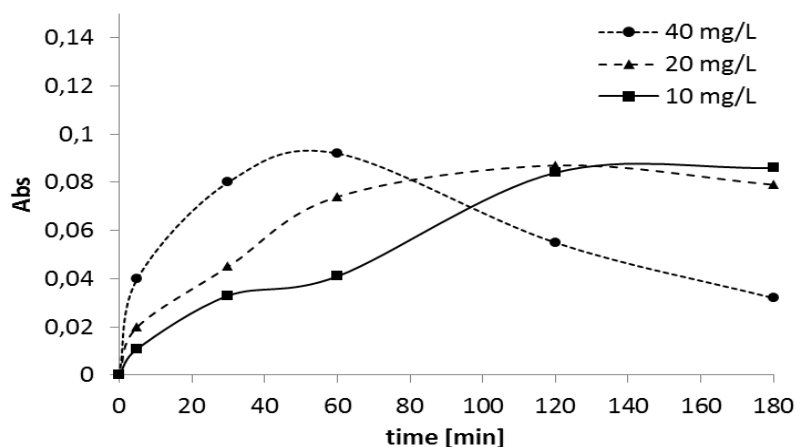


Figure 23. Formation of the temporary intermediates of ibuprofen in aqueous solution during photocatalytic treatment over Zr-TiO₂ photocatalyst based on UV-Vis absorbance at λ_{\max} 262 nm for different cat conc.: 10, 20 and 40 mg/L, IBP conc.: 10 ppm.

In Table 6 the relative and absolute abatements and corresponding experimental effective mean first order reaction rates of ibuprofen over Zr-doped titania derived from the abatement curves are summarized.

Table 6. Data of the photocatalytic abatement of ibuprofen (10 ppm) in water during photocatalytic treatment over Zr-TiO₂ photocatalyst (cat conc.: 10, 20 and 40 mg/L). Relative and absolute abatements (A) and corresponding experimental effective mean first order reaction rates (r) calculated after 30, 120 and 180 min of treatment.

irradiation time of IBP [min]	rel. A	abs. A	r	rel. A	abs. A	r	rel. A	abs. A	R
	[%]	[mg/L]	[min ⁻¹]	[%]	[mg/L]	[min ⁻¹]	[%]	[mg/L]	[min ⁻¹]
	10 mg/L			20 mg/L			40 mg/L		
5	5	0.5	0.0100	6	0.6	0.0060	11	1.1	0.0055
30	12	1.2	0.0040	19	1.9	0.0032	36	3.6	0.0030
120	35	3.5	0.0029	54	5.4	0.0023	84	8.4	0.0018
180	56	5.6	0.0031	71	7.1	0.0020	89	8.9	0.0012

As is expected, the relative and absolute abatement increases with reaction time and increasing photocatalyst loading (cat-to-sub ratio). However, the absolute abatement per mg of photocatalyst decreases with increasing photocatalyst amount. E.g. after 30 min of treatment, the specific abatements decrease from 0.12, 0.095 and 0.09 mg/L IBP per mg of photocatalysts with increased photocatalyst amount from 10 to 40 mg/L, respectively. Therefore, the mean reaction rates also decrease in the same order. The decrease of the mean reaction rate at high photocatalyst loading (40 mg/L) between 120 and 180 min of reaction is due to photocatalyst deactivation. The abatement increases only slightly. This finding is surprising, because the IBP concentration (10 ppm) is low compared to the photocatalyst. Finally, the apparent

photocatalyst efficiency is decreased with growing cat-to-sub ratio, but the total abatement is improved. Probably, the photocatalyst is faster deactivated by formed reaction intermediates. A similar effect is observed with titania after 30 min of reaction (Tab. 4). Finally, the abatement over titania is higher (up to 100 %) due its high onset activity, which has been ascribed to the presence of highly active electron holes.

The adsorption of ibuprofen over titania and Zr-doped TiO₂ is shown in Figure 24. The Zr-doping of titania significantly enhanced the adsorption of IBP compared to non-doped TiO₂.

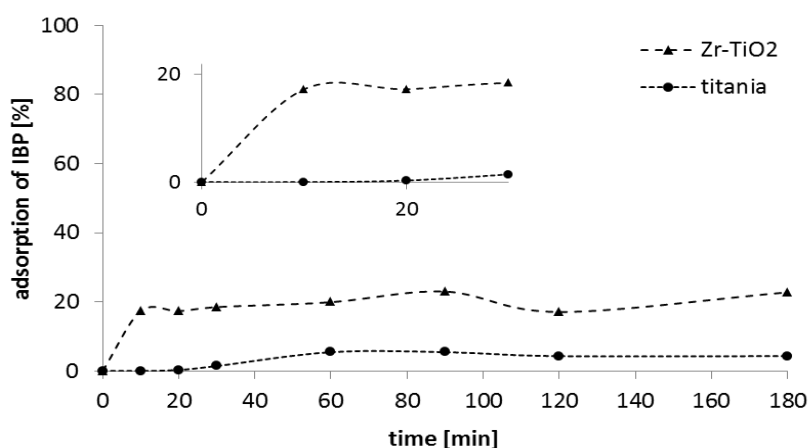


Figure 24. Adsorption of ibuprofen on titania P25 and Zr-TiO₂ photocatalysts in the dark; IBP conc.: 10 ppm, cat conc.: 100 mg/L; (inset) magnification of adsorption curves between 0 and 30 min; cat-to-sub ratio of 10:1.

Already at short contact time the IBP is adsorbed on Zr-TiO₂. *Ca.* 20 % abatement of ibuprofen is achieved by adsorption from a low concentrated solution containing 10 ppm IBP with 100 mg/L of photocatalyst. This improved adsorption is maintained at long contact time of 180 min in aqueous solution. In contrast, adsorption on titania is comparably low. The significant enhanced adsorption at Zr-doped titania can be explained by both, the increased specific surface area and the presence of mesoporosity of 0.25 cm³/g and pores of 8 - 9 nm size (compare A 1.1, Fig. 9) compared to the titania photocatalyst.

The photocatalytic abatements of **tetracycline** over Zr-doped titania photocatalyst (10, 20 and 40 mg/L) has been studied at constant concentration of 10 ppm (Fig. 25).

The photocatalytic behaviour of the TC abatement is similar to that of IBP, reported above. However, the achieved abatement is lower with *ca.* 37 to 70 % for 10 to 40 mg/L photocatalyst loading, respectively. The photocatalytic abatement of TC increases nearly continuously after the first 5 min of treatment up to 120 min. Beyond 120 min the abatement proceeds slowly leading to a lower slope of the abatement curve especially for higher cat-to-sub ratio of 2 or 4. The photocatalyst deactivation observed after 120 min of reaction increases markedly with the increased cat-to-sub ratios.

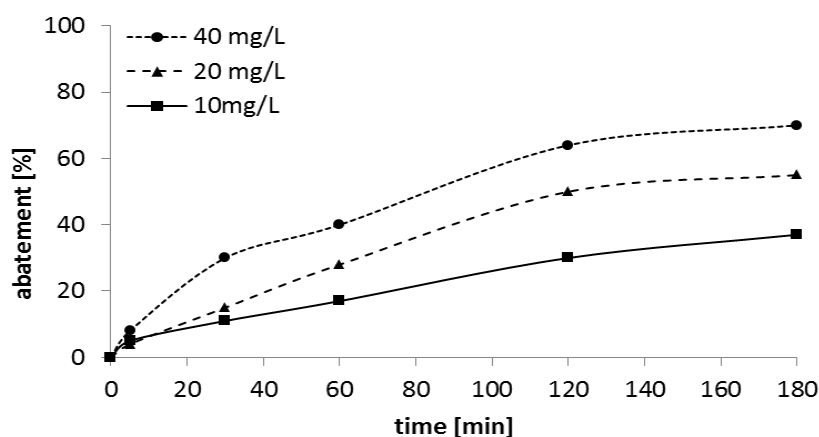


Figure 25. Photocatalytic abatement of tetracycline in aqueous solution over Zr-TiO₂ photocatalyst under UV-Vis irradiation; TC conc.: 10 ppm, cat conc.: 10, 20 and 40 mg/L.

The mean first order reaction rates of TC and IBP are similar and decrease with increasing reaction time and photocatalyst amounts (Tab. 7).

Table 7. Data of the photocatalytic abatement of tetracycline (10 ppm) in water during photocatalytic treatment over Zr-TiO₂ photocatalyst (cat conc.: 10, 20 and 40 mg/L). Relative and absolute abatements (A) and corresponding experimental effective mean first order reaction rates (r) calculated after 30, 120 and 180 min of treatment.

irradiation time of TC [min]	rel. A	abs. A	r	rel. A	abs. A	r	rel. A	abs. A	r
	[%]	[mg/L]	[min ⁻¹]	[%]	[mg/L]	[min ⁻¹]	[%]	[mg/L]	[min ⁻¹]
	10 mg/L			20 mg/L			40 mg/L		
5	4	0.4	0.0080	5	0.5	0.0050	8	0.8	0.0040
30	11	1.1	0.0036	15	1.5	0.0025	30	3	0.0025
120	30	3	0.0025	50	5	0.0020	64	6.4	0.0013
180	37	3.7	0.0021	55	5.5	0.0015	70	7	0.0009

Zr-doped TiO₂ shows lower abatements in the abatement of tetracycline due to the lower onset activity (Fig. 26). Contrary to, the high onset activity of titania is due to improved photocatalytic activity. Zr-doped titania, is markedly contributed by absorption, at the onset abatement, due to the improved adsorption properties.

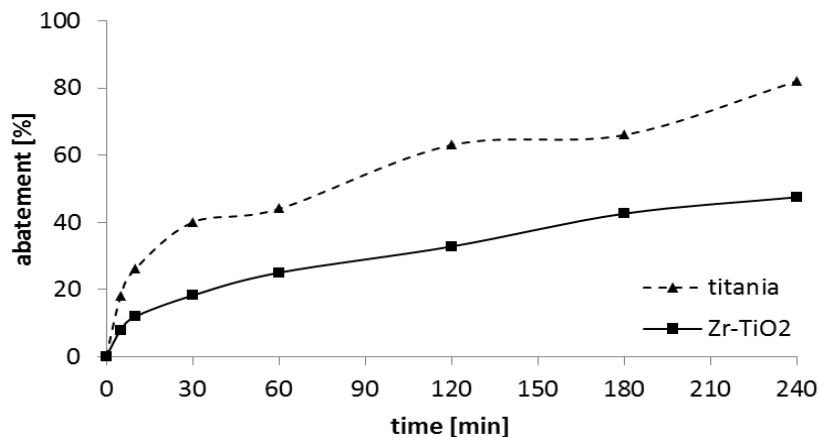


Figure 26. Photocatalytic abatement of tetracycline in aqueous solution over titania P25 and Zr-TiO₂ photocatalysts under UV-Vis irradiation; TC conc.: 20 ppm, cat conc.: 20 mg/L.

Influence of pH solution

The photocatalytic abatement of **ibuprofen** over Zr-TiO₂ photocatalyst is significantly improved with decreasing pH value. Rapid photocatalytic abatement is observed at the very beginning of the treatment (5 min), especially at acidic conditions. It increases by a factor of 6 with simultaneous decreasing the pH value from 9 to 2. Thereafter, degradation of ibuprofen proceeds continuous, but slower, as was already noted (Fig. 27).

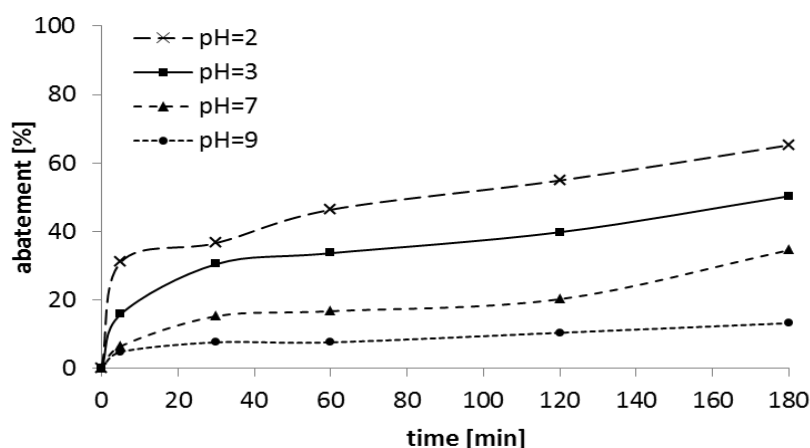


Figure 27. Influence of pH value of the reaction solution on the photocatalytic abatement of ibuprofen in aqueous solution over Zr-TiO₂ photocatalyst under UV-Vis irradiation; IBP conc.: 20 ppm, cat conc.: 10 mg/L.

The noticeable improvement of the photocatalytic activity is explained by the changed surface properties of titania after Zr-doping. Obviously, the material behaves more hydrophobic. Therefore, non - polar molecules are preferentially adsorbed. The dissociation of the carboxylic acid group of ibuprofen is diminished with decreasing pH value, because ibuprofen is a weak acid ($pK_a = 4.4$). This will favour the interaction of the IBP with the photocatalyst surface. Alignment of IBP molecules on the photocatalyst surface and in solution can be improved by hydrogen bonding between non - dissociated carboxyl groups. This effect can markedly enhance the adsorption/enrichment of the substrate at the photocatalyst surface. The self - agglomeration tendency of IBP is also shown by the formation of agglomerated species in the starting reaction solution. The polar hydrophilic intermediates, that are formed, are readily released from the hydrophobic photocatalyst surface into solution.

The influence of the pH value of the **tetracycline** solution on the activity of Zr-doped titania (Zr-TiO₂) photocatalyst has been also checked (Fig. 28).

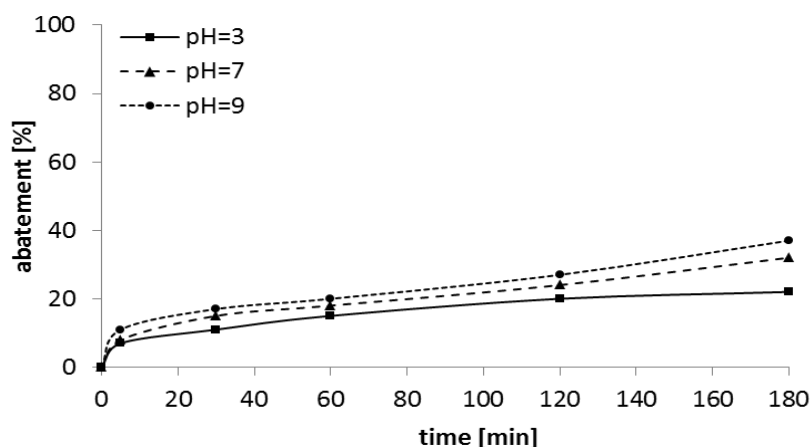


Figure 28. Influence of pH value of the reaction solution on the photocatalytic abatement of tetracycline in aqueous solution over Zr-TiO₂ photocatalyst under UV-Vis irradiation; IBP conc.: 20 ppm, cat conc.: 10 mg/L.

In contrast to ibuprofen, the influence of the pH value of the reaction solution is low showing the importance of the nature of the substrate molecule. At all three pH values applied, the tetracycline is mainly ambivalent charged (compare A 1.2, Fig. 30).

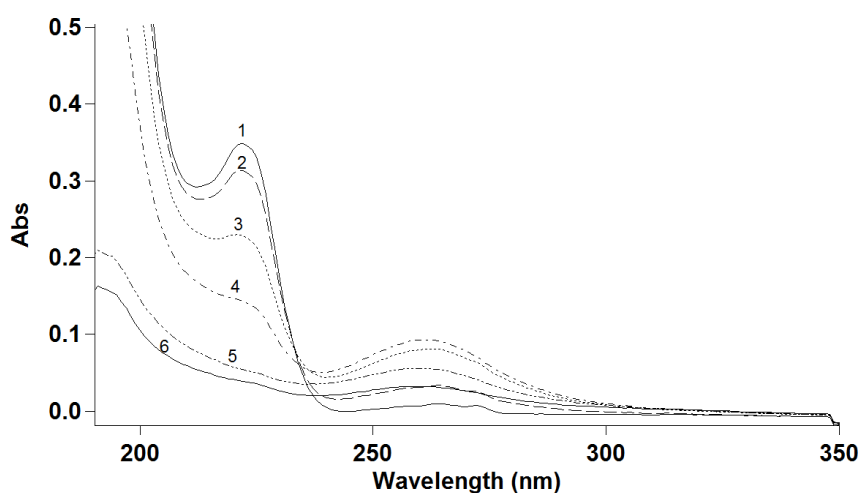
The variation of the pH value does not change the general finding that the photocatalytic degradation of IBP and TC proceeds faster over titania and that ibuprofen IBP is easier converted than tetracycline.

Formation of ibuprofen intermediates

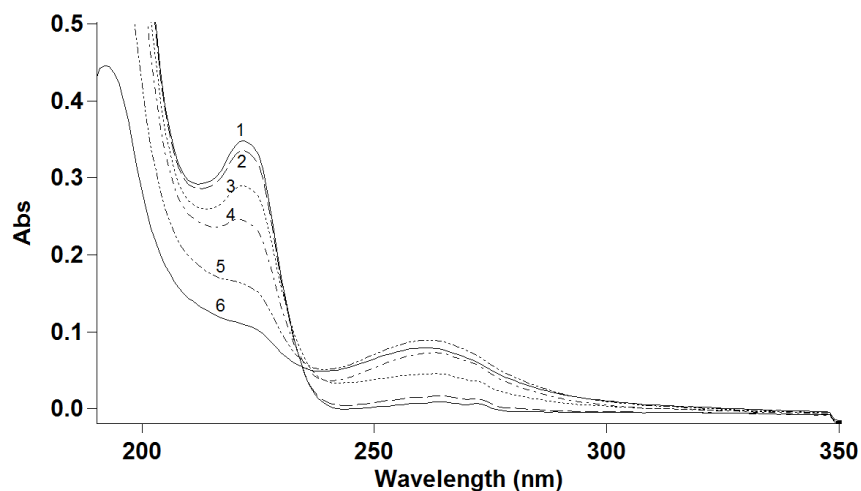
The photocatalytic decomposition behaviour of ibuprofen over Zr-TiO₂ was followed by UV-Vis spectroscopy based on the intensity of the 222 nm absorbance of the aromatic ring of IBP. The decrease of this absorption band during photocatalytic treatment is accompanied by the simultaneous appearance and increase of a new absorbance at 262 nm, which has been used to characterize the formation of reaction intermediates. ESI-TOF-MS measurements (after 30 and 240 min of treatment) have been performed to detect qualitatively the formation of different types of intermediates.

Figure 29 shows the corresponding UV-Vis spectra of reaction solutions after different reaction times. During the course of treatment, IBP is decomposed as indicated by the decrease of the 222 nm absorbance of IBP. The decrease of the 222 nm band is related to the cat-to-sub ratio in the order 1:1 < 2:1 < 4:1, with increased photocatalyst amount. At the same time, the formation of intermediates is increased and is higher with increased photocatalyst amount. However, after 180 min of reaction the concentration of intermediates is decreased again due to the ongoing photocatalytic degradation

a)



b)



c)

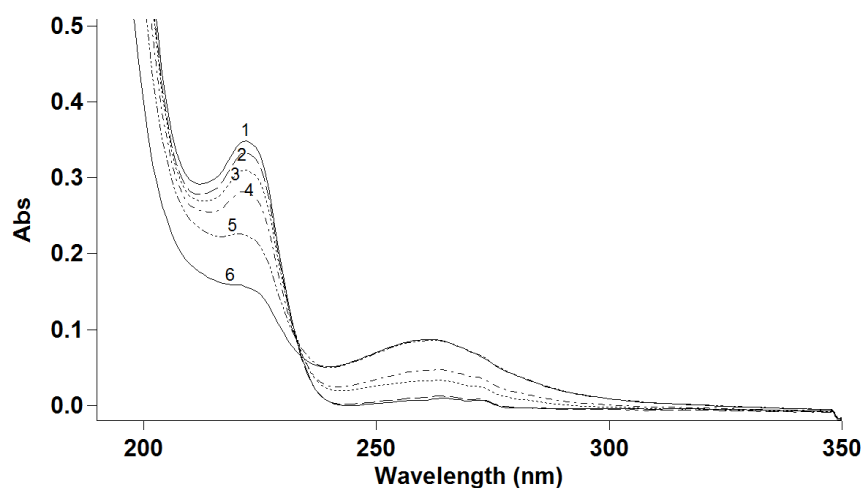


Figure 29. UV-Vis spectra of an aqueous ibuprofen solution after photocatalytic treatment over Zr-TiO₂ photocatalyst at different cat-to-IBP ratio a) 4:1; b) 2:1; c) 1:1 under UV-Vis irradiation: (1) starting IBP solution (10 ppm) and after (2) 5 min, (3) 30 min, (4) 60 min, (5) 120 min, (6) 180 minutes of photocatalytic treatment. Concentration of ibuprofen determined based on the absorbance at 222 nm. Experimental conditions: IBP conc.: 10 ppm, cat conc.: 10, 20 and 40 mg/L, pH=7.

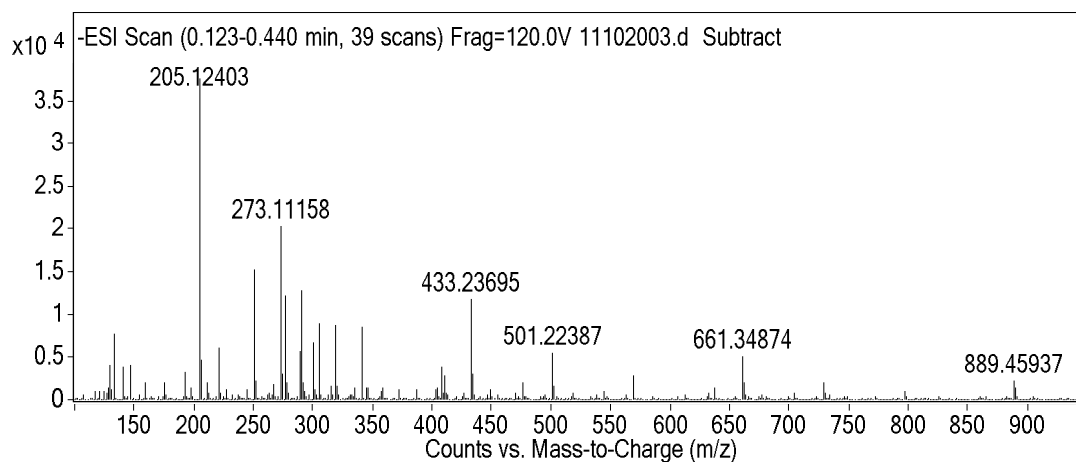
Additionally, ESI-TOF-MS measurements were carried out to follow the ibuprofen decomposition process (Fig. 30). Beside the m/z 205 peak related to the ibuprofen anion, higher mass-to-charge peaks are observed at m/z 433, 661 and 889 in the starting solution (compare A 1.2, Fig. 34). These peaks indicate the presence of agglomerated IBP species. The mass increment of 228 between the signals at m/z 205 and m/z 433, 661 and 889 indicates ibuprofen sodium salt units. Some impurities, e.g.

at m/z 273 and corresponding agglomerated species of ibuprofen sodium salt, as indicated by peaks arising at m/z 501 and 729, are also observed in ESI-TOF-MS spectrum.

In the case of chemical bonding by C - C coupling of IBP (formation of polymers), the mass increments between the peaks would lower due to the release of hydrogen atoms. Therefore, these species (Fig. 30 a) should be aggregates of IBP and the impurity (m/z 273) held together by ionic interactions between the negatively charged carboxylic groups and the sodium ions and by non - polar interactions between the hydrophobic tails of the ibuprofen molecules. These aggregates are decomposed by photocatalytic treatment (Fig. 30 b). After 30 min of photocatalytic treatment, the m/z peak intensities of agglomerated species decrease markedly. IBP is still present as indicated by the peak of the ibuprofen anion at m/z 205 [M-H].

Additional peaks appear at higher and lower m/z values. Obviously, they belong to photocatalytic oxidation and decomposition products.

a)



b)

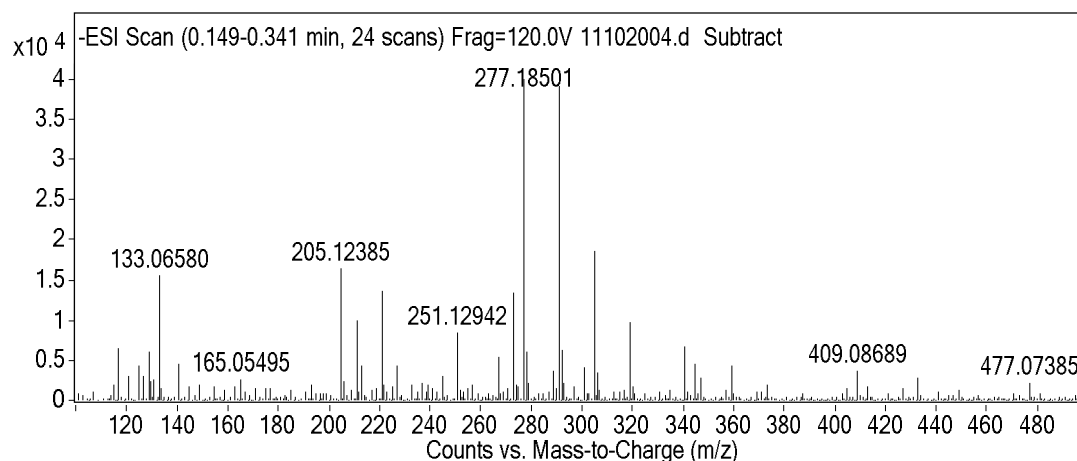
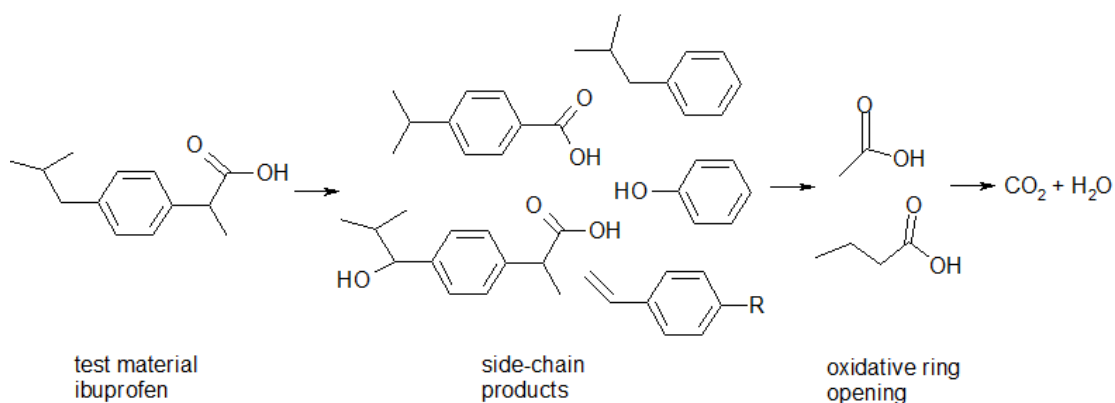


Figure 30. Negative ESI-TOF-MS spectrum of the aqueous ibuprofen solution after a) 30 min and b) 240 min of photocatalytic treatment over Zr-TiO₂ photocatalyst under UV-VIS irradiation; IBP conc.: 20 ppm, cat. conc.: 20 mg/L.

The possible oxidation by-products of ibuprofen of higher masses are due to side chain hydroxylation and carboxylation as initial oxidation processes. Lower mass products are formed by dimethylation and decarboxylation combined with hydroxylation during oxidation. Accordingly, the observed higher mass m/z $[M-H]^-$ peaks at 221, 251 and higher are assigned to hydroxy ibuprofen (221), carboxylated hydroxyl ibuprofen (251) and related different side chain oxidation products (Scheme 2). Such oxygenated species decompose readily under photocatalytic conditions.

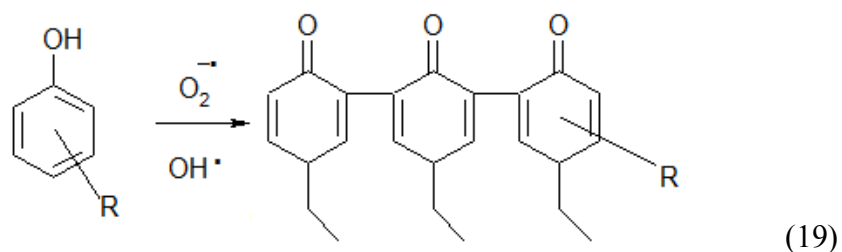
It is concluded that the observed higher mass molecule fragments ($m/z > 300$) point to the formation of polymeric species. They can be formed from phenols, alcohols or aldehydes present in the reaction solution giving rise to lower mass peaks $m/z < 205$. For example, the $[M-H]^-$ peak at (133) could be due to formation of 4-ethylbenzaldehyde or 2-methyl-1-phenylpropane, (149) to 4-isobutylphenol, (163) to 4-acetylbenzoic acid, (175) to 4-isobutylacetophenon or 4-(hydroxyisobutyl)ethyl benzene, (177) to 1-(isobutylphenyl)-1-ethanol and others.^[182-185]



Scheme 2. Possible formation of side-chain products, its deep oxidation products and open ring intermediates formed during photocatalytic abatement of ibuprofen.

Even after an extended treatment time of 240 min (Fig. 30 b), ibuprofen is not fully converted as indicated by the presence of the ibuprofen anion peak at m/z 205. A couple of intermediate decomposition products are still present in the reaction solution, which were not mineralized. They give rise to a variety of signals in the ESI-TOF-MS spectrum of the photocatalytic treated solution. The lower mass peaks at m/z <205 are expected to belong to oxidation products like phenols or ketones and others as discussed above.^[182,184,186,187] These peaks show the presence of some aromatics and reaction intermediates, giving rise to absorbance bands at 222 nm and 262 nm, respectively.

Additionally, new signals appear after photocatalytic treatment at higher m/z values of 277, 291, 305 and 319 (Fig. 30 b). The observed mass differences, with constant increments of 14, implies that they likely represent methyl substitutes of the compound giving rise to the m/z 277 signal. It is proposed that they belong to trimeric quinonic compounds as shown schematically in Equation 19.



This proposal is supported by recent studies. They show the possibility of the polymerization of aromatics, e.g. phenols, in low concentrated aqueous solution catalysed by peroxidase enzyme.^[188-190] The observation of oligomeric species during photocatalytic treatment of ibuprofen is new and has been found with titania photocatalyst, recently for the first time.^[191]

For comparison, the negative ESI-TOF-MS spectra of the aqueous ibuprofen solution after 30 and 240 min of photocatalytic treatment over titania P25 photocatalyst are shown in Figure 31.

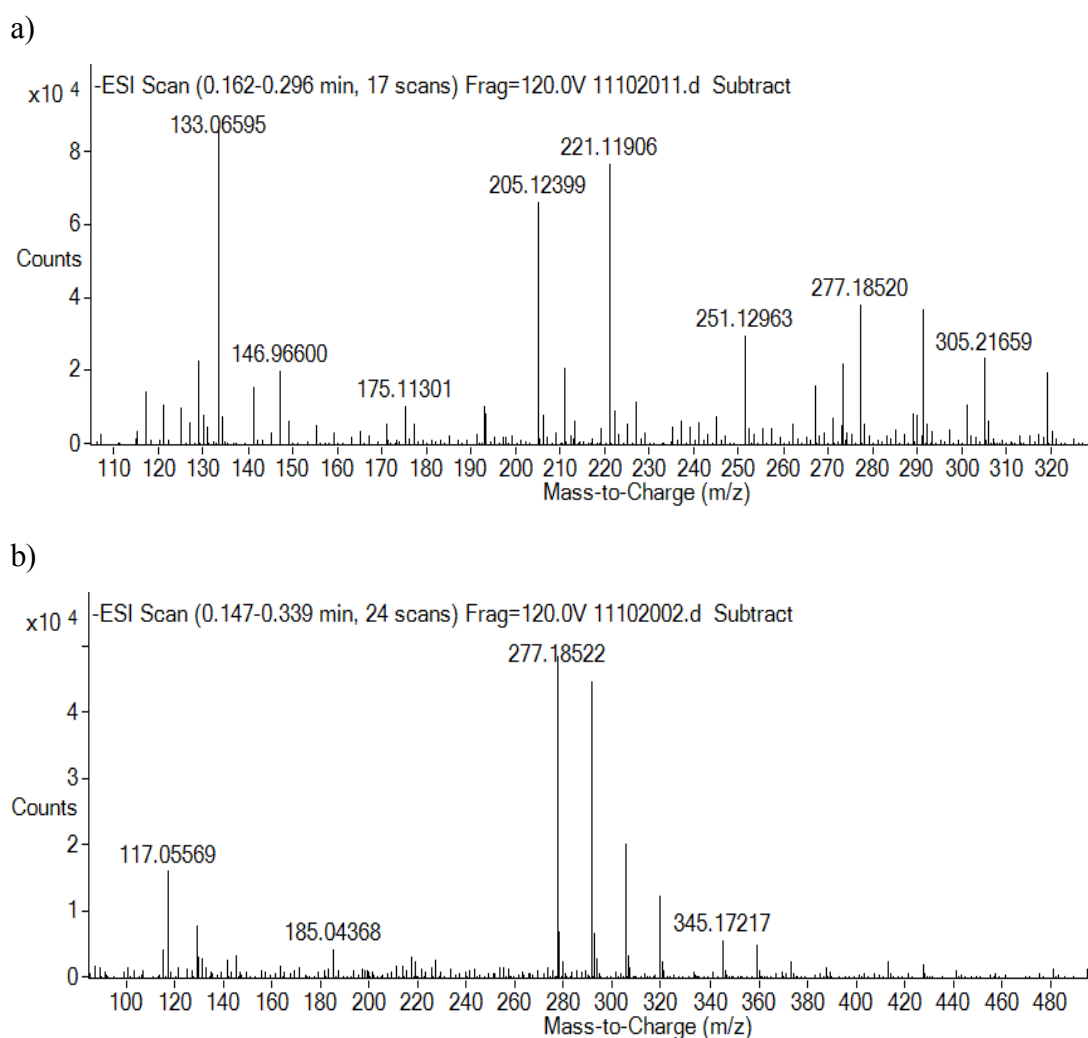


Figure 31. Negative ESI-TOF-MS spectrum of the aqueous ibuprofen solution after a) 30 min and b) 240 min of photocatalytic treatment over titania P25 photocatalyst under UV-VIS irradiation; IBP conc.: 20 ppm, cat. conc.: 20 mg/L.

After 30 min of photocatalytic treatment, mass signals of oligomeric products of the starting solution disappear (Fig. 31 a). Besides, the ibuprofen anion peak $[M-H]^-$ at m/z 205, peaks at m/z 221, 251, 277, 305, 319 and others appear. Obviously, these higher molecular mass peaks belong to partial oxidation products of IBP and reaction products of intermediates e.g. the m/z 221 and 251 peaks, which belong to side-chain oxidation products, which have been identified by Méndez - Arriaga, Caviglioli and Madhavan.^[182,184,187]

Lower mass $[M-H]^-$ peaks arising at m/z 146, 133, 129 and lower likely belong to deeper oxidized degradation products like aromatic ketones, carboxylic acids or phenols. It has to be noted that at this point, the 262 nm absorbance in the UV-Vis spectrum related to intermediates reaches maximum intensity (Fig. 32). After 240 min of photocatalytic treatment, the m/z 205 peak of the IBP anion disappeared completely. In addition, the intensities of lower m/z peaks decreased substantially. Low intense peaks at m/z 117 and 129 remained probably belonging to aromatic oxidation products. Interestingly, new peaks of higher molecular mass appear at m/z 277 as well as 291 and 305 (Fig. 31 b). The mass differences of 14 between these peaks points to methyl substitution. It is proposed that these peaks belong to oligomerization products of aromatics compounds like phenols formed during the photocatalytic decomposition of IBP. These peaks start to arise already after 30 min of photocatalytic treatment.

These data indicate that the photocatalytic properties of Zr-TiO₂ and TiO₂ differ. In case of Zr-TiO₂ more reaction by-products are present in photocatalytic treated solutions. The comparison shows that reaction intermediates formed over titania are almost successively decomposed during the course of photocatalytic treatment (Fig. 8). Finally, mainly polymeric species remain in the reaction solution. In contrast, formed reaction intermediates are more difficult to decompose over Zr-TiO₂.

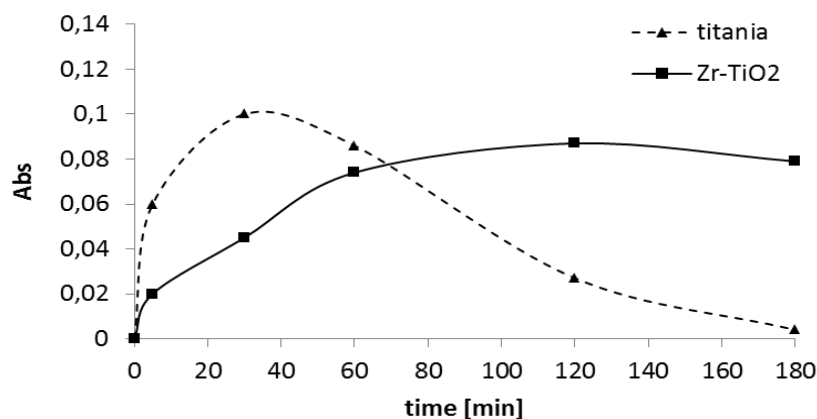


Figure 32. Formation of the temporary intermediates of ibuprofen in aqueous solution during photocatalytic treatment over titania 25 and Zr-TiO₂ photocatalyst based on UV-Vis absorbance at λ_{\max} 262 nm; IBP conc.: 20 ppm, cat conc.: 20 mg/L.

Formation of tetracycline intermediates

The formation of TC intermediates over Zr-TiO₂ and titania and has been studied by ESI-TOF-MS measurements (Fig. 33-35). The negative ESI-TOF-MS spectrum of starting tetracycline solution is shown in Figure 33. The starting solution exhibits one main peaks located at m/z 443 nm related to the tetracycline $[M-H]^-$ peak. Other present molecular peaks at *ca.* m/z 155, 501 and 909 indicate some impurities.

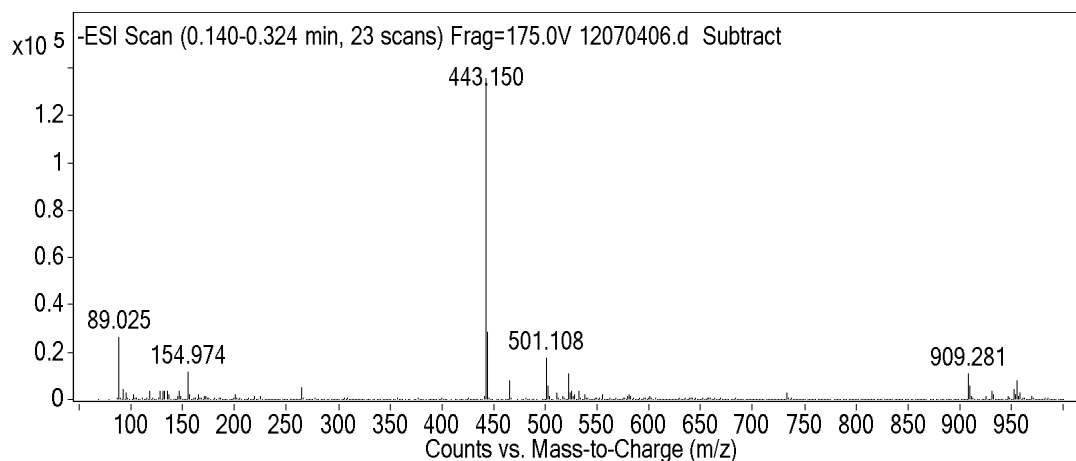
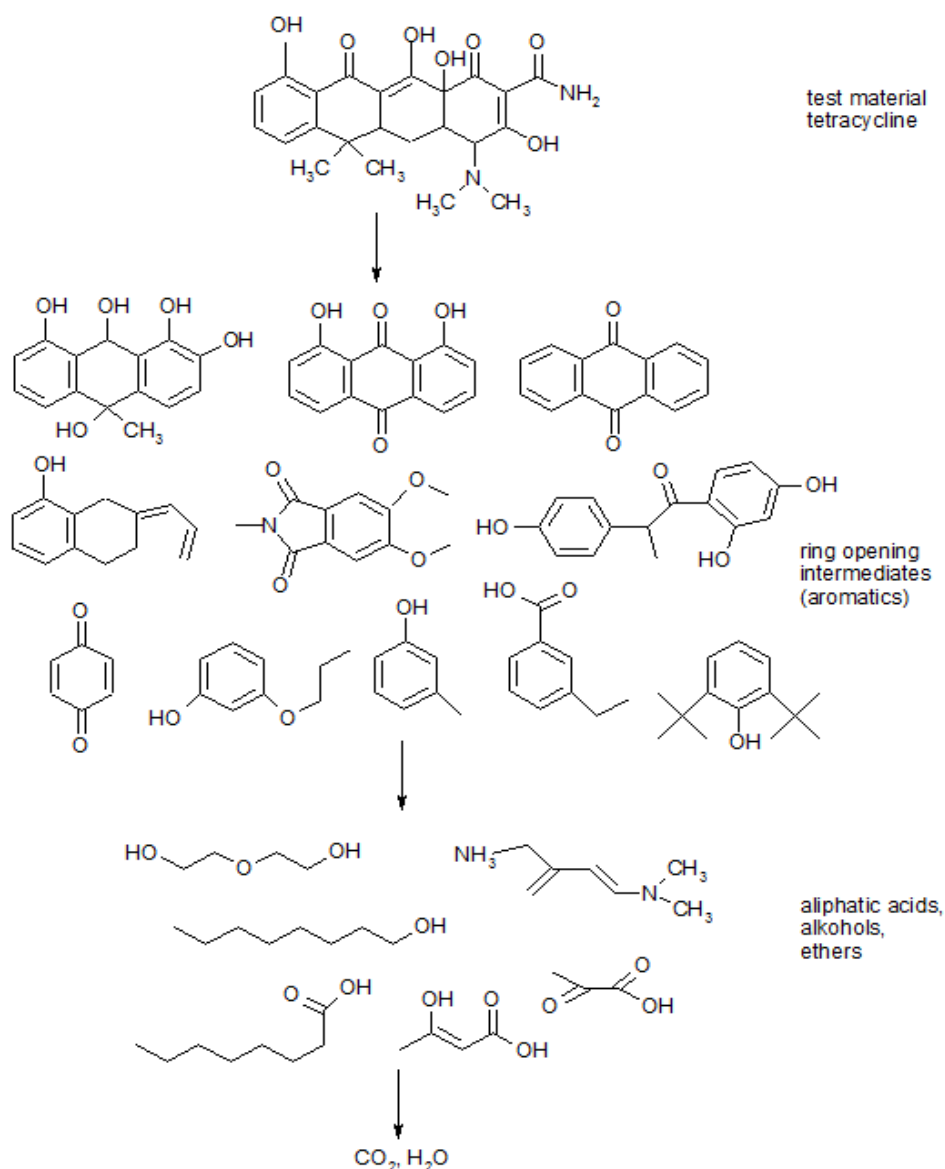


Figure 33. Negative ESI-TOF-MS spectrum of the starting aqueous tetracycline solution (20 ppm).

After 30 min of photocatalytic treatment over Zr-TiO₂, the main mass-to-charge peak $[M-H]^-$ of the TC still appears at m/z 443 (Fig. 34). Besides, some new lower molecular mass-to-charge peaks are observed around *ca.* m/z 170, and very low intense peaks around m/z 130 - 140 and <100 . After 240 min an additional m/z peak arises at *ca.* m/z 265.

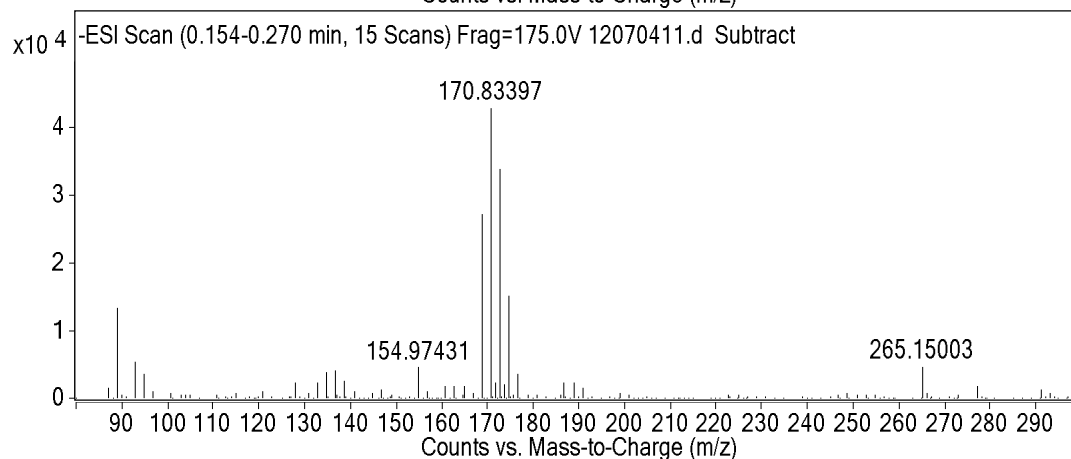
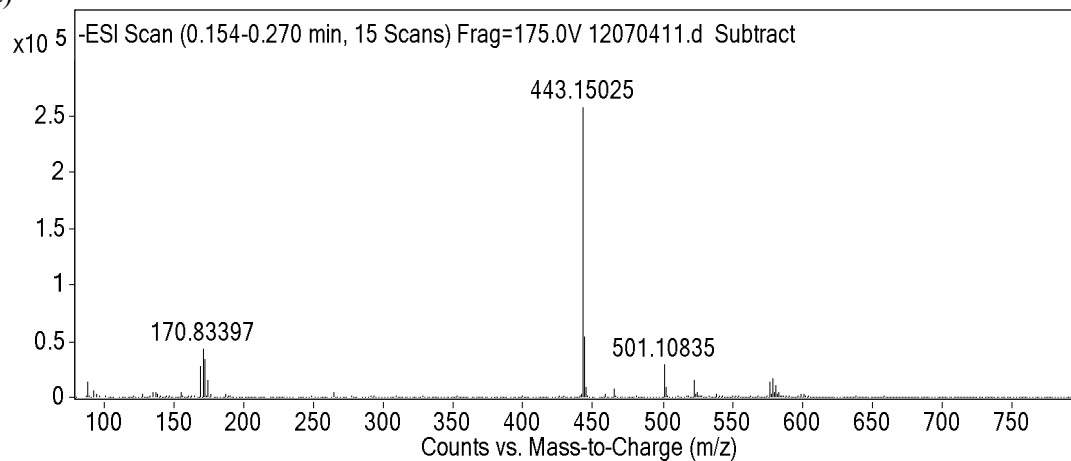


Scheme 3. Proposed possible formation of ring opening tetracycline intermediates (i.g. three, two and one ring aromatics^[192] followed by formation of aliphatic compounds (i.g. aliphatic acids, alcohols, ethers).

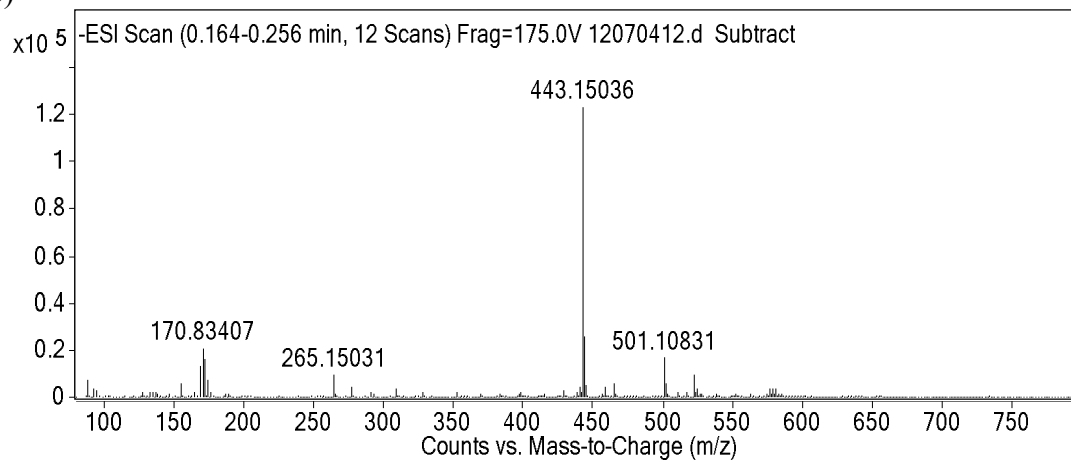
According to Zhu and Niu^[177,193] the degradation of TC, consisting of four aromatic, olefinic and aliphatic 6-membered hydrocarbon rings, proceeds via non-selective oxidation of the non-aromatic part producing reaction intermediates through ring opening. This way mainly substituted aromatics based on benzenes are formed probably via quinone formation (Scheme 3).

As a results, a couple of different intermediates of medium mass ($m/z < 210$) related to anthraquinone, quinone derivates,^[194] benzoic acid derivates, substituted benzene and phenol derivates are formed and further decomposed to low mass ($m/z < 100$) aliphatic acids, alcohols and ethers.

a)



b)



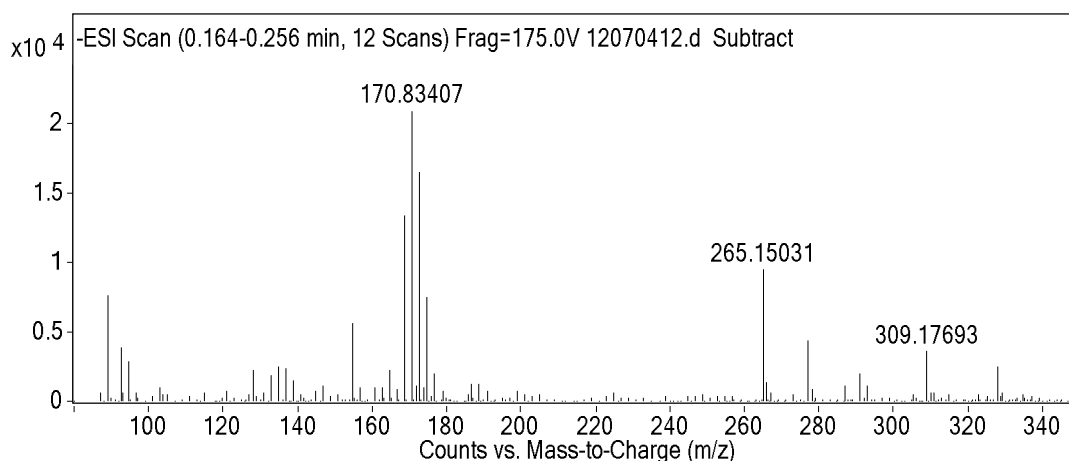
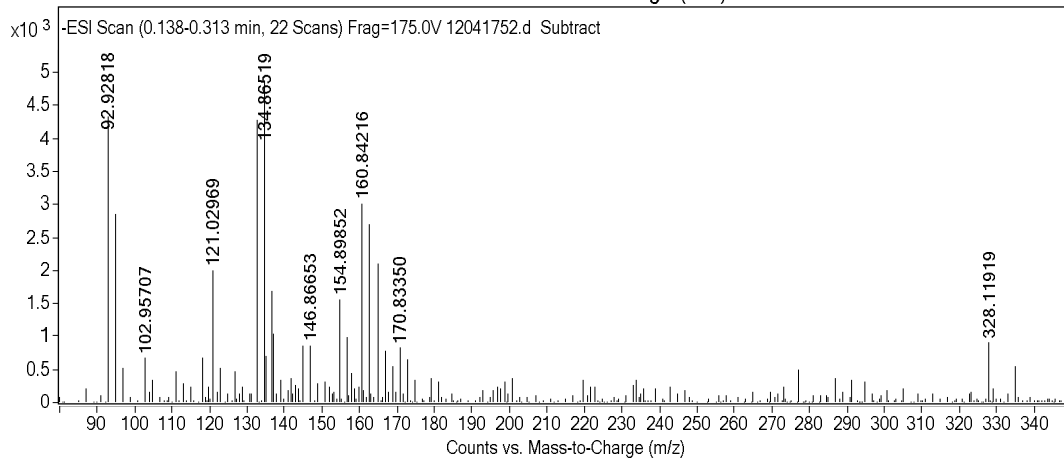
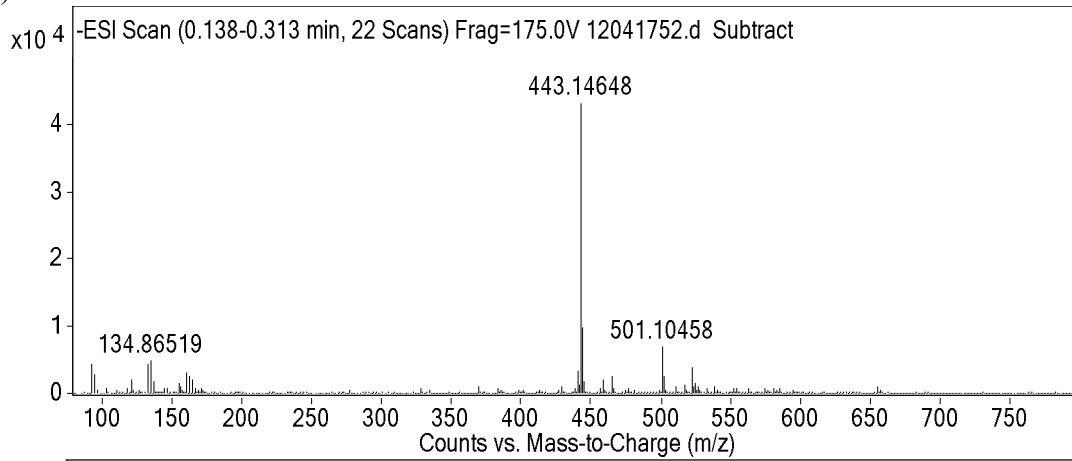


Figure 34. Negative ESI-TOF-MS spectrum of the aqueous tetracycline solution after a) 30 min and b) 240 min of photocatalytic treatment over Zr-TiO₂ photocatalyst under UV-VIS irradiation, including higher magnifications (given below); TC conc.: 20 ppm, cat conc.: 20 mg/L.

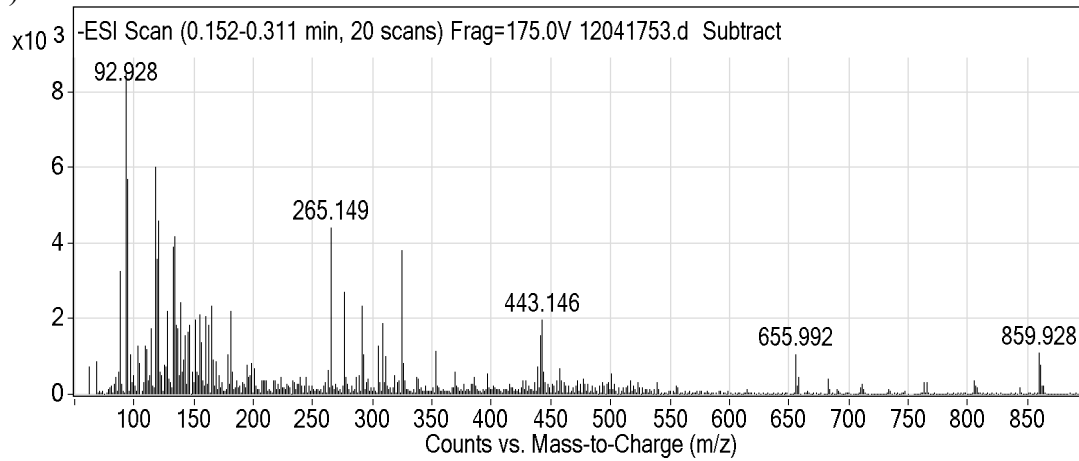
ESI-TOF-MS data reveal incomplete abatement of TC over Zr-doped titania and formation of minor amounts of reaction intermediates, which are not decomposed even after 240 min of photocatalytic treatment. The findings are confirmed by the results of the photocatalytic abatement studies under similar conditions (Fig. 25). They degradation curve shows that only *ca.* 53 % of tetracycline is abated over Zr-doped titania after 240 min of treatment.

For comparison, ESI-TOF-MS measurements have been performed for the photocatalytic decomposition of tetracycline over titania P25 (Fig. 35). After 30 min, distinctly more tetracycline is converted compared to the Zr-doped titania photocatalyst. The intensity (counts) of the TC related peak at m/z 443 is decreased. Additionally, a couple of by - products with $m/z < 170$ are formed. However, the peak intensities are low. After 240 min of treatment, the TC is markedly diminished showing as indicated by the low intensity of the corresponding m/z peak, which is in the same order of magnitude as the intermediates. Indeed, the photocatalytic testing shows *ca.* 95 % of degradation of TC after four hours of treatment. A broad distribution of low concentrated different reaction intermediates given rise to signals in the m/z range between 200 and 50 are present in the solution, indicating deeper oxidation of TC over titania. Additionally, m/z peaks at 265, 277, 291, 309 and 325 are observed, which might be related to substituted anthraquinones and hydroquinones^[195] (structures containing three six - membered rings).

a)



b)



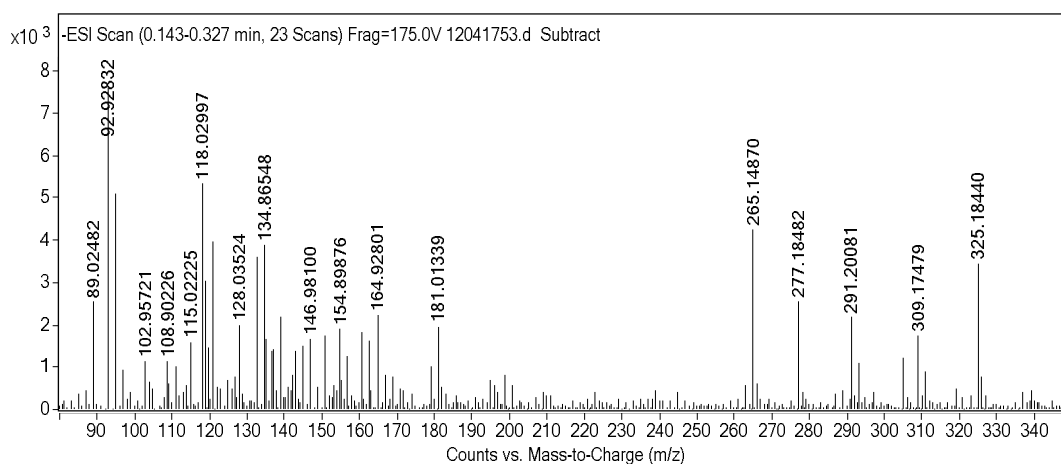


Figure 35. Negative ESI-TOF-MS spectrum of the aqueous tetracycline solution after a) 30 min and b) 240 min of photocatalytic treatment over titania P25 photocatalyst under UV-VIS irradiation, including higher magnifications (given below); TC conc.: 20 ppm, cat conc.: 20 mg/L.

The ESI-TOF-MS measurement shows that the spectrum of formed intermediates over Zr-doped and non-doped titania are different compared to the data given in the literature.^[177,193] Fewer types of intermediates are formed with Zr-doped titania. This might be due to its lower photocatalytic activity (Fig. 34 b and 35 b). In contrast to ibuprofen, the photocatalytic degradation of the large polyketide tetracycline results in the formation of a couple of aromatic intermediates.

Re-use experiments

The photocatalytic activity of Zr-TiO₂ has been checked in re-use experiments during abatement of **ibuprofen** (10 mg/L of photocatalyst per 10 ppm of IBP) under neutral reaction conditions using cycling experiments. Decomposed IBP was replaced by fresh IBP portion.

The achieved abatement of ibuprofen decreased from *ca.* 55 % in the first run to 21 % and 19 % in the second and third run, respectively (Fig. 36). The photocatalyst deactivation is highest after the first run indicating the blocking of most active sites.

Indeed, formation of reaction intermediates is found after the first run (Fig. 37) and increases with the cycling experiments. This indicates incomplete decomposition of the IBP followed by cycling experiments.

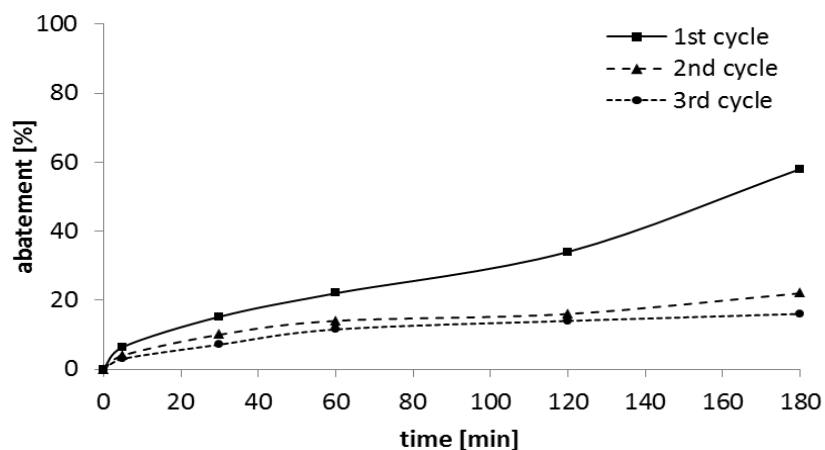


Figure 36. Photocatalytic abatement of ibuprofen in aqueous solution over Zr-TiO₂ photocatalyst under UV-Vis irradiation after 3 runs of treatment; IBP conc.: 10 ppm, cat conc.: 10 mg/L.

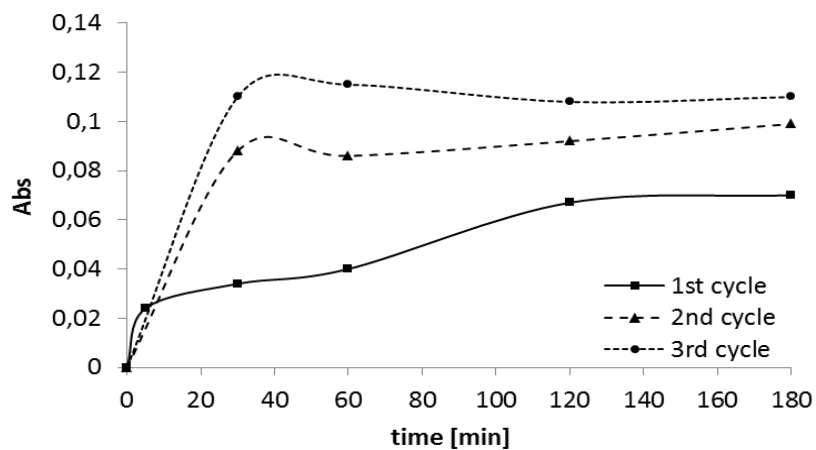


Figure 37. Formation of the temporary intermediates of ibuprofen in aqueous solution during photocatalytic treatment over Zr-TiO₂ photocatalyst based on UV-Vis absorbance at λ_{\max} 262 nm after 3 runs of treatment; IBP conc.: 10 ppm, cat conc.: 10mg/L.

The photocatalytic abatements of **tetracycline** over Zr-TiO₂ was investigated in 3 runs of photocatalytic treatment (Fig. 38). The cycling experiment shows that the photocatalyst can be re-used also in the case of tetracycline. However, as is generally observed, the abatement decreases with the cycling.

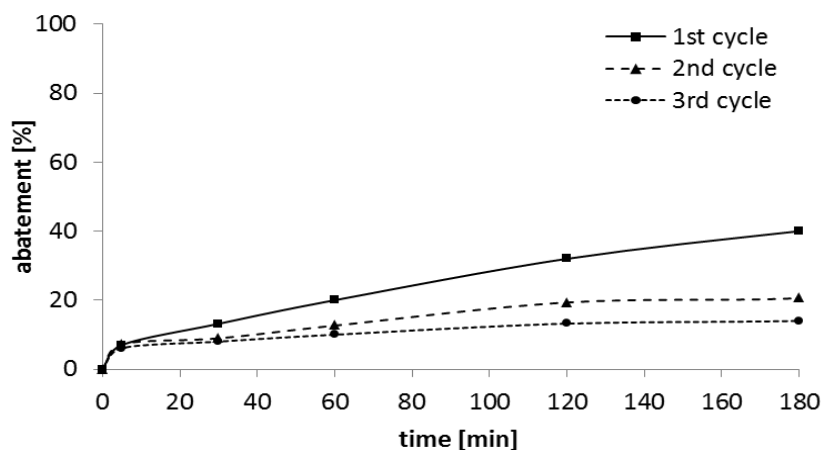


Figure 38. Photocatalytic abatement of tetracycline in aqueous solution over Zr-TiO₂ photocatalyst under UV-Vis irradiation after 3 runs of treatment; TC conc.: 10 ppm, cat conc.: 10 mg/L.

The final comparison of the re-use experiments with ibuprofen and tetracycline over non-doped and Zr-doped titania is shown in Figure 39. Both materials are subject of the photocatalyst deactivation during cycling (re-use) experiments. The deactivation is more pronounced with Zr-doped titania. The decomposition of formed reaction intermediates is more efficient over titania, probably by the reducing of photocatalyst poisoning.

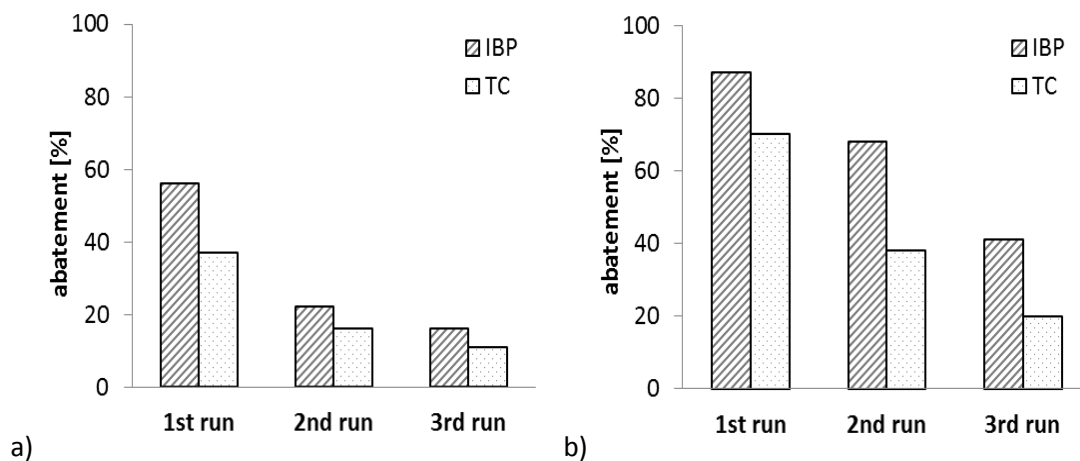


Figure 39. Representative graphs of the photocatalytic abatements of ibuprofen and tetracycline over a) Zr-TiO₂ and b) titania after 180 min of treatment in 3 runs under UV-Vis irradiation; TC and IBP conc.: 10 ppm, cat conc.: 10 mg/L.

Summary

- The impact of the titania doping with zirconium on the photocatalytic activity has been checked during the course of ibuprofen and tetracycline abatement and compared with commercial titania P25.
- The doped material showed lower onset activity compared to titania P25.
- The lower onset activity is followed by faster composition, due to higher adsorption. The contribution of adsorption significantly increases what is attributed to higher specific surface area ($100 \text{ m}^2/\text{g}$) and the presence of mesoporosity.
- The deactivation in the second stage of reaction (between 30 and 180 min) is lower compare to titania. The reaction rates of Zr-TiO₂ amount *ca.* 0.0036 and 0.0022 for the IBP and TC abatements, respectively.
- The change pH value of solution influences the ibuprofen degradation. The best photocatalytic abatement of IBP over Zr-TiO₂ is observed at acidic conditions. This finding is explained by more hydrophobic character of Zr-doped titania and therefore increased affinity toward non-polar IBP molecule. In contrast, the variation of pH value of TC solution does not change the ambivalent character of TC molecule.
- Zr-doped titania forms more IBP intermediates. Especially, after 240 min of treatment a couple of oligomeric species are observed in the solution (intermediates with lower masses). In contrast, the degradation of IBP over titania proceeds faster and more effective (the spectrum seems to be more clean). The ESI-TOF-MS spectra of TC show incomplete decomposition. A lot of minor TC intermediates are formed. After 240 min of treatment, these by-products are still present. A couple of different TC intermediates of medium masses are related to anthraquinone derivates.

3.3. Photocatalytic abatement of low concentrated (ppb-low ppm) tetracycline over novel titania based photocatalysts

Novel titania (Ti) - based photocatalysts as doped titania, titania nanotubes (TNs), metal-organic framework based photocatalysts namely Ti/MIL-101 composites and MIL-125 have been investigated in the photocatalytic degradation of very low concentrated (0.1 or 0.5 ppm) antibiotic tetracycline from aqueous solution. The aim was to test whether improved adsorption properties of these porous materials and enhanced use of visible light, in the case of doped titania and the Ti/MIL-101 composite, will facilitate the photocatalytic degradation.

Photocatalytic abatement of tetracycline over titania and titania doped materials (Zr-TiO₂, Fe-TiO₂ and N-TiO₂)

Photocatalytic testing of titania doped materials (Zr-TiO₂, Fe-TiO₂ and N-TiO₂) was checked during decomposition of tetracycline in very low concentration (500 ppb). The course of photocatalytic abatements shows the contribution of power of the UV-Vis solarium lamp, with part of solar (visible) range, on the decomposition of tetracycline in low concentrated solution.

Figure 40 shows the course of photocatalytic abatement of tetracycline over commercial titania photocatalyst. It has to be noticed that this experiment has been performed at very low catalyst concentration (2 mg/L) and low cat-to-sub ratio of 4. As is observed, with higher concentrated solution (compare Chapter 3.1), rapid degradation occurs at the onset of reaction (initial 1st stage), followed by continuous but slowly abatement between 10 and 60 min. *Ca.* 70 and 90 % of abatement of tetracycline has been achieved after 10 and 60 min, respectively.

At low pollutants concentration of 500 ppb increase of electric power has no impact on the photocatalytic abatement. Obviously, low pollutants concentration requires only weak radiation power, which allows for application of sunlight. Also blank irradiation tests in the absence of the photocatalyst were carried out in order to check a possible contribution of photolysis. The TC concentration was diminished by only 10 % after 3 hours of irradiation.

Additionally, adsorption experiments were carried out with photocatalysts in the dark. Figure 41 shows the photocatalytic treatment of tetracycline over titania photocatalyst and the corresponding adsorption. Clearly, adsorption contributes significantly to the abatement at low pollutant concentration. Especially, at the onset of reaction the adsorption is high on the titania photocatalyst (ca. 30 %), which is different from the behaviour at high ppm pollutant concentration.

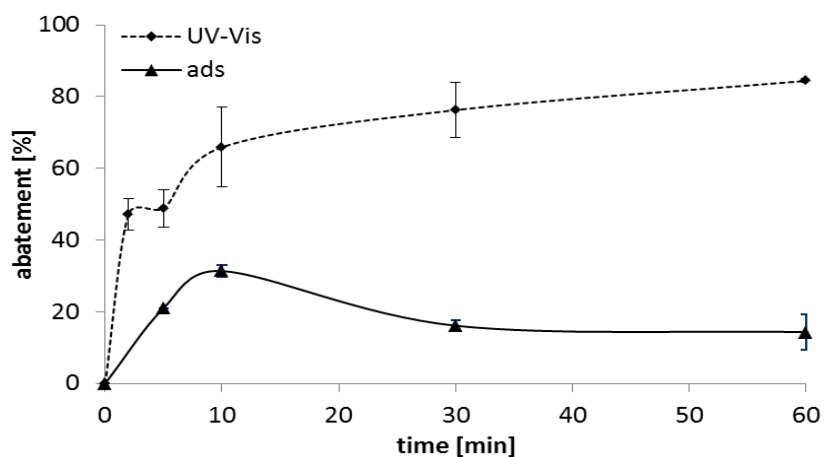


Figure 41. Adsorption and photocatalytic abatement of tetracycline in aqueous solution over titania P25 photocatalyst; TC conc.: 500 ppb, cat. conc.: 2 mg/L, cat-to-sub ratio of 4.

The influence of the dopant of titania e.g. with zirconium (Zr-TiO₂), iron (Fe-TiO₂) and the nitrogen (N-TiO₂) has been tested on the photocatalytic abatement of tetracycline. The courses of photocatalytic abatement of TC at low concentration and corresponding adsorption curves are shown in Figures 42-44.

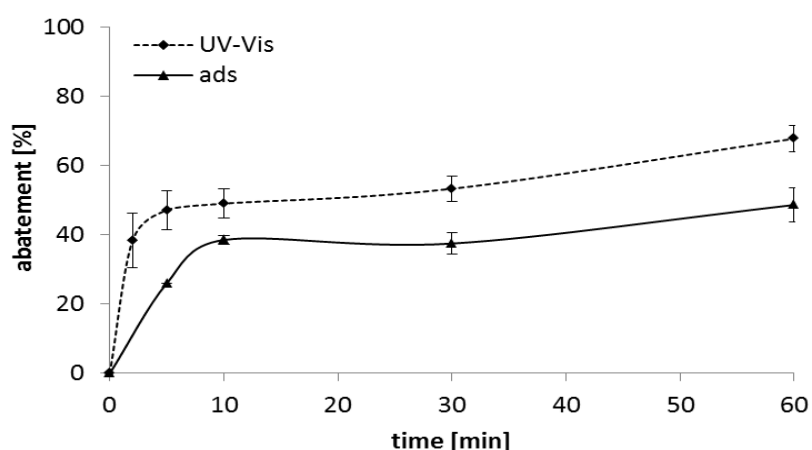


Figure 42. Adsorption and photocatalytic abatement of tetracycline in aqueous solution over Zr-TiO₂ photocatalyst; TC conc.: 500 ppb, cat. conc.: 2 mg/L, cat-to-sub ratio of 4.

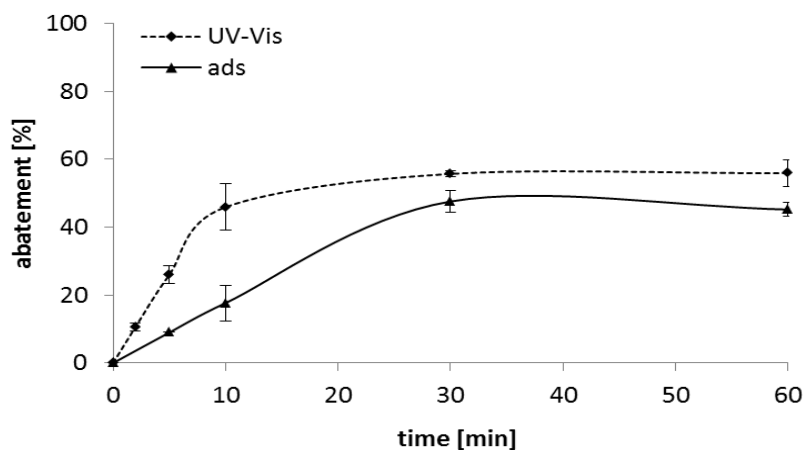


Figure 43. Adsorption and photocatalytic abatement of tetracycline in aqueous solution over Fe-TiO₂ photocatalyst; TC conc.: 500 ppb, cat. conc.: 2 mg/L, cat-to-sub ratio of 4.

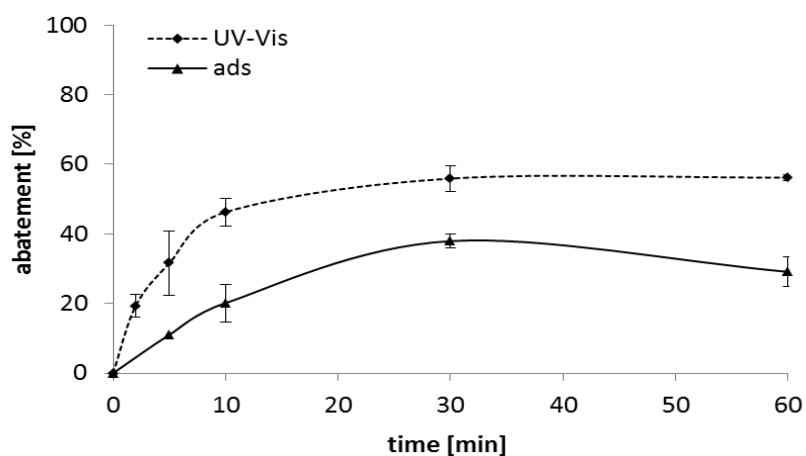


Figure 44. Adsorption and photocatalytic abatement of tetracycline in aqueous solution over N-TiO₂ photocatalyst; TC conc.: 500 ppb, cat. conc.: 2 mg/L, cat-to-sub ratio of 4.

In the initial stage of treatment, after 10 min, *ca.* 50 % of abatement is achieved with all the doped titania photocatalysts. Further prolongation of the treatment time enhances the abatement over Zr-doped TiO₂ and very slightly in the case of Fe-TiO₂ and N-TiO₂ (Fig. 43 and 44). In all cases, adsorption contributes significant to the abatement (*ca.* 30-40 %), The high contribution of adsorption found with doped materials is due to the improved mesoporosity and enhanced surface area of *ca.* 100-180 m²/g compared to *ca.* 55 m²/g of the non-doped titania. Zr-TiO₂ exhibits a distinctly higher onset activity and adsorption.

The contribution of adsorption of low concentrated TC solution has been summarized in Table 8. The observed tetracycline up-takes of up to 90 µg per mg of photocatalyst

exceed the estimated monolayer coverage of TC on titania of *ca.* 15 $\mu\text{g}_{\text{TC}}/\text{mg}_{\text{cat}}$. These high up-takes can be achieved by multilayer adsorption or in the confined space of the mesopores. It has to be noticed that the adsorption is much lower at higher concentration (ppm range) even at similar reaction conditions and cat-to-sub ratio. Obviously, at very low concentration (ppb range) the adsorption of TC on the photocatalyst surface by vertical alignment is preferred, compared to molecular solution in the water. This might be due to the hydrophobic part of the flat TC molecule limiting hydration.

At higher concentration, beyond the critical micelle formation concentration (CMC) or aggregate formation concentration (aggregation concentration, *ca.* 44 ppm range), formation of aggregates^[196] may facilitate solution competing with decreased adsorption of TC at the photocatalyst surface.

Table 8. Data of the adsorption of low concentrated tetracycline solution (0.5 ppm) over titania and titania doped photocatalysts (cat conc.: 2 mg/L). Relative and absolute adsorption data (A) and corresponding photocatalyst loading calculated after 5, 30 and 60 min of treatment; cat-to-sub ratio of 4:1.

Adsorption of low TC concentration (0.5 ppm)						
adsorption time of TC [min]	rel. A [%]	abs. A [mg/L]	loading [mg/mg]	rel. A [%]	abs. A [mg/L]	loading [mg/mg]
	titania			Zr-TiO ₂		
5	21	0.1050	0.0525	26	0.1300	0.0650
30	16.1	0.0805	0.0403	37.5	0.1865	0.0938
60	14.3	0.0715	0.0357	48.6	0.243	0.1251
adsorption time of TC [min]	rel. A [%]	abs. A [mg/L]	loading [mg/mg]	rel. A [%]	abs. A [mg/L]	loading [mg/mg]
	Fe-TiO ₂			N-TiO ₂		
5	9	0.045	0.0225	11	0.0550	0.0275
30	47.6	0.238	0.1190	38	0.1900	0.0950
60	45.2	0.226	0.1130	29	0.1450	0.0725

The relative and absolute photocatalytic abatements of tetracycline in the ppb concentration range over titania, Zr-TiO₂, Fe-TiO₂ and N-TiO₂ photocatalysts and corresponding experimental effective mean first order reaction rates (r) calculated after 5, 30 and 60 min of treatment are summarized in Table 9.

Table 9. Data of the abatement of low concentrated tetracycline solution (500 ppb) during photocatalytic treatment over titania and titania doped photocatalysts (cat conc.: 2 mg/L). Relative and absolute abatements (A) and corresponding experimental effective mean first order reaction rates (r) calculated after 5, 30 and 60 min of treatment; cat-to-sub ratio of 4:1.

Low concentration of TC (500 ppb)						
irradiation time of TC [min]	rel. A [%]	abs. A [mg/L]	r [min ⁻¹]	rel. A [%]	abs. A [mg/L]	r [min ⁻¹]
	titania			Zr-TiO₂		
5	48.8	0.244	0.0244	47	0.235	0.0235
30	76.2	0.381	0.0063	53.2	0.266	0.0044
60	84.4	0.422	0.0035	67.8	0.339	0.0028
irradiation time of TC [min]	rel. A [%]	abs. A [mg/L]	r [min ⁻¹]	rel. A [%]	abs. A [mg/L]	r [min ⁻¹]
	Fe-TiO₂			N-TiO₂		
5	26	0.13	0.013	31.6	0.158	0.0158
30	55.8	0.279	0.0047	56	0.28	0.0047
60	55.8	0.279	0.0023	60	0.3	0.0025
High concentration of TC (10 ppm)						
irradiation time of TC [min]	rel. A [%]	abs. A [mg/L]	r [min ⁻¹]	rel. A [%]	abs. A [mg/L]	r [min ⁻¹]
	titania			Zr-TiO₂		
5	34.5	3.45	0.0173	10.9	1.09	0.0055
30	68.4	6.84	0.0057	36.8	3.68	0.003
60	86.8	8.68	0.0036	59.8	5.98	0.0025

The initial photocatalytic abatement rates are higher for titania and distinctly lower for the doped titania photocatalysts. They decrease with reaction time due to the deactivation of the photocatalysts in the TiO₂, Zr-TiO₂, Fe-TiO₂ and N-TiO₂. The photocatalytic abatement rates of the initial stage (5 min) over titania and Zr-TiO₂ obtained with low tetracycline concentration (0.5 ppm) have been compared with that of high TC concentration (10 ppm), but at the same cat-to-sub ratio of 4:1 (Tab. 9). The abatement rates achieved at low concentration are markedly higher than those found at high concentration (10 ppm), even the cat-to-sub ratio is equal (Fig. 45). This finding is in line with the adsorption data, which showed enhanced specific adsorption at low concentration (ppb range).

It is concluded that the increased adsorption and therefore, enrichment of the substrate at photocatalyst surface, facilitates the photocatalytic degradation.

On the catalyst surface the reactive oxidative species e.g. hydroxyl radicals ([•]OH) and superoxide radicals (O₂^{•-}) as well as electron holes (h⁺) are formed.

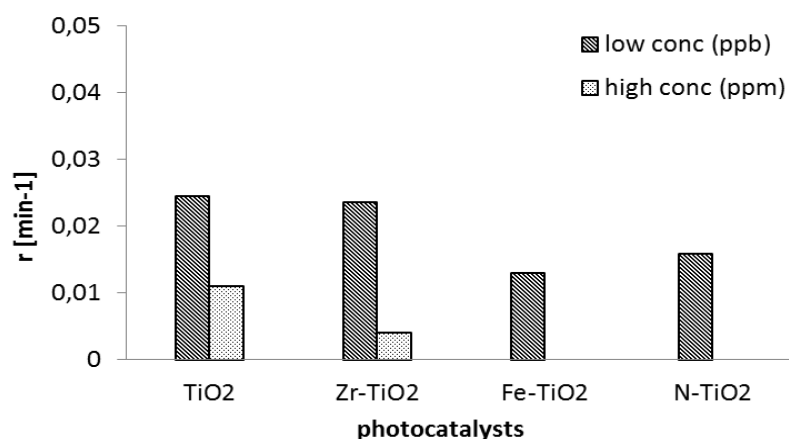


Figure 45. Comparison of the mean experimental first order reaction rates of tetracycline abated at low (ppb) and high (ppm) concentrated solutions over titania, Zr-TiO₂, Fe-TiO₂ and N-TiO₂ photocatalysts, estimated after 5 min of treatment, cat-to-sub ratio of 4:1.

Photocatalytic abatement of tetracycline over new porous titania-based photocatalysts

Beside titania and doped titania photocatalysts, the photocatalytic abatement of low concentrated tetracycline solution (100 ppb) has been tested also over new ordered porous titania based materials as titania nanotubes, titania/MOF MIL-101 composite as well as a the titanium containing porous metal - organic framework MIL-125. The photocatalytic tests were carried out with 100 ppb TC solution and 0.2 mg of photocatalyst. In order to differentiate between adsorption and photocatalytic degradation in one experiment, the reaction solution containing the TC and the photocatalysts were stirred in the dark (adsorption part) and then irradiated with the UV-Vis light (photocatalytic part).

The photocatalytic abatement of tetracycline over titania and titania nanotubes from a 100 ppb aqueous solution is shown in Figure 46. After 30 min of adsorption *ca.* 40 % of TC are adsorbed over as-synthesised TNs, and then the photocatalytic treatment was started (switching on the UV-Vis solarium lamps).

The abatement is increased up to *ca.* 60 % after 60 min of irradiation and slightly increases to *ca.* 66 % after 180 min.

The calcination of nanotubes at 700°C improves the adsorption as well as the photocatalytic activity (Fig. 46). The adsorption is increased to *ca.* 60 % compared to the as-synthesized TN sample. After 60 min of irradiation the abatement increases to *ca.* 74 % and reaches 90 % after 180 min. Although the specific surface area is

decreased after calcination from *ca.* 220 to 100 m²/g,, the adsorption is enhanced by *ca.* 50 % compared to the as-synthesized ones.

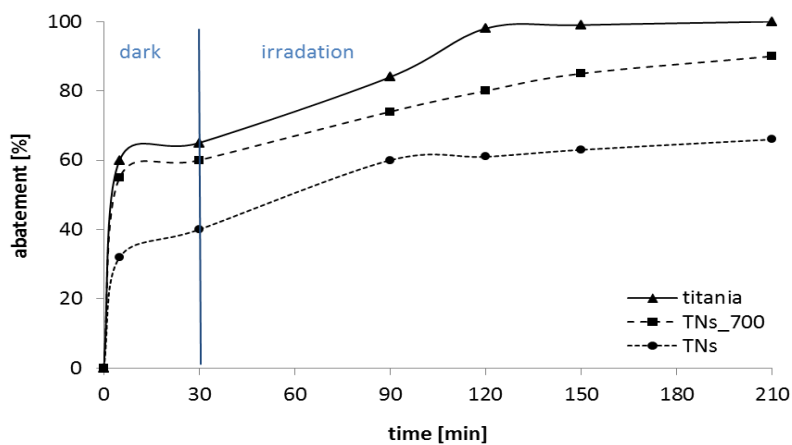


Figure 46. Adsorption (in the dark) and photocatalytic abatement of tetracycline in aqueous solution over as-synthesized titania nanotubes (TNs), calcined nanotubes (TN_700) and titania; TC conc.: 100 ppb, cat. conc.: 0.2 mg/L, cat-to-sub ratio of 2.

The specific loading per area is increased by a factor of four. TEM images show that titania needles are changed to more compact, different shaped nanoparticles resulting in the decrease of the specific surface area (compare A 1.1, Fig. 22 and 23).

The markedly enhanced specific loading (adsorption of TC) points to a change in the nature of the surface. The inspection of samples by XPS showed that the un-calcined TNs contain much more Ti-OH groups than the calcined ones. The latter is in part converted to anatase, rutile and unidentified phases (compare A 1.1, Fig. 21).

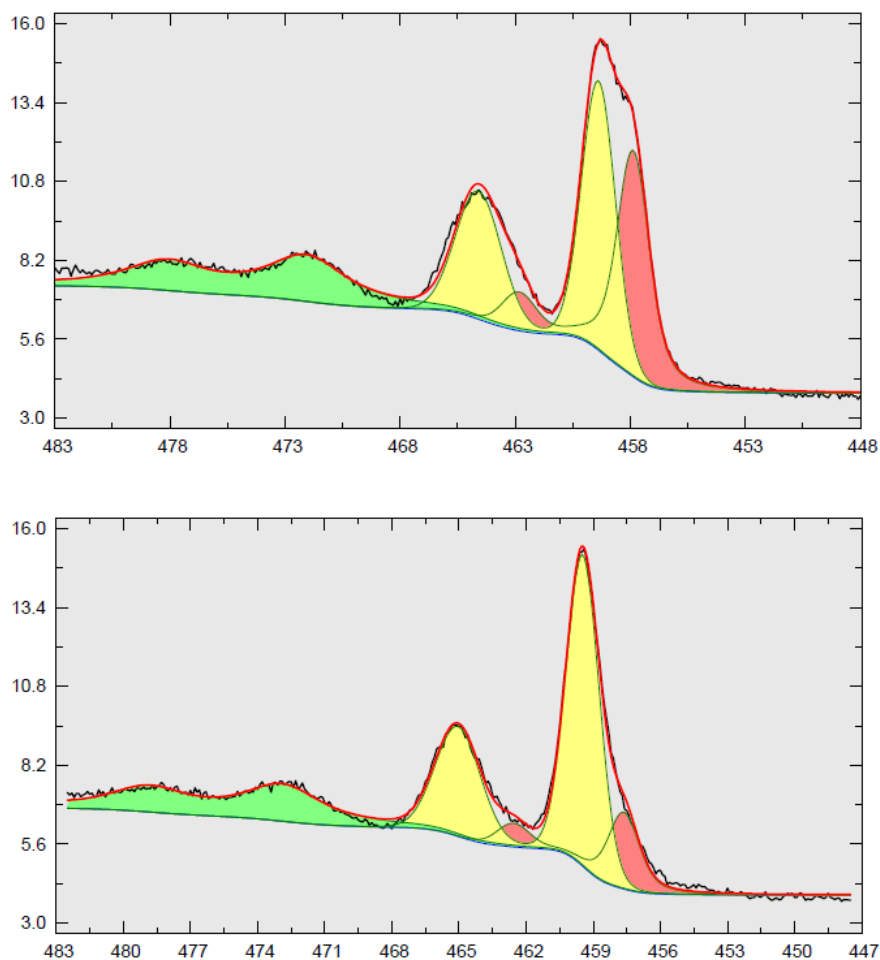


Figure 47. XPS of Ti_{2p} states of titania nanotubes: (top) as-synthesized and (bottom) calcined.

The intensity of the Ti_{2p} doublet signal at 462.82 eV related to Ti of TiO_6 octahedra is increased on the expense of the signal at 464.57 eV, assigned to titania connected with OH groups (Fig. 47). At the same the O_{1s} signal of TiO_6 octahedra at 530.95 eV is increases and the corresponding -OH group signal at 533.96 eV is substantially decreased (Fig. 48). Calcination results in condensation of the titania network, leading to a markedly decrease of the hydrophilic nature of the catalyst, resulting in a decreased affinity to water and improved adsorption of TC.

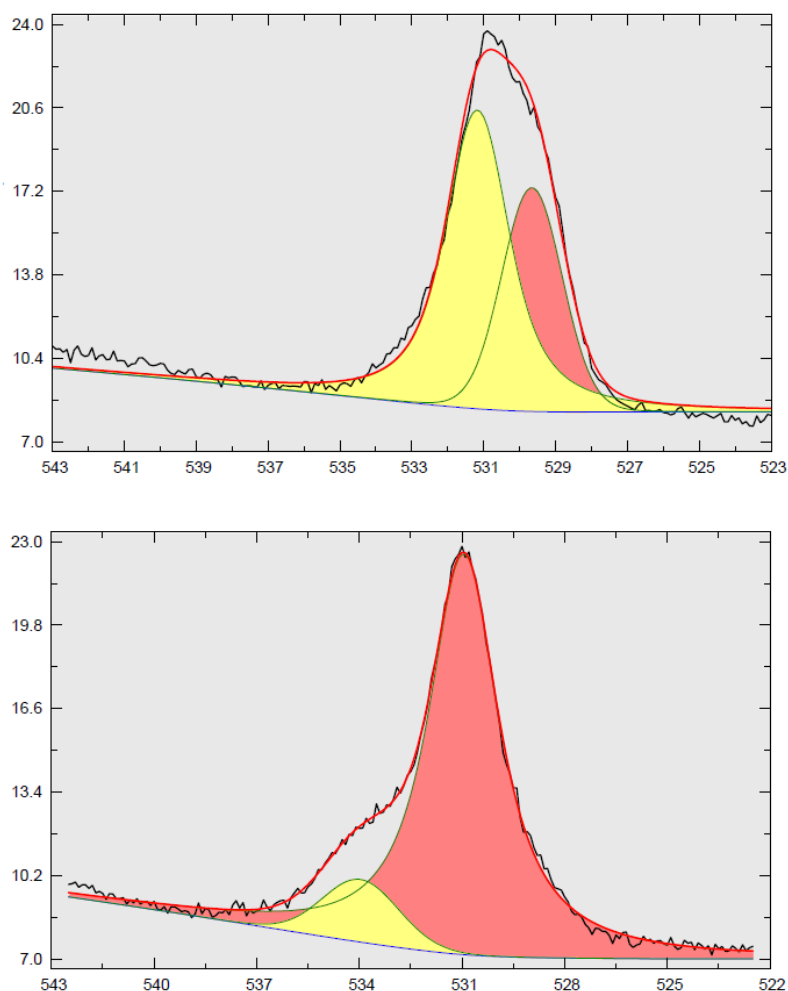


Figure 48. XPS of O_{1s} states of titania nanotubes: (top) as-synthesized and (bottom) calcined.

The increase in the photocatalytic activity is due to the formation of anatase, which is known to be a photocatalytic active titania phase.

For the comparison, titania P25 photocatalyst has been included. After 30 min of reaction, *ca.* 65 % of TC is adsorbed. Titania nanoparticles are very effective in the photocatalytic abatement of TC (Fig. 46). They show nearly 100 % of abatement of TC from low concentrated solution after 90 min of treatment. These findings confirm the importance of the formation of anatase for photocatalytic properties of the calcined TNs. Therefore, the construction of titania nanotubes consisting of anatase is a challenge.

The photocatalytic abatement of tetracycline over titania/MIL-101 composites and MIL-125 is shown in Figure 49. Adsorption of tetracycline over titania/MIL-101 composite reached *ca.* 40 % and increase with adsorption time and the increased titania content. Irradiation enhances the abatement of TC by photocatalytic degradation. *Ca.* 40 % of abatement is achieved after 60 min and increases to *ca.* 65 and 80 % after 6 hours of treatment for the 6.6 and 10.94 wt.% of Ti containing samples, respectively (Fig. 49). The photocatalytic activity is lower than that of the titania nanotubes. However, it should be taken into account that the active titania content is much lower and is not compensated by a contribution of the MOF chromium.

The MIL-125 photocatalyst shows a similar behaviour, but the adsorption is somewhat higher (*ca.* 50 %) due to the high porosity of this porous metal-organic framework material. The TC abatement reached *ca.* 60 % by photocatalytic treatment of 60 min and increased slightly to *ca.* 80 % after 360 min (Fig. 49). The results confirm that titania MOFs are promising new porous materials for photocatalytic applications.

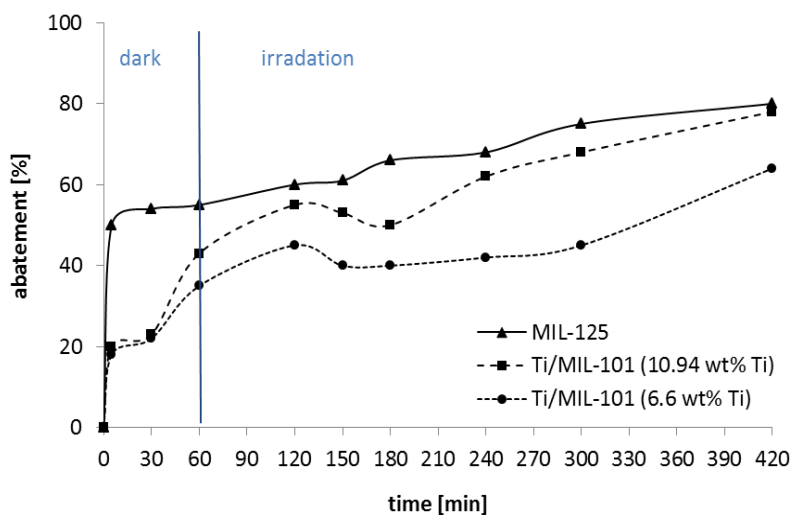


Figure 49. Adsorption and photocatalytic abatement of tetracycline in aqueous solution over MIL-125 and Ti/MIL-101 photocatalysts; TC conc.: 100 ppb, cat. conc.: 0.2 mg/L, cat-to-sub ratio of 2; Ti percent weight (wt. %) of 6.6 and 10.94.

Summary

- New titania based photocatalytic materials (titania doped, titania nanotubes and titania/MOF composites) with improved texture and porosity have been tested in the degradation of low concentrated tetracycline solution.
- All doped titania photocatalysts show high initial photocatalytic abatement of tetracycline at low concentration (500 ppb) of *ca.* 55 % after 10 min of reaction.
- Abatement of TC over titania at low ppb range at the same cat-to-sub ratio proceeds faster compared to high concentration range (ppm). *Ca.* 65 % and 35 % is removed from solution in ppb and ppm range, respectively. The improved adsorption at low concentration is due to formation of TC micelles (beyond CMC, below 44 ppm), which is preferred to TC self-aggregation in solution. This close contact of TC micelles facilitates the high adsorption.
- The adsorption might be also explained by improved texture, porosity (mesoporosity) and higher specific surface area of titania/MOF and nanotubes (*ca.* 100-180 m²/g compared to 55 m²/g for titania).
- The texture of titania nanotubes after calcinations was changed. Resulted increase in the photocatalytic activity of TNs is due to the formation of anatase phase at 700°C. This confirms the importance of the anatase presence for the photocatalytic activity.
- Porous titania containing MOFs are also promising photocatalytic materials, due to high adsorption and stable increase in the abatement with treatment time.

3.4. Photocatalytic abatement of ibuprofen and tetracycline over two types of nanosized ZnO photocatalysts

The photocatalytic performance of ZnO nanoparticles of different sizes in the abatement of tetracycline and ibuprofen from water have been investigated in detail. The influence of different reaction factors like: different substrate concentrations and corresponding cat-to-sub ratios, pH values and formation of TC and IBP by-products during the course of treatment have been investigated. The possibility of the re-use of the photocatalyst (re-use experiments) has been checked. The contributions of adsorption over ZnO nanoparticles (in the dark) have been also checked in case of low concentrated (ppb range) and at high concentrated (ppm scale) TC and IBP solutions. The smaller, *ca.* 15-30 nm, sized ZnO_e particles were prepared from ethanolic solution. The larger, *ca.* 100 nm, sized ZnO_w particles were obtained from aqueous solution.

Photocatalytic activity

Photocatalytic abatement of **ibuprofen** was carried out over two types ZnO nanoparticles (Fig. 50 and 51). As is observed in Figure 50, the better abatement data are obtained in case of smaller (*ca.* 15-30 nm) ZnO_e nanoparticles. With increasing the cat-to-sub ratios from 1 to 4, the photocatalytic abatement of ibuprofen proceeds faster and more effective and reaches (after 180 min of reaction) *ca.* 72, 51 and 31 %, at 10, 20 and 40 mg/L of photocatalysts, respectively.

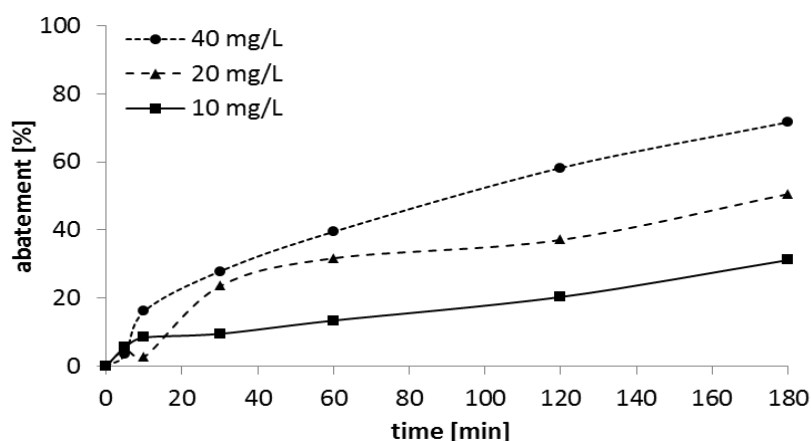


Figure 50. Photocatalytic abatement of ibuprofen in aqueous solution over ZnO_e photocatalyst under UV-Vis irradiation; IBP conc.: 10 ppm, cat conc.: 10, 20 and 40 mg/L.

In case of larger crystals ZnO_w the abatement is lower (Fig. 51) with *ca.* 19 % at a cat-to-sub ratio of 1:1 compared to ZnO_e . The ZnO_w shows a lower onset activity in the abatement. The abatement increases significantly to finally *ca.* 68 % with the increased photocatalyst amount (cat-to-sub ratio of 1 to 4). Even the specific surface area of ZnO_w is *ca.* 5 times lower than that of ZnO_e , the observed abatements are only somewhat lower.

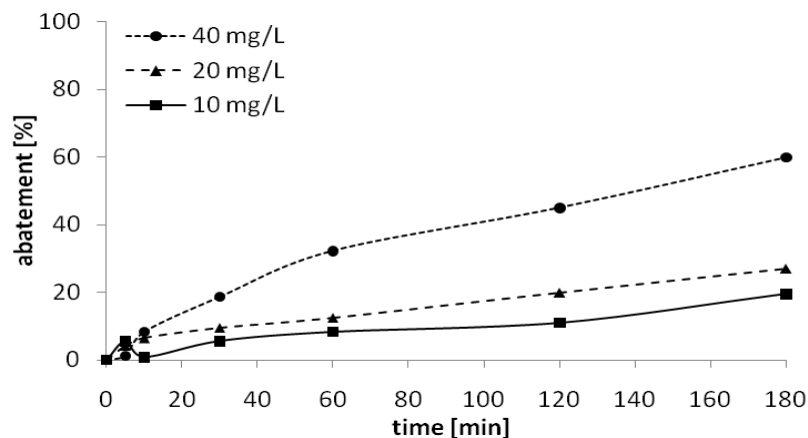


Figure 51. Photocatalytic abatement of ibuprofen in aqueous solution over ZnO_w photocatalyst under UV-Vis irradiation; IBP conc.: 10 ppm, cat conc.: 10, 20 and 40 mg/L.

Additionally, the contribution of the adsorption of ibuprofen over ZnO nanoparticles has been checked in detail (Fig. 52). This experiment strongly confirms high contribution of adsorption to the abatement. *Ca.* 15 and 11% of IBP are adsorbed after 60 min of contact time.

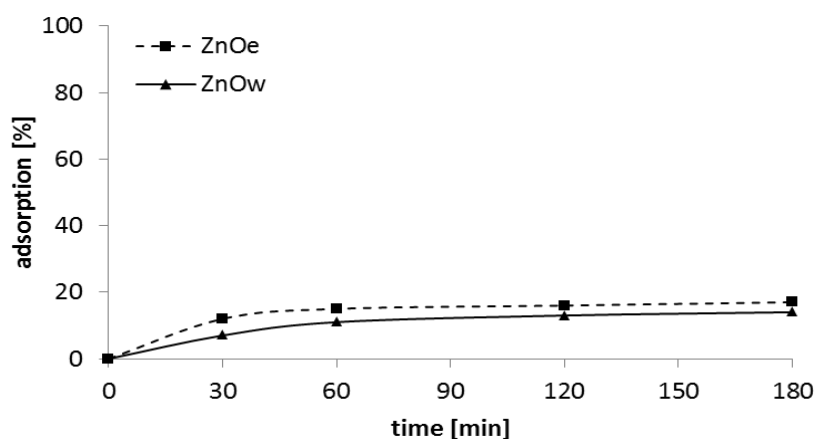


Figure 52. Adsorption of ibuprofen in aqueous solution over ZnO_e and ZnO_w photocatalysts in the dark; IBP conc.: 10 ppm, cat conc.: 40 mg/L.

Again, adsorption is high for both photocatalysts. It is very likely that the higher onset activity of ZnO_e is related to the higher adsorption of IBP compared to ZnO_w. Finally, the observed abatements and the effective mean first reaction rates (Tab. 10) are slightly lower with the larger ZnO_w nanoparticles compared to the smaller sized ZnO_e.

Table 10. Data of the abatement of ibuprofen (10 ppm) in aqueous solution during photocatalytic treatment over ZnO_e (top) and ZnO_w (bottom) at cat conc.: 10, 20 and 40 mg/L. Relative and absolute abatements (A) and corresponding experimental effective mean first order reaction rates (r) calculated after 30, 120 and 180 min of treatment.

ZnO _e									
irradiation time of IBP [min]	rel. A [%]	abs. A [mg/L]	r [min ⁻¹]	rel. A [%]	abs. A [mg/L]	r [min ⁻¹]	rel. A [%]	abs. A [mg/L]	r [min ⁻¹]
	10 mg/L			20 mg/L			40 mg/L		
5	3.3	0.33	0.0066	4.9	0.49	0.0049	5.5	0.55	0.0028
30	10.9	1.09	0.0036	23.4	2.34	0.0039	27.7	2.77	0.0023
120	20	2	0.0017	37	3.7	0.0015	58	5.8	0.0012
180	31.1	3.11	0.0017	50.5	5.05	0.0014	71.6	7.16	0.0010
ZnO _w									
irradiation time of IBP [min]	rel. A [%]	abs. A [mg/L]	r [min ⁻¹]	rel. A [%]	abs. A [mg/L]	r [min ⁻¹]	rel. A [%]	abs. A [mg/L]	r [min ⁻¹]
	10 mg/L			20 mg/L			40 mg/L		
5	5.5	0.55	0.0110	4.2	0.42	0.0042	6.3	0.63	0.0032
30	5.5	0.55	0.0018	9.4	0.94	0.0016	18.7	1.87	0.0016
120	11.1	1.11	0.0009	20	2	0.0008	45	4.5	0.0009
180	19.4	1.94	0.0011	27	2.7	0.0007	60	6	0.0008

Additionally, the photocatalytic abatement of **tetracycline** over the ZnO photocatalysts has been studied using different amounts of the ZnO nanoparticles (10, 20 and 40 mg/L) at a constant TC concentration of 10 ppm (Fig. 53).

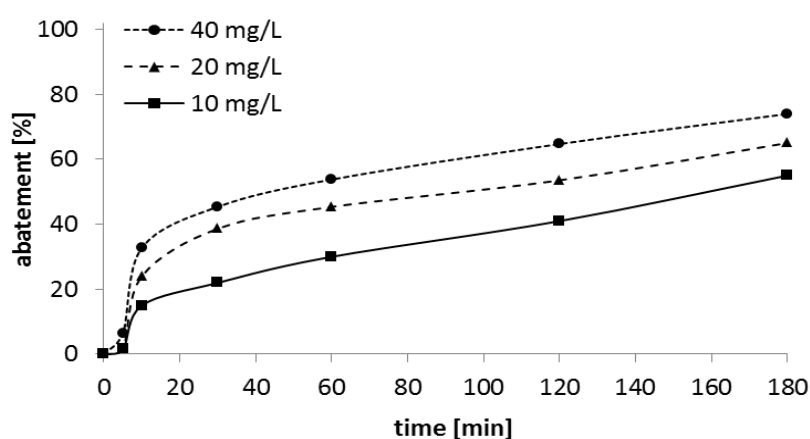


Figure 53. Photocatalytic abatement of tetracycline in aqueous solution over ZnO_e photocatalyst under UV-Vis irradiation; TC conc.: 10 ppm, cat conc.: 10, 20 and 40 mg/L.

The photocatalytic behaviour of the TC abatement is similar to that of IBP. *Ca.* 74 and 55 % of TC has been removed from solution after 180 min using 40 and 10 mg/L of photocatalyst, respectively (Tab. 11).

Table 11. Data of the abatement of tetracycline (10 ppm) in aqueous solution during photocatalytic treatment over ZnO_e (top) and ZnO_w (bottom) at cat conc.: 10, 20 and 40 mg/L. Absolute abatement (A) and corresponding experimental effective mean first order reaction rates (r) calculated after 30, 120 and 180 min of treatment.

ZnO _e									
irradiation time of TC [min]	rel. A [%]	abs. A [mg/L]	r [min ⁻¹]	rel. A [%]	abs. A [mg/L]	r [min ⁻¹]	rel. A [%]	abs. A [mg/L]	r [min ⁻¹]
	10 mg/L			20 mg/L			40 mg/L		
5	1.6	0.16	0.0032	1.6	0.16	0.0016	6.5	0.65	0.0033
30	22	2.2	0.0073	38.6	3.86	0.0064	45	4.5	0.0038
120	41	4.1	0.0034	53	5.3	0.0022	64	6.4	0.0013
180	55	5.5	0.0031	65	6.5	0.0018	73.9	7.39	0.0010
ZnO _w									
irradiation time of TC [min]	rel. A [%]	abs. A [mg/L]	r [min ⁻¹]	rel. A [%]	abs. A [mg/L]	r [min ⁻¹]	rel. A [%]	abs. A [mg/L]	r [min ⁻¹]
	10 mg/L			20 mg/L			40 mg/L		
5	0.9	0.09	0.0018	1.1	0.11	0.0011	6.04	0.604	0.0030
30	15	1.5	0.0050	22	2.2	0.0037	26	2.6	0.0022
120	35	3.5	0.0030	39.9	3.99	0.0017	57.9	5.79	0.0012
180	50	5	0.0028	57	5.7	0.0016	64.7	6.47	0.0008

However, ZnO_e shows a comparatively high onset activity in the first 10 min of reaction, followed by a continuous abatement in the second step, between 30 and 180 min of photocatalytic treatment. With increasing photocatalyst amount, the abatement also increases.

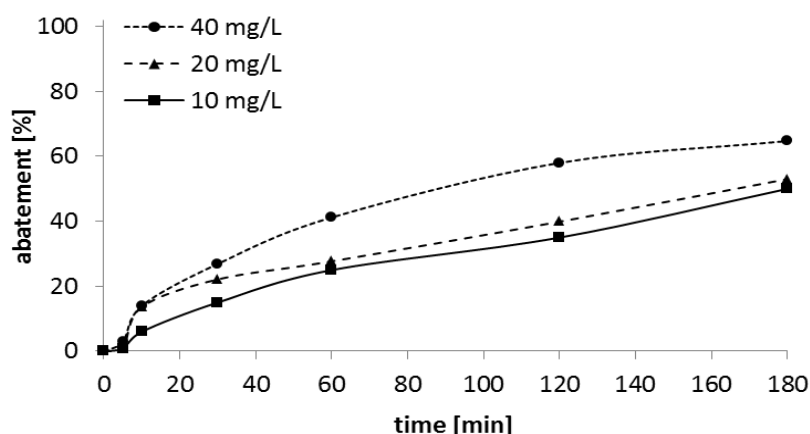


Figure 54. Photocatalytic abatement of tetracycline in aqueous solution over ZnO_w photocatalyst under UV-Vis irradiation; TC conc.: 10 ppm, cat conc.: 10, 20 and 40 mg/L.

The photocatalytic abatement of TC over ZnO_w nanoparticles and corresponding effective mean first order reaction rates are only slightly lower. However, ZnO_w shows no distinct increase in the onset activity (Fig. 54).

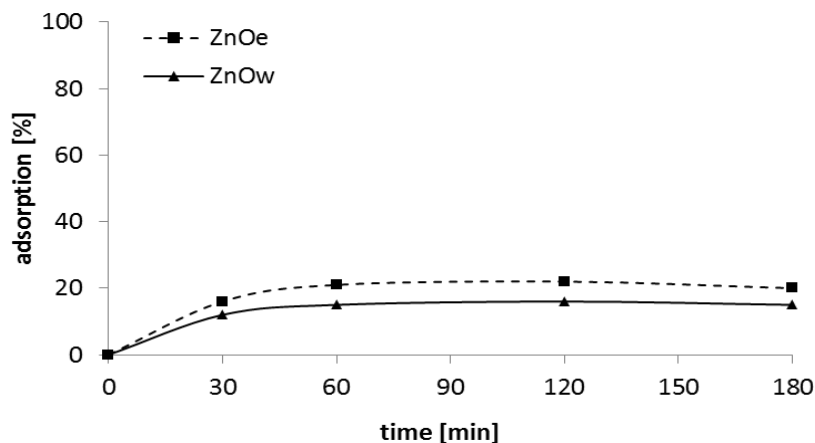


Figure 55. Adsorption of tetracycline in aqueous solution over ZnO_e and ZnO_w photocatalysts in the dark; TC conc.: 10 ppm, cat conc.: 40 mg/L.

The adsorption of TC on the photocatalyst surface is high and reaches *ca.* 12 and 19 % after 60 min (Fig. 55). The loadings of tetracycline over ZnO are higher than that found with IBP (Fig. 52), reflecting the different structure and molecular weight of the molecules.

In order to differentiate between the photocatalytic performance of small and large sized ZnO nanoparticles, the influence of the concentration of **ibuprofen and tetracycline** on the course of abatement has been tested. The IBP and TC concentrations were increased from 5 and 60 ppm at constant photocatalyst content of 10 mg/L. The results are summarized in Table 12.

The course of photocatalytic abatement of ibuprofen over ZnO_e, the more active photocatalyst, is shown in Figure 56. With increasing substrate concentration, the relative abatement decreases, however the absolute abatement is enhanced from 2.95 to 14.4 mg/L. Remarkably, the abatement nearly continuously increases with time, indicating stable operation of the catalyst.

At low substrate concentration of 5 ppm and photocatalyst in excess by mass, at cat-to-sub ratio of 2:1, the onset abatement is increased (Fig. 56). It is larger with ZnO_e compared to ZnO_w and larger for TC than for IBP.

Table 12. Influence of the drug concentration on the relative (Rel.%) and absolute abatement (A) of tetracycline and ibuprofen over zinc oxide photocatalysts: ZnO_e (top) and ZnO_w (bottom) and the apparent photocatalytic reaction rate [$\text{mg}_{\text{sub}}/\text{mg}_{\text{cat}} \times \text{min}^{-1}$] derived from the second stage of the course of abatement between 60 and 180 min; catalyst conc.: 10 mg/L.

ZnO_e								
Conc. of drug [ppm]	rel. abatements [%]			abatements				reaction rates
	initial	after		10 min	180 min	between 60 to 180 min		2 nd stage
	10 min	60 min	180 min	A [mg/L]	A [mg/L]	Rel. [%]	A [mg/L]	min ⁻¹
IBP								
5	7	36	59	0.35	2.95	23	1.25	0.0104
10	7	18	41	0.7	4.1	23	2.3	0.0192
20	5	17	33	1.0	6.6	16	3.2	0.0267
40	4	14	26	1.6	10.4	12	4.8	0.04
60	1	13	24	0.6	14.4	11	6.6	0.055
TC								
5	38	50	75	1.9	3.75	25	1.25	0.0104
10	17	44	65	1.7	6.5	21	2.1	0.0175
20	12	23	42	2.6	8.4	19	3.8	0.0317
40	8	5	15	3.2	6	10	4	0.0333
60	5	4	11.5	3	6.9	7.5	4.5	0.0375
ZnO_w								
Conc. of drug [ppm]	rel. abatements [%]			abatements				reaction rates
	initial	after		10 min	180 min	between 60 to 180 min		2 nd stage
	10 min	60 min	180 min	A [mg/L]	A [mg/L]	Rel. [%]	A [mg/L]	min ⁻¹
IBP								
5	13	32	36	0.65	1.8	4	0.2	0.002
10	5	17	27	0.5	2.7	10	1	0.008
20	5	17	25	1	5	8	1.6	0.013
40	5	14	21	2	8.4	7	2.8	0.023
60	3	10	14	1.8	8.4	4	2.4	0.02
TC								
5	25	39	65	1.25	3.25	26	1.3	0.0108
10	6	33	55	0.6	5.5	22	2.2	0.0183
20	4	21	38	0.8	7.6	17	3.4	0.0283
40	1.2	2	12	0.48	4.8	10	4	0.033
60	0.3	2	3	0.18	1.8	1	0.6	0.005

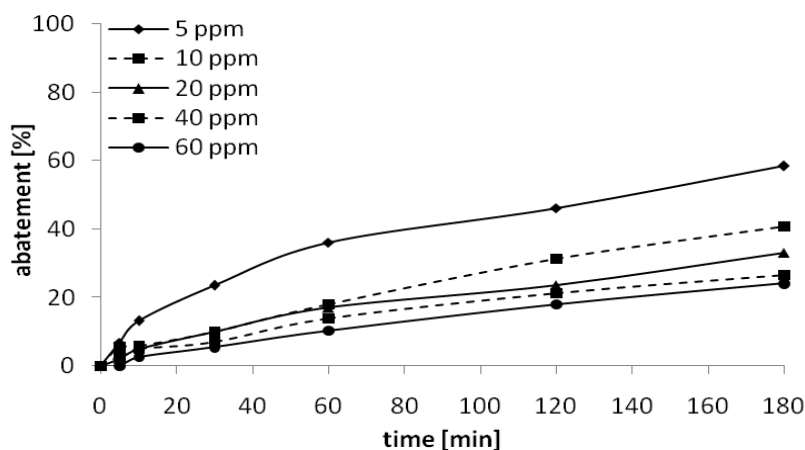


Figure 56. Photocatalytic abatement of ibuprofen in aqueous solution over smaller *ca.* 15-30 nm ZnO_e crystals under UV-Vis irradiation; IBP conc.: 5, 10, 20, 40 and 60 ppm, ZnO conc.: 10 mg/L.

Generally, the found abatement is higher with ZnO_e than with ZnO_w nanoparticles. E.g. *ca.* 24 % of 60 ppm concentrated IBP solution is converted over ZnO_e compared to *ca.* 14 % over ZnO_w after 180 min of treatment. It is observed that the abatement of IPB is markedly larger than that of TC, with *ca.* 11 and 3 %, respectively, under before mentioned conditions. ZnO_w undergoes severe deactivation especially at higher substrate concentration, i.e. at low cat-to-sub ratio. With ZnO_w photocatalyst, the absolute abatement is markedly decreased from 7.6 to 1.8 mg/L, with growing the TC concentration from 20 to 60 ppm. Whereas with ZnO_e only a slightly decrease from 8.4 to 6.9 mg/L is observed. This decrease is also reflected in the reaction rates (Tab. 12). With increased substrate concentration, larger nanocrystals (ZnO_w) are faster deactivated, compared to smaller ZnO_e ones. This might be due to lower specific surface area of ZnO_w.

The photocatalytic abatement of TC has been also studied at very **low concentration of 200 ppb**, similar to that of the new emerging pollutants, at low photocatalyst amount of 0.5 mg/L (Fig. 57). It is characterized by an increase of abatement after short treatment time (5 min). Then, it is followed by a nearly continuous increase of the abatement curves. *Ca.* > 90 % of TC is abated after 180 min. ZnO_e and ZnO_w behaves similar. The adsorption measurements show a high affinity of the ZnO towards TC. At very low substrate concentration. *Ca.* 15 % of TC is adsorbed on 0.5 mg photocatalyst (Fig. 58).

Obviously, the adsorption contributes to the initial abatement in the first 5 min, which amounts to *ca.* 32 and 18 % over ZnO_e and ZnO_w, respectively. The results show that nanosized zinc oxide is an effective catalyst for the depollution of TC in low contaminated water.

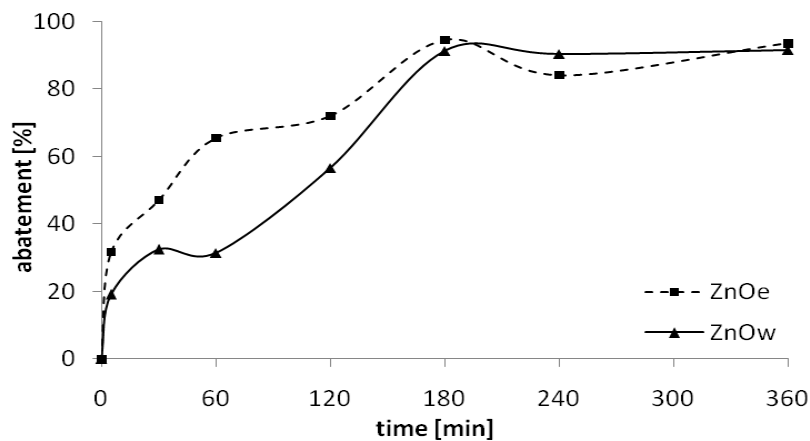


Figure 57. Photocatalytic abatement of tetracycline in aqueous solution over ZnO_e and ZnO_w photocatalysts under UV-Vis irradiation; TC conc.: 200 ppb, cat conc.: 0.5 mg/L, cat-to-sub ratio of 2.5.

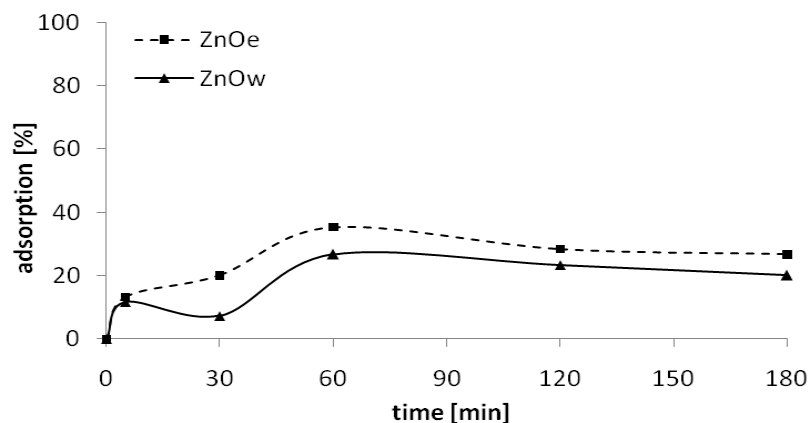


Figure 58. Adsorption of tetracycline in aqueous solution over ZnO_e and ZnO_w photocatalysts in the dark; TC conc.: 200 ppb, cat conc.: 0.5 mg/L, cat-to-sub ratio of 2.5.

The adsorption behaviour at low and high TC concentrations, but similar cat-to-sub ratio, has been compared (Tab. 13).

Table 13. Data of the adsorption TC at low (top) and high (bottom) concentration over ZnO_e and ZnO_w (cat conc.: 0.5 (top) and 10 mg/L (bottom)). Relative and absolute adsorption (A) and corresponding specific loadings calculated after 30, 60, 120 and 180 min of adsorption; cat-to-sub ratios of 2.5 (top) and 2 (bottom).

Adsorption of TC at low concentration (200 ppb)						
adsorption time of TC [min]	rel. A [%]	abs. A [mg/L]	loading [mg/mg]	rel. A [%]	abs. A [mg/L]	loading [mg/mg]
	ZnO _e			ZnO _w		
30	20	0.040	0.080	7.5	0.015	0.030
60	35.5	0.071	0.142	26.5	0.053	0.106
120	28.5	0.057	0.114	23.5	0.047	0.094
180	26.5	0.053	0.106	20	0.040	0.080
Adsorption of TC at high concentration (5 ppm)						
adsorption time of TC [min]	rel. A [%]	abs. A [mg/L]	loading [mg/mg]	rel. A [%]	abs. A [mg/L]	loading [mg/mg]
	ZnO _e			ZnO _w		
30	5.6	0.28	0.0280	4	0.200	0.020
60	9.6	0.48	0.0480	3.9	0.195	0.016
120	3.4	0.17	0.0170	2.3	0.115	0.012

It is surprisingly found that the specific TC loading [mg_{TC}/mg_{cat}] on the photocatalysts is markedly enhanced at very low (200 ppb) compared to higher (5 ppm) concentration. The inspection at higher concentration shows that this effect of enhanced adsorption in low concentrated solution, but at similar cat-to-sub ratio, starts already below 10 ppm (Fig. 59).

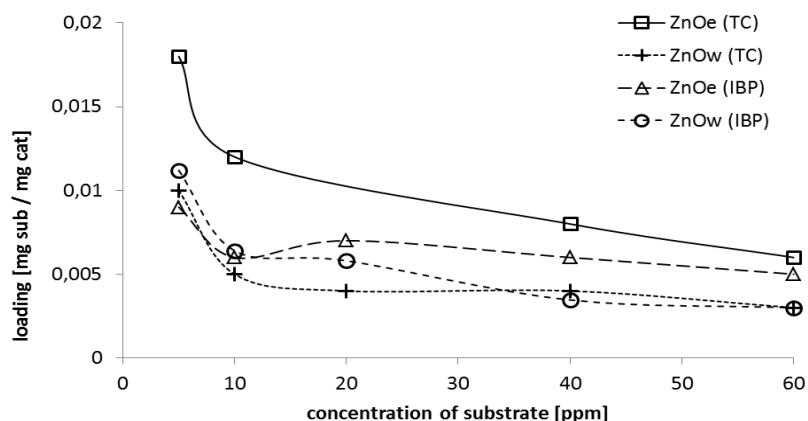


Figure 59. The ZnO photocatalysts loading [mg_{sub}/mg_{cat}] of tetracycline and ibuprofen in the aqueous solution at high substrate concentration. Conditions of measurements: adsorption time: 5 min; ZnO conc.: 10 mg/L; asterisk (*) indicates the cat-to-sub ratio of 1.

The specific loading changes (increase and decrease) with contact time probably due to changes of the surface (hydration). At low concentration and low photocatalyst amount, the loading further increases markedly with growing TC concentration (Fig.

60 inset). But the effect of higher loading at low substrate and catalyst concentration is maintained, with prolonged contact time (Tab. 13).

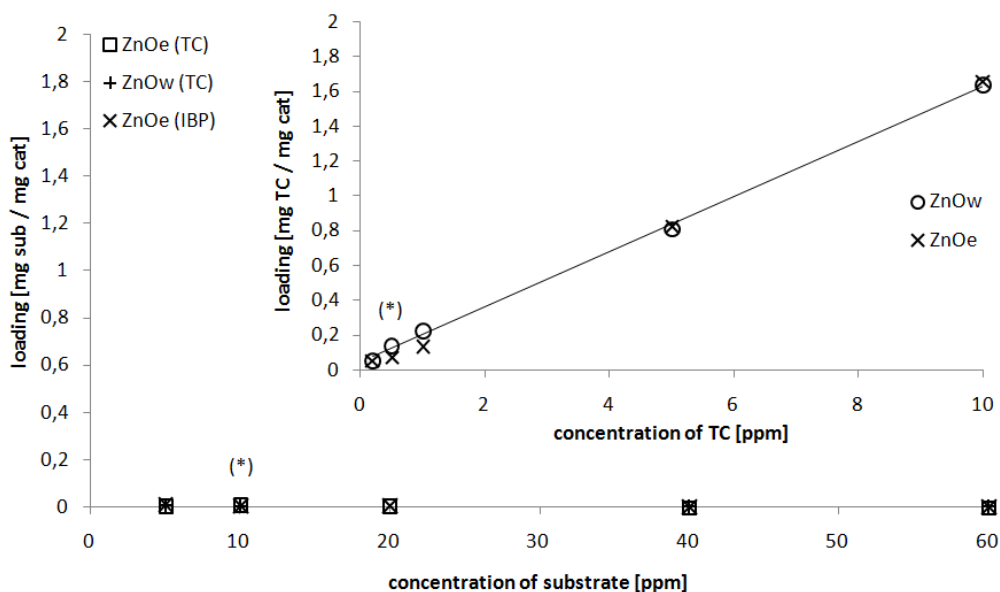


Figure 60. The ZnO photocatalysts loading [$\text{mg}_{\text{sub}}/\text{mg}_{\text{cat}}$] of tetracycline and ibuprofen in the aqueous solution at high and low (inset) substrate concentrations. Conditions of measurements: adsorption time: 5 min; ZnO content: 10 mg/L at high, and 0.5 mg/L at low concentrations; asterisk (*) indicates the cat-to-sub ratio of 1.

The high TC loading per milligram of ZnO photocatalyst, at low concentrated solution, is also observed with titania (compare Chapter 3.3).

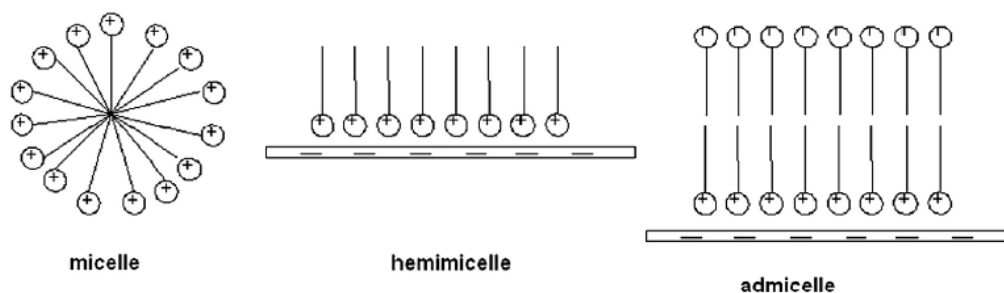


Figure 61. Schematic representation of micelles, hemimicelle and admicelle formation; depending on arrangement of molecules.^[197]

Own estimations show that these loadings exceed the monolayer adsorption capacity of *ca.* 0.011 and 0.002 $\text{mg}_{\text{TC}}/\text{mg}_{\text{cat}}$ for ZnO_e and ZnO_w , respectively. They require

multilayer adsorption as can be realized with aligned adsorbed molecules (Langmuir Blodgett - type) and admicelles formation with amphiphilic molecules and solid particles as well as their aggregation binding high amounts of substrate (Fig. 61). The large crystal faces of the ZnO_w favour the formation of mono- and multilayer (Fig. 62).

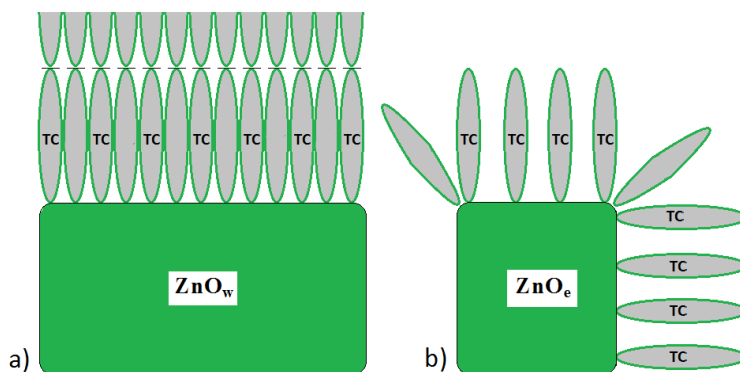


Figure 62. Schematic representation of the adsorption of tetracycline on zinc oxide nanoparticles a) multilayer adsorption on large size ZnO_w crystals, b) monolayer adsorption on small size ZnO_e crystals.

In contrast, at higher (ppm range) TC concentration, the formation micelles in solution competes with the adsorption on the particles rendering the formation of multilayers or admicelles more difficult.

Influence of pH solution

The influence of the pH value (varied between 3 and 9) has been studied during photocatalytic abatement of ibuprofen and tetracycline.

The activity of the ZnO photocatalysts under acidic, neutral and alkaline reaction conditions has been tested at the cat-to-sub ratio of 2, using 20 mg/L of photocatalyst and 10 ppm of drug (Fig. 63-66).

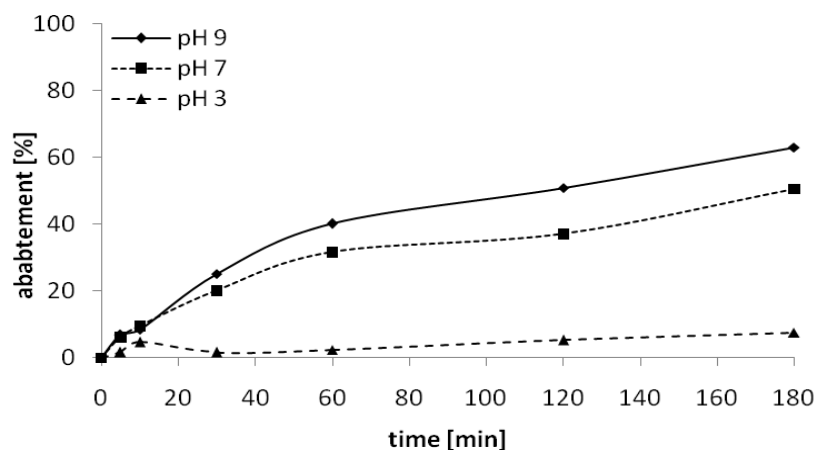


Figure 63. Influence of pH value of the reaction solution on the photocatalytic abatement of ibuprofen in aqueous solution over ZnO_e photocatalyst under UV-Vis irradiation; IBP conc.: 10 ppm, cat conc.: 20 mg/L.

The photocatalytic abatement of **ibuprofen** over ZnO_e and ZnO_w is strongly influenced by pH of solution (Fig. 63 and 64). The abatement of IBP is markedly dropped under acidic conditions (pH=3). The lower activity of the zinc oxide can be explained by the increased electrostatic repulsion between the protonated surface of the ZnO nanoparticles and the substrate molecules. After 180 min of treatment, only ca. 8 and 5 % of IBP is abated in the acidic conditions over ZnO_e and ZnO_w nanoparticles, respectively.

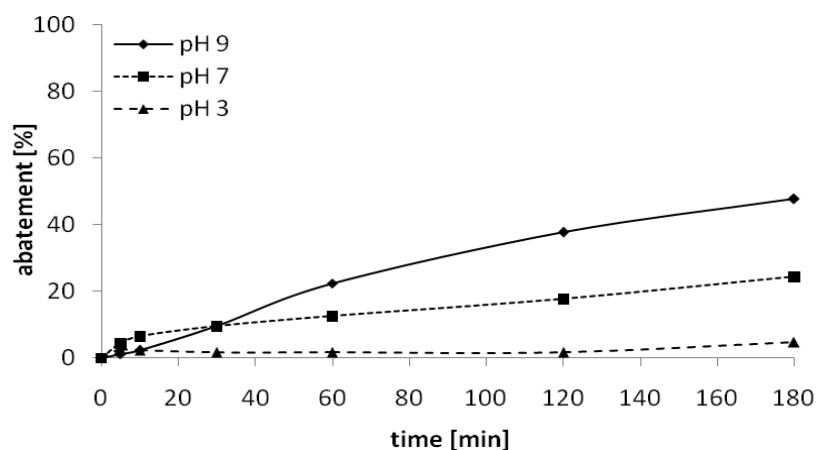
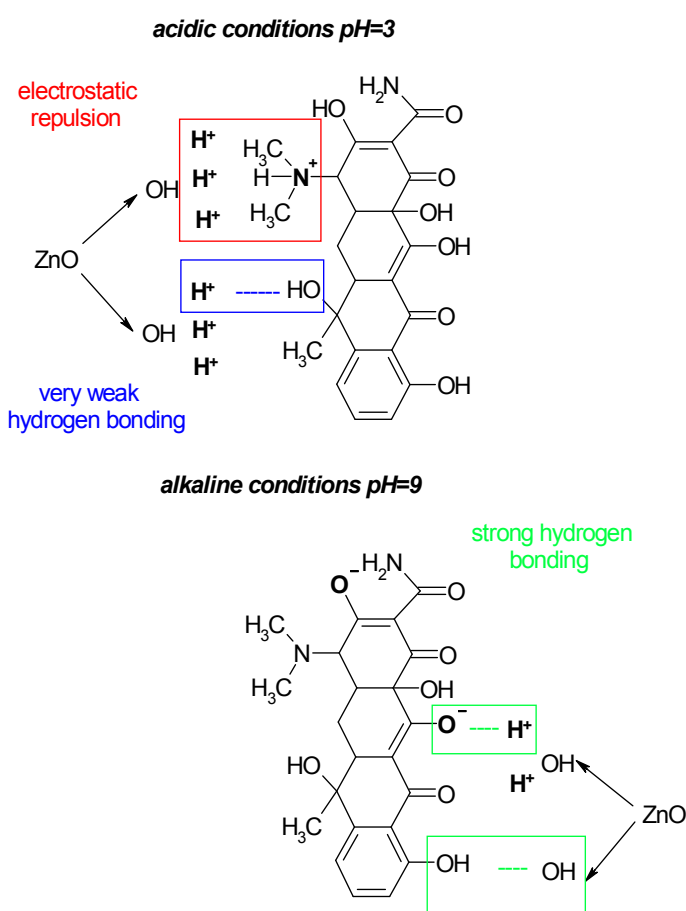


Figure 64. Influence of pH value of the reaction solution on the photocatalytic abatement of ibuprofen in aqueous solution over ZnO_w photocatalyst under UV-Vis irradiation; IBP conc.: 10 ppm, cat conc.: 20 mg/L.

The influence of pH value on the photocatalytic abatement of **tetracycline** over ZnO_e and ZnO_w has been also investigated (Fig. 65 and 66). The abatement is markedly

decreased over both ZnO type catalysts under acidic conditions due to the improved electrostatic repulsion between the positively charged TC (ab^+c species, compare A 1.2 Fig. 29) and the positive charged catalyst surface in aqueous solution (P_{zc} of ZnO is *ca.* 9^[198,199]). Enhanced degradation of TC is observed under alkaline conditions (Fig. 65 and 66). This is due to improved interaction of the hydroxylated photocatalyst surface and negatively charged TC (deprotonated -OH groups) by strong hydrogen bonding (Scheme 4). The enhancement of the pH value from 7 to 9 leads finally to an increase of the photocatalytic abatement of tetracycline from *ca.* 65 to 90 % over ZnO_e and from *ca.* 50 to 85 % over ZnO_w, respectively.



Scheme 4. Schematic representation of the interactions between ZnO hydroxylated surface and tetracycline molecule at acidic and alkaline solutions.

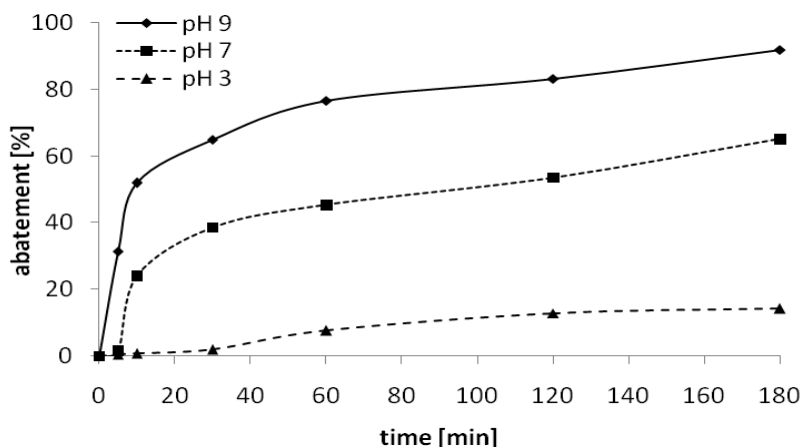


Figure 65. Influence of pH value of the reaction solution on the photocatalytic abatement of tetracycline in aqueous solution over ZnO_e photocatalyst under UV-Vis irradiation; TC conc.: 10 ppm, cat conc.: 20 mg/L.

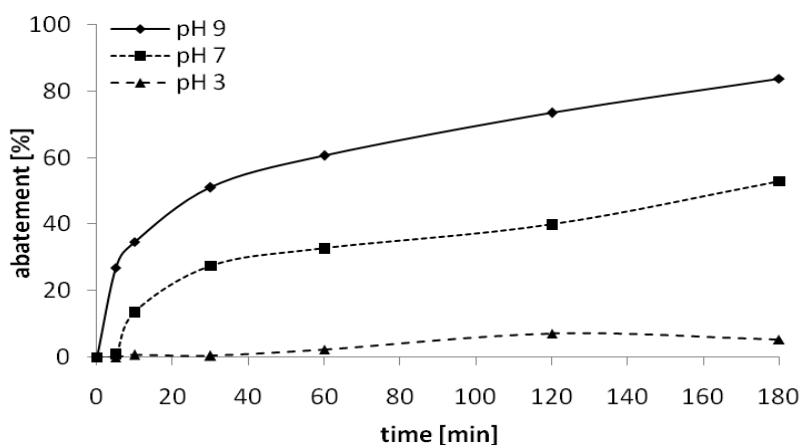


Figure 66. Influence of pH value of the reaction solution on the photocatalytic abatement of tetracycline in aqueous solution over ZnO_w photocatalyst under UV-Vis irradiation; TC conc.: 10 ppm, cat conc.: 20 mg/L.

Therefore, also the adsorption of IBP and TC is increased at pH=9 and markedly decreased at low pH=3 (Fig. 67). This finding shows the close relation between the adsorption and the photocatalytic abatement properties observed with the ZnO nanoparticle photocatalysts. The adsorption of TC on the ZnO is higher than that of IBP due to amphiphilic, zwitterionic nature and the higher polarity (polar substituents) of tetracycline compared to ibuprofen, which possess only one -COOH polar group (compare A 1.2, Fig. 28).

These special TC properties improve the polar interactions with the photocatalyst surface. The adsorption on the photocatalyst surface increases with contact time due to increased surface hydroxylation.

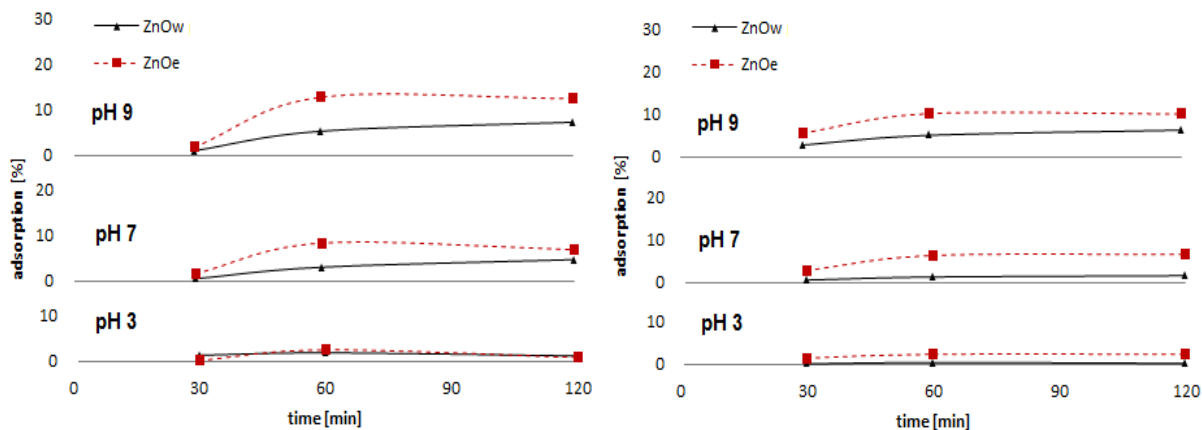


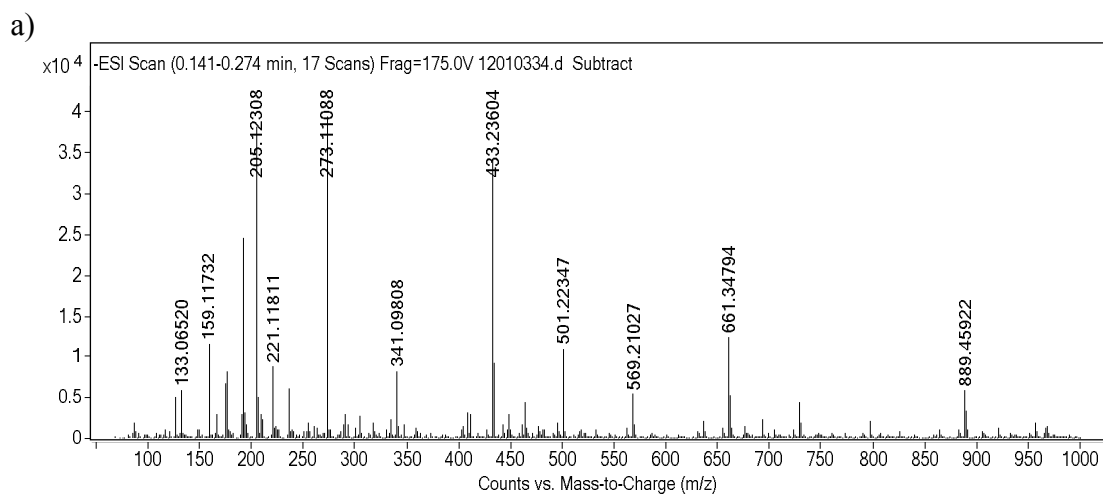
Figure 67. Influence of the pH value on the adsorption of tetracycline (left) and ibuprofen (right) in aqueous solution over ZnO_e and ZnO_w. TC and IBP conc.: 10 ppm, cat conc.: 20 mg/L, cat-to-sub ratio of 2.

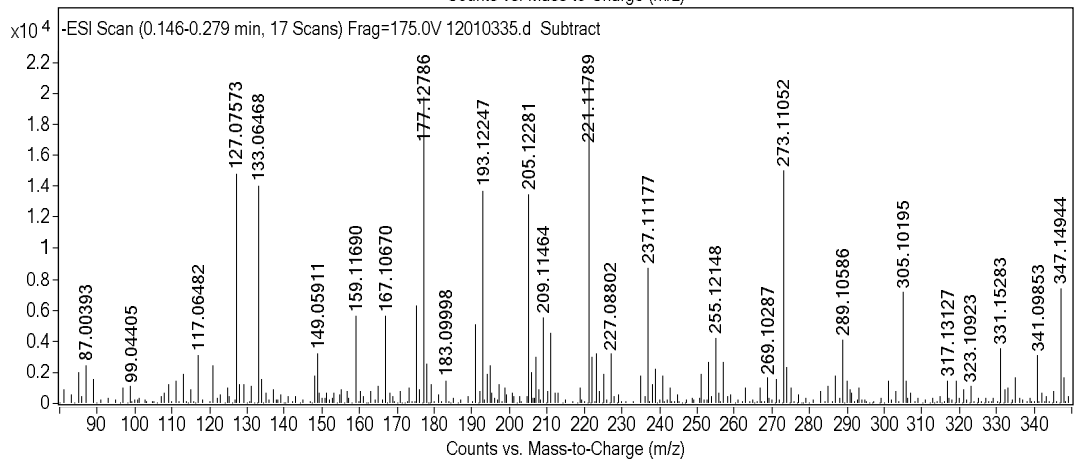
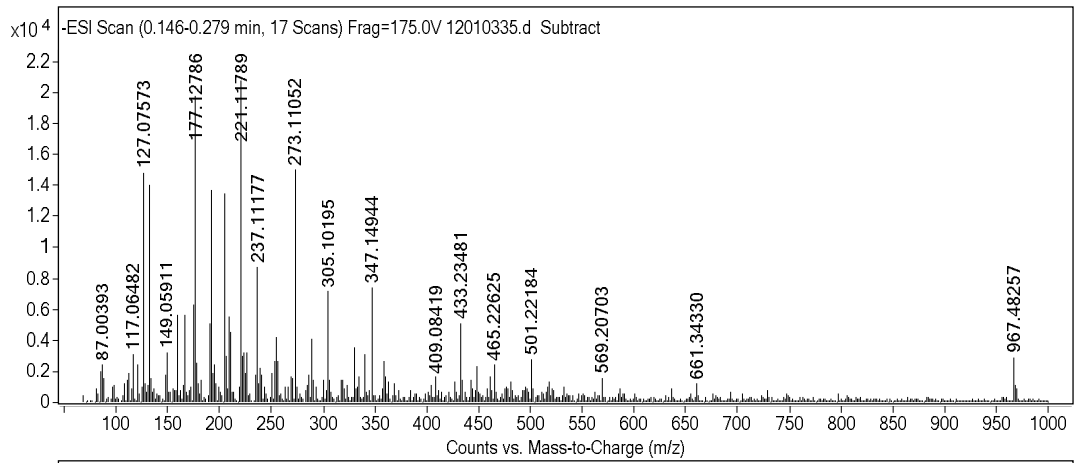
Formation of ibuprofen and tetracycline intermediates

The formation of reaction intermediates of ibuprofen and tetracycline during the course of photocatalytic treatment over the two different sized ZnO nanoparticles have been followed by ESI-TOF-MS measurements. The ESI-TOF-MS spectra of starting IBP and TC solution have been explained before (compare A 1.2, Fig. 35 and 33). The molecular peaks [M-H]⁻ of IBP and TC formed in the negative ionization mode appear at m/z 205 and 443, respectively.

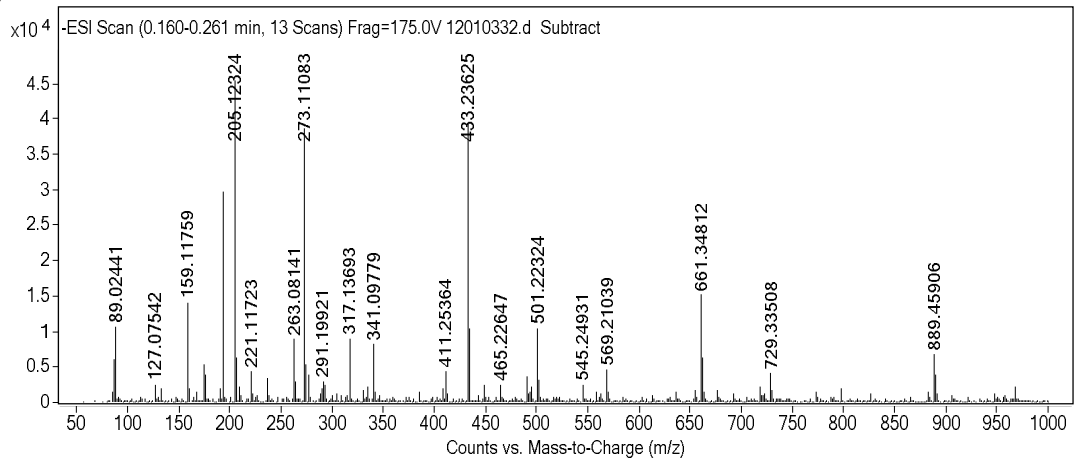
The photocatalytic abatement of **ibuprofen** under UV-Vis irradiation over smaller and larger ZnO crystals is accompanied by the formation of reaction intermediates (Fig. 68). After 30 min of treatment a lot of IBP intermediates with different masses formed over ZnO_e appear in the solution (Fig. 68 a). With prolonged time (240 min) the majority of high intensity molecular peaks appear in the m/z range between 90 and 350. They are probably related to the formation of the benzene derivatives (one ring aromatics) and deeper oxidation intermediates (e.g. ring opening, aliphatic acids).

The magnification of this range shows a special pattern of peak distribution. It consists of distinguished intermitting single groups of m/z peaks which differ by *ca.* 20 m/z . Besides a couple of low intensity peaks appear in the m/z range between 400 - 550, and around 661 and higher. Besides, some IBP aggregates are shown at m/z 273, 443, 501, 661 and 889 (also present in the starting IBP solution, compare A 1.2, Fig. 34). The abatement of IBP over ZnO leads to the formation of a huge amount of different high molecular masses by-products. Based on ESI-TOF-MS spectra, the formation of IBP intermediates over the smaller and larger ZnO_w nanoparticles looks similar (Fig. 68). However the IBP absorption bands (UV-Vis spectra, data not shown) monitored during the course of treatment differ in the intensity by 264 nm. The formation of ibuprofen by-product is higher with ZnO_e than with ZnO_w. This observation is in an agreement with the adsorption data (Fig. 52 and 59). The formation of intermediates increases steadily during the course of treatment up to 180 min (Fig. 69). This finding related to the formation of IBP intermediates is different from that of titania (compare Chapter 3.1, Fig. 9).





b)



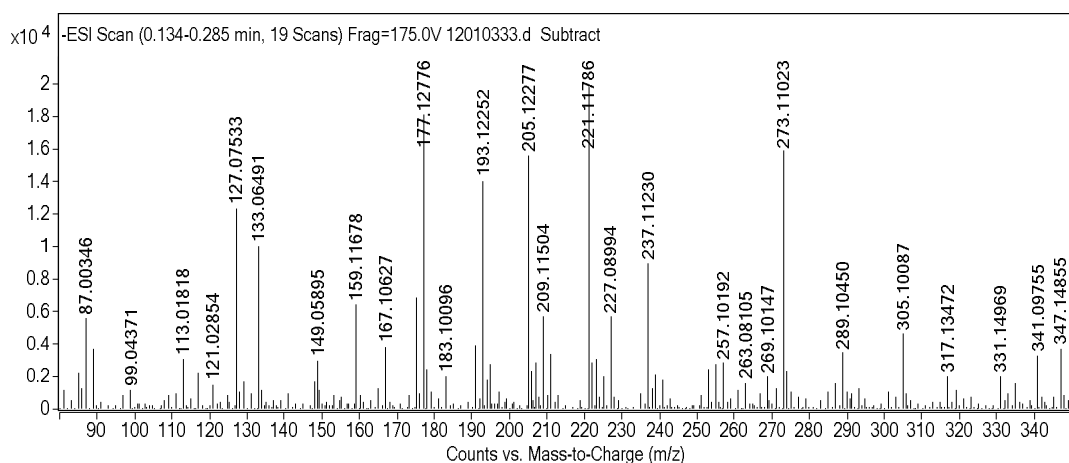
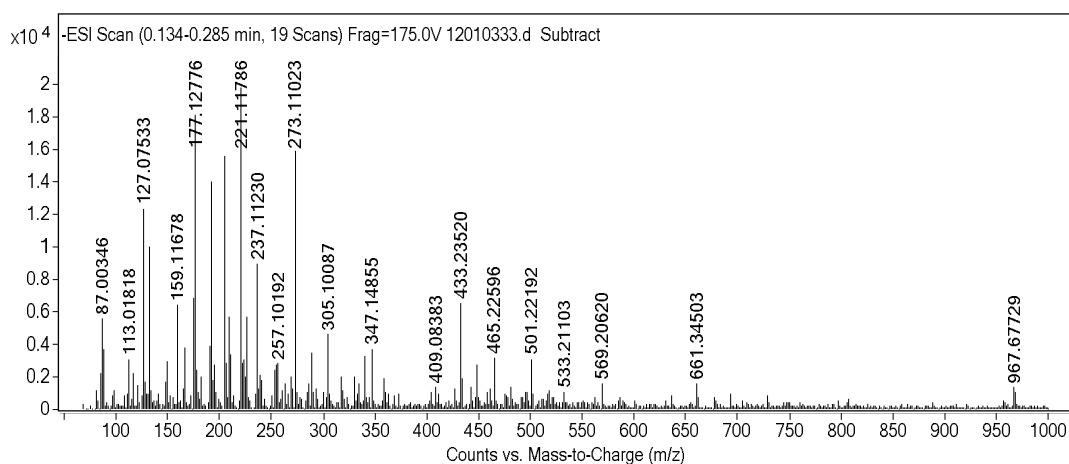


Figure 68. Negative ESI-TOF-MS spectra of the aqueous ibuprofen solution after photocatalytic treatment over (a) ZnO_e after 30 (top) and 240 min (middle), including higher magnification of spectrum after 240 min (bottom); and over (b) ZnO_w after 30 (top) and 240 min (middle), including higher magnification of spectrum after 240 min (bottom). Reaction conditions: UV-VIS irradiation, IBP conc.: 20 ppm, cat conc.: 20 mg/L; cat-to-sub ratio of 1.

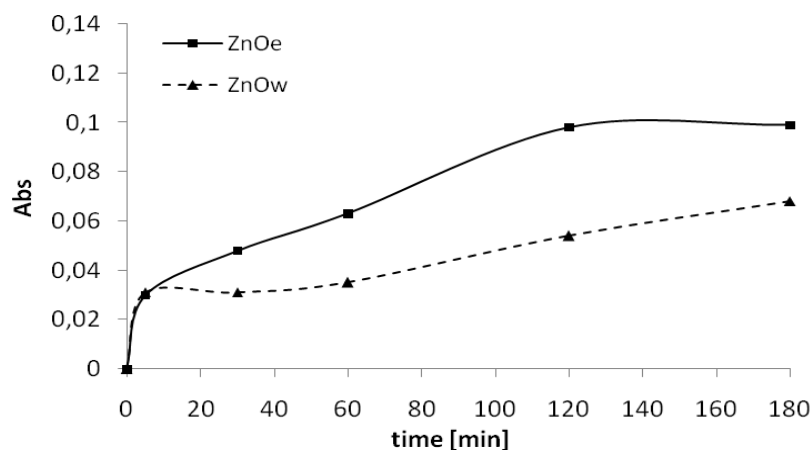
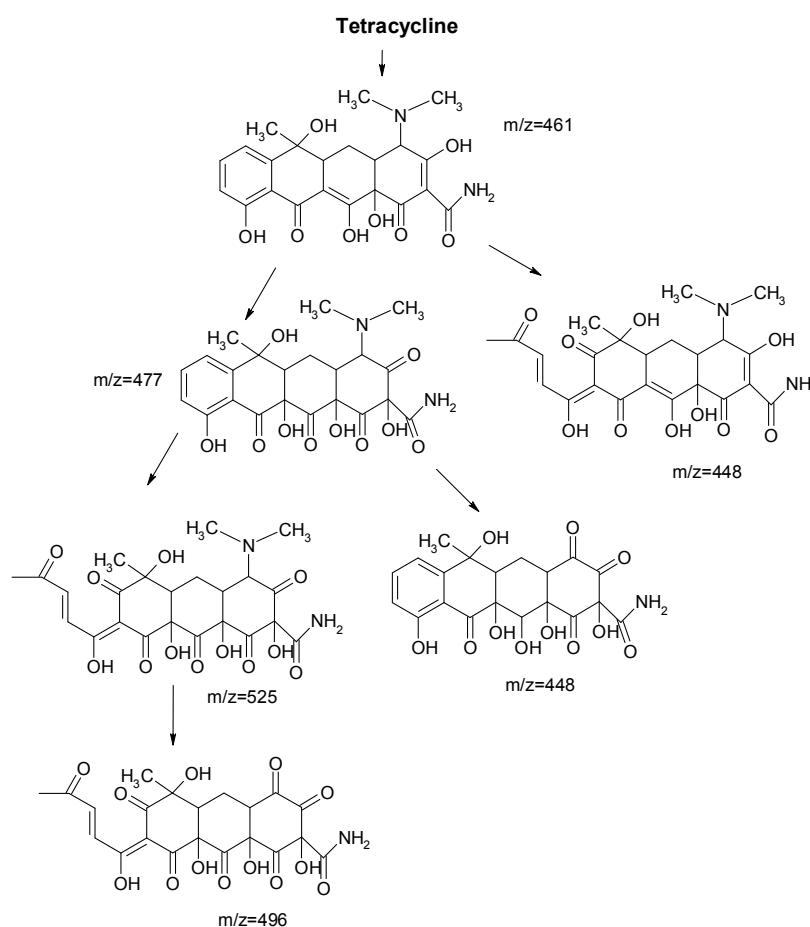


Figure 69. Formation of the temporary intermediates of ibuprofen in aqueous solution during photocatalytic treatment over ZnO photocatalyst based on UV-Vis absorbance at λ_{max} 262 nm; IBP conc.: 20 ppm, cat conc.: 20 mg/L.

Additionally, the formation of **tetracycline** intermediates has been checked during the course of photocatalytic abatement (Fig. 70). The ESI-TOF-MS spectra of TC by-products show also typically peak group pattern by location and intensity. Three groups of peaks arise around m/z 100, 136 and 170 and lower intense peaks around m/z 250 and 350 and higher. This pattern is not changed with treatment.

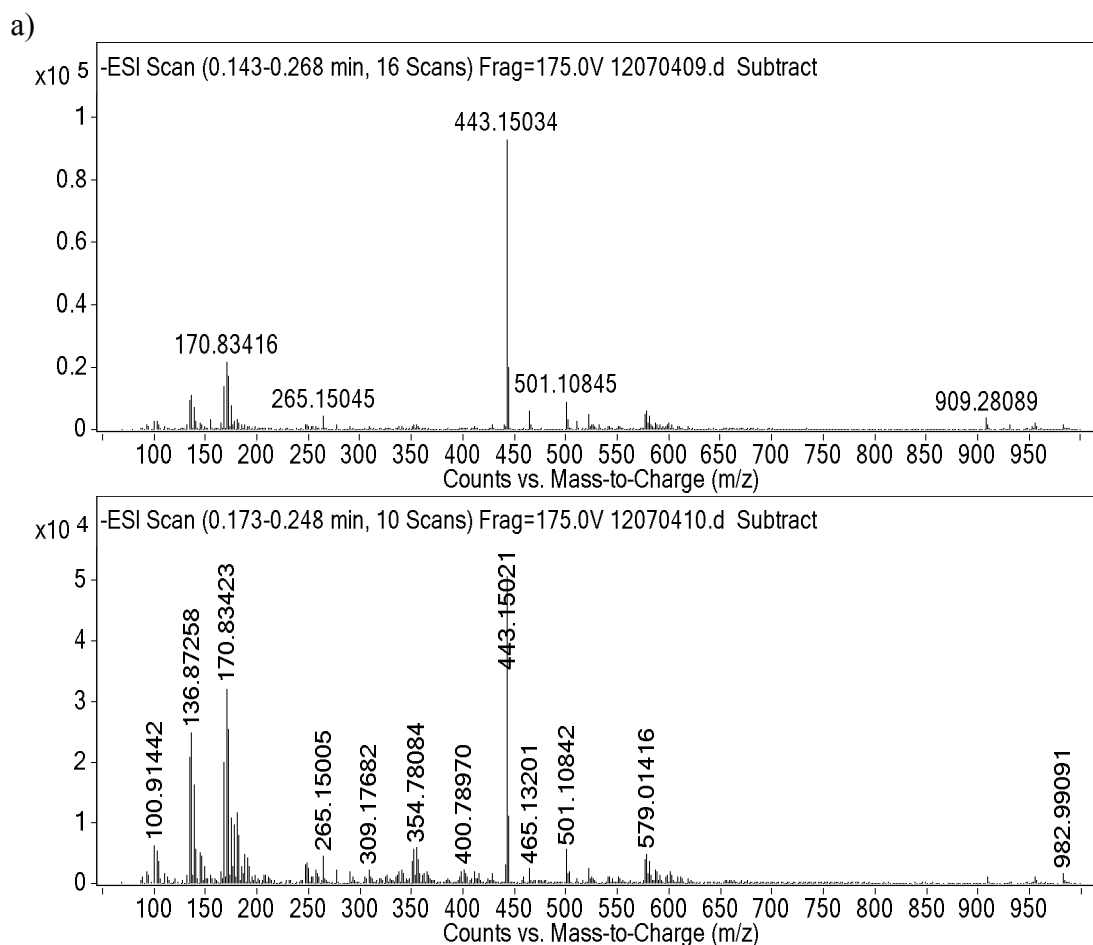
In detail after 30 min of UV-Vis irradiation higher mass peaks are formed. Peaks m/z at 579, 501, and 465 are higher than mass of TC (m/z 443). These peaks probably belong to partial oxidised by-products enhancing the molecular mass by oxygen insertion (Scheme 5).

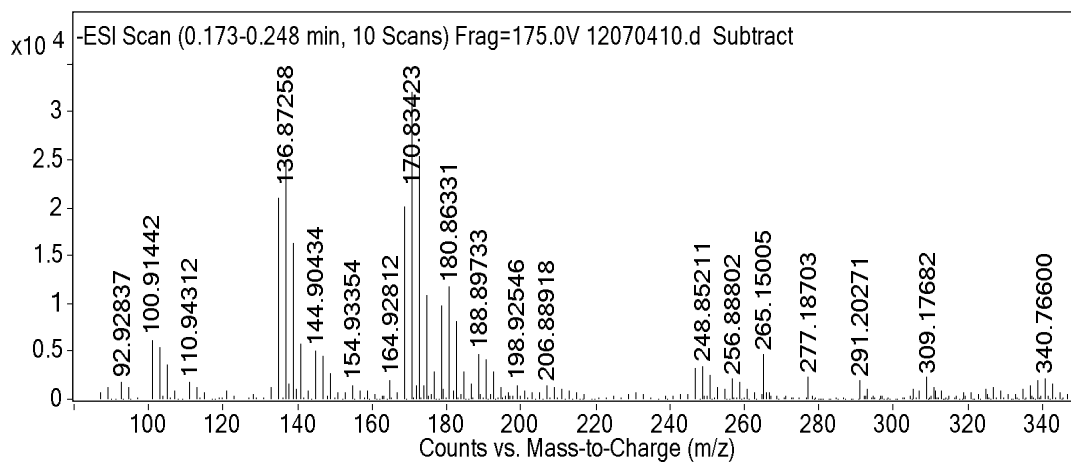


Scheme 5. The proposed degradation pathway of tetracycline; arrow indicates degradation by oxidant agent like ozone or hydroxyl radicals.^[200]

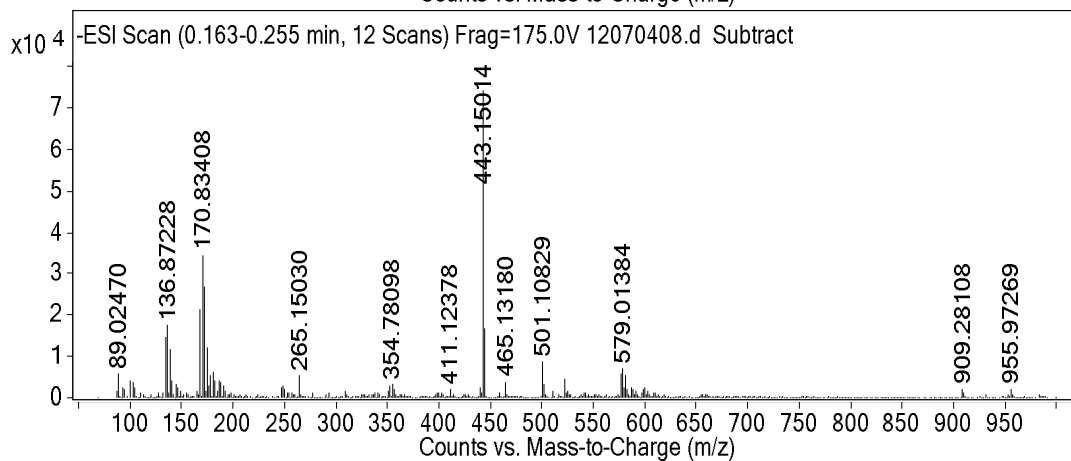
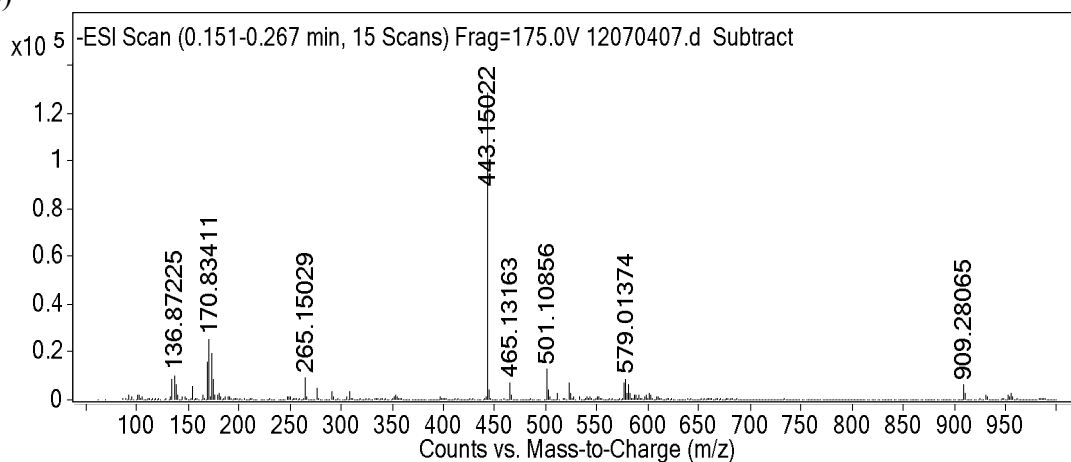
The intensity of these peaks slight decreases during prolonged abatement. After 240 min formation of some intermediates gives rise at m/z peaks below $m/z < 400$. The main intense signals located between m/z 100 and 200, mainly around m/z 102, 133 and 170, likely belong to decomposition products, especially related to anthraquinone,

quinone derivatives, benzoic acid derivatives, substituted benzene and phenol derivatives which are further decomposed to aliphatic acids, alcohols and ethers with lower than 100 m/z (compare Chapter 3.2). Higher m/z peaks at 180, 188, 265 and 354 also appear. These peaks are new and differ from that found with titania. They can be assigned to by-products containing three or two 6-membered aliphatic or aromatic rings. It is observed that the photocatalytic abatement of TC over both ZnO photocatalysts is very similar (Fig. 70 a and b). Number and amount of by-products of TC is reduced, compared to IBP.





b)



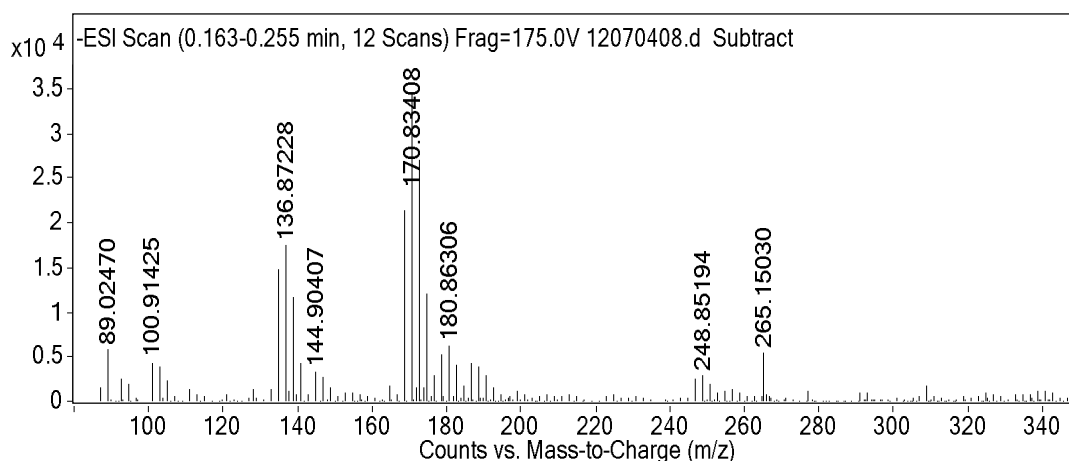


Figure 70. Negative ESI-TOF-MS spectra of the aqueous tetracycline solution after photocatalytic treatment over (a) ZnO_e after 30 (top) and 240 min (middle), including higher magnification of spectrum after 240 min (bottom); and over (b) ZnO_w after 30 (top) and 240 min (middle), including higher magnification of spectrum after 240 min (bottom). Reaction conditions: UV-VIS irradiation, TC conc.: 20 ppm, cat conc.: 20 mg/L; cat-to-sub ratio of 1.

Re-use experiments

The re-usability of ZnO nanoparticles has been checked by cycling (re-use) experiments during photocatalytic abatement of ibuprofen and tetracycline. These experiments were carried using 10 mg/L of ZnO photocatalysts and a drug concentration of 10 ppm; i.e. at equal cat-to-sub ratio of 1.

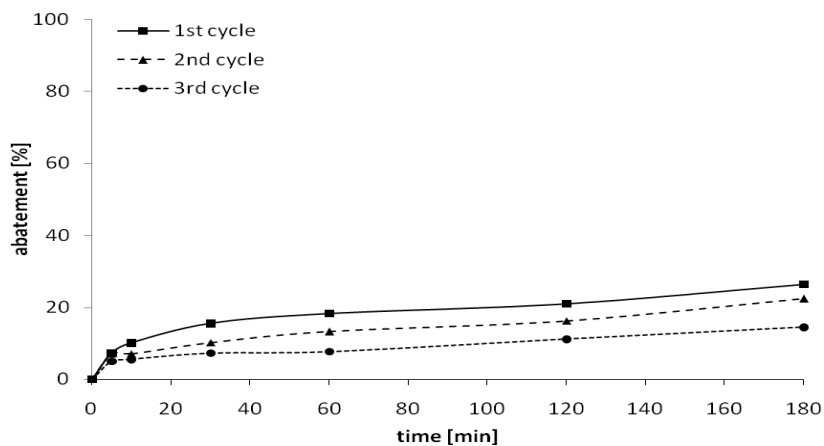


Figure 71. Photocatalytic abatement of ibuprofen in aqueous solution over ZnO_e photocatalyst under UV-Vis irradiation after 3 runs of treatment; IBP conc.: 10 ppm, cat conc.: 10 mg/L.

The photocatalytic abatement of **ibuprofen** over smaller ZnO_e and larger ZnO_w nanoparticles in three runs of treatment is shown in Figures 71 and 72. The abatement of ibuprofen over smaller ZnO_e nanoparticles decreased from *ca.* 26, 22 to 14 % after

first, second and third run, after 180 min of treatment, respectively (Fig. 71). The somewhat lower photocatalyst activity is observed with larger ZnO nanoparticles (Fig. 72). *Ca.* 18, 12 and 7 % is abated over ZnO_w photocatalyst after 3 runs of treatment at the same time. *Ca.* 50 % loss of activity in the IBP abatement after 3rd run is observed for both ZnO photocatalysts.

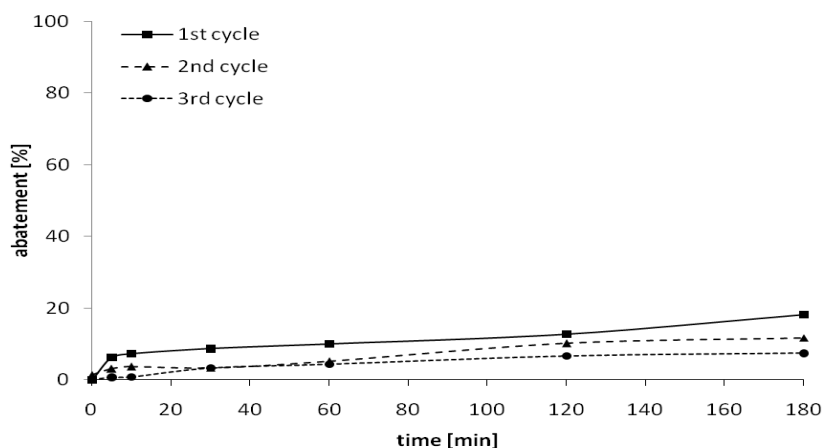


Figure 72. Photocatalytic abatement of ibuprofen in aqueous solution over ZnO_w photocatalyst under UV-Vis irradiation after 3 runs of treatment; IBP conc.: 10 ppm, cat conc.: 10 mg/L.

Additionally, re-use experiments over ZnO nanoparticles during photocatalytic abatement of **tetracycline** are shown in Figures 73 and 74. Again, the smaller nanoparticles show higher abatement of tetracycline and *ca.* 69, 58 and 31 % of TC is removed from the solution, after 180 min of each run, respectively (Fig. 73). Lower abatement is obtained with larger ZnO_w crystals, where *ca.* 57, 32 and 29 % of TC is removed from the solution after 1st, 2nd and 3rd run, respectively (Fig. 74). Finally, *ca.* 50 % loss of activity of TC is observed after the 3rd run over smaller and larger ZnO crystals, which is similar to IBP.

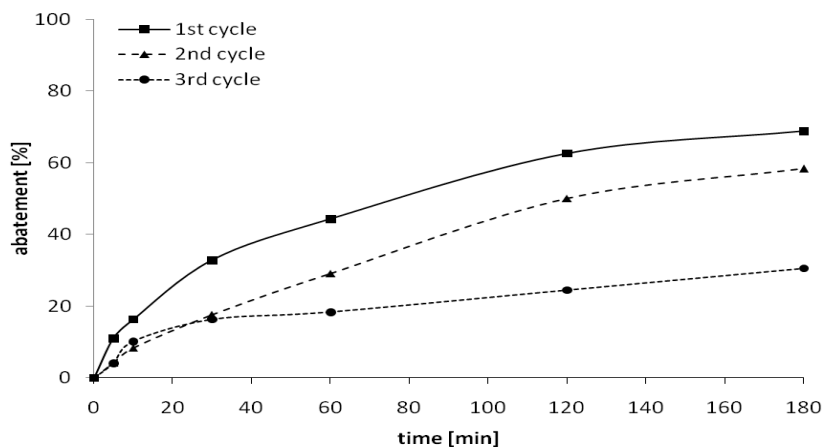


Figure 73. Photocatalytic abatement of tetracycline in aqueous solution over ZnO_e photocatalyst under UV-Vis irradiation after 3 runs of treatment; TC conc.: 10 ppm, cat conc.: 10 mg/L.

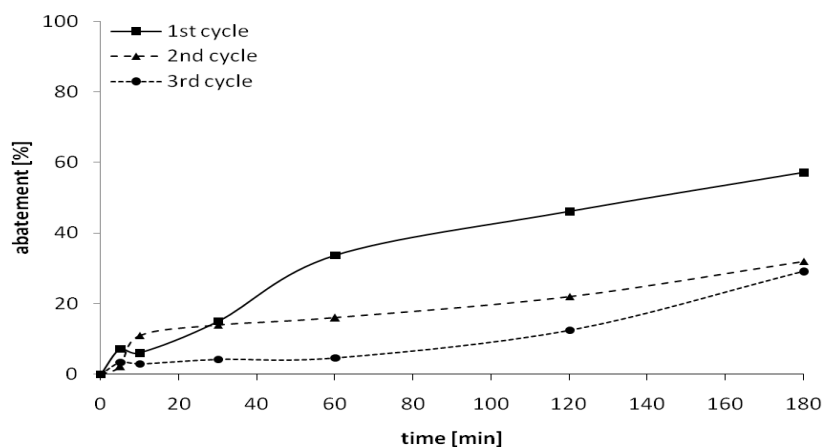


Figure 74. Photocatalytic abatement of tetracycline in aqueous solution over ZnO_w photocatalyst under UV-Vis irradiation after 3 runs of treatment; TC conc.: 10 ppm, cat conc.: 10 mg/L.

The experimental findings of the re-use experiments are in line with former presented photocatalytic results which show higher conversion of TC compared to IBP over ZnO and but larger formation of by-products with IBP over larger ZnO_w particles.

The activity of re-used catalysts decrease in the order:

$$\text{ZnO}_e \text{ TC} > \text{ZnO}_w \text{ TC} > \text{ZnO}_e \text{ IBP} > \text{ZnO}_w \text{ IBP};$$

whereas the relative decrease in activity after the 3rd run is about 50 % and similar for all the ZnO photocatalysts - drug combinations.

Summary

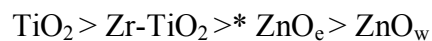
- The influence of particle size and texture effect of two nanosized ZnO photocatalysts on the abatement of ibuprofen and tetracycline has been investigated.
- The activity of larger (ZnO_w) nanoparticles is somewhat lower than that of smaller (ZnO_e) one. Even the larger ZnO_w nanoparticles have *ca.* 5 times lower adsorption capacity than ZnO_e , the photocatalytic activity is still high. *Ca.* 50 and 27 % of IBP and 65 and 57 % of TC have been effectively abated from solution (cat-to-sub ratio of 2, 180 min of treatment, 60 W of lamps) over ZnO_e and ZnO_w , respectively.
- High onset activity (first 10 min) of ZnO_e is due to high adsorption (influence of nanoporosity), whereas initial activity observed with ZnO_w is lower because of lower adsorption.
- It is observed that adsorption of TC and catalysts loadings are higher at low ppb range. Again, the self-agglomeration of TC molecule close to catalyst surface facilitates the high adsorption. Additionally, calculation showed that the surface coverage of TC at low concentration requires the multilayer adsorption formation for ZnO_w (with monolayer adsorption of *ca.* 0.002 $\text{mg}_{\text{TC}}/\text{mg}_{\text{cat}}$) and monolayer adsorption formation for ZnO_e (*ca.* 0.011 $\text{mg}_{\text{TC}}/\text{mg}_{\text{cat}}$).
- Both ZnO sized nanoparticles shows similar properties during formation of IBP and TC intermediates. However, the formation of IBP intermediates is somewhat higher for smaller ZnO_e crystals. A broaden range of peaks distribution (with masses between 90 - 350 and 400 - 550) appears on the ZnO_e surface. This might be due to high specific loading (adsorption) of IBP on ZnO_e . Formation of TC intermediates is similar for both ZnO. Photocatalytic abatement of tetracycline is slightly higher than that of ibuprofen. This is also confirmed by different type of intermediates formation. The formation of TC intermediates with higher mass >200 (aromatic and cyclic aliphatic rings) is observed, but the number of TC intermediates is reduced compared to IBP.

3.5. Final conclusions

- Besides commercial TiO₂ (P25, Degussa), novel titania (doped titania, titania nanotubes, titania/MOF composites, and T-MOF-125) and two different sized nanoparticulate zinc oxide based photocatalysts have been prepared, characterized and tested in the photocatalytical decomposition of two pharmaceuticals ibuprofen (IBP) and tetracycline (TC).
- These materials differ in the texture, morphology and specific surface area and were characterized by the XRD, TEM and N₂ adsorption-desorption measurements.
- Photocatalytic performances have been tested under more reliable photocatalytic conditions; at low cat-to-sub ratio, at low photocatalyst and substrate concentrations, and at low irradiation intensity (sun light). These severe conditions are usually not considered in the literature.

IBP and TC at ppm range

- The photocatalytic abatement of IBP and TC at low ppm range (5 - 60 ppm of substrate) was carried out over titania, titania doped photocatalysts and zinc oxide nanoparticles (Tab. 15).
- The formation of IBP and TC intermediates has been investigated by ESI-TOF-MS measurements. Influence of pH on the degradation, re-use of catalysts and its adsorption behaviours have been also tested during the course of abatement.
- The samples show still high photocatalytic activity (abatement/degradation of pharmaceuticals) even most severe conditions which have been applied.
- Titania shows the highest activity which is assigned to very reactive species like electron holes (h⁺) and titania redox pairs (Ti³⁺/Ti⁴⁺), whereas ZnO is less active, but is known to be an efficient in the formation of reactive [•]OH radicals. The oxidation potential of hydroxyl radicals is lower than for h⁺.
- The doping of titania does not increased the photocatalytic efficiency. It leads to decrease of the onset activity, compared to titania. Over all, the abatement achieved with the photocatalysts decreases in the order:



(*) with exception in TC abatement, where $\text{ZnO}_e > \text{Zr-TiO}_2$.

- The adsorption of IBP and TC on ZnO nanoparticles is higher than on titania. The enrichment by adsorption contributes to the comparatively high photocatalytic performance of ZnO nanoparticles.
- Over titania a lot of intermediates are formed, but they are decomposed during the course of photocatalytic treatment. Doping of titania with zirconium reduces the formation of intermediates, however, they are not decomposed and block the catalyst surface. Poisoning of the catalyst makes the re-use more difficult.
- Over ZnO the formation of by-product increases. It is assigned to the significantly enhanced specific loading (adsorption) of pharmaceuticals on ZnO surface compared to titania, which facilitates the formation of partial oxidation by-products nearby the surface of the catalyst (Tab. 14).

TC at ppb range

- Decomposition of tetracycline at ppb range has been studied with titania, doped titania and porous titania based materials (titania nanotubes (TNs), Ti/MIL composites and porous MIL-125 materials). At low catalyst concentration and at low cat-to-sub ratio of *ca.* 2, all samples show high activities in the TC abatement.
- The very high adsorption of samples, contributes significantly to the TC abatement (40 - 65 %). All materials behave also photocatalytic and degrade the TC. With titania nearly 100 % of abatement is observed after 90 min of treatment.
- The photocatalytic abatement decrease in the order:

titania (*ca.* 100 %) > TNs (*ca.* 90 %) >
MIL-125 (*ca.* 80 %) > Ti/MIL-101 (*ca.* 64 %)

- At very low substrate concentration unexpected increase of the adsorption (specific TC loading) on the catalysts surface is observed. This high TC adsorption at low concentration is explained by multilayer or admicelle formation by amphiphilic TC molecules. At high concentration (ppm) range, formation of self-aggregates and admicelles in the solution compete with (and decrease) the adsorption on the photocatalyst.

Therefore, the photocatalytic abatement behavior at **low (ppb) concentration is different from high (ppm) concentration**.

- The results show that the **photocatalysis is of high potential**. It can be successfully used for the photocatalytic remediation of water from very low concentrated emerging pharmaceutical pollutants.

Table 14. Data of the photocatalytic abatement of ibuprofen and tetracycline (10 ppm) in water during photocatalytic treatment over titania, Zr-TiO₂ and ZnO photocatalysts (cat conc.: 10, 20 and 40 mg/L). Relative and abatements (A) and corresponding experimental effective mean first order reaction rates (r) calculated after two stages of reaction 0-5 and 60-180 min.

Conc. of titania P25 [mg/L]	between 0-5 min			between 60-180 min			final abatement [%]
	rel. A [%]	abs. A [mg/L]	r [min ⁻¹]	rel. A [%]	abs. A [mg/L]	r [min ⁻¹]	
ibuprofen							
10	17	1.7	0.0340	22.7	2.27	0.0019	88
20	27	2.7	0.0270	25.4	2.54	0.0011	97
40	34	3.4	0.0170	13.2	1.32	0.0003	100
tetracycline							
10	11	1.1	0.0220	24.5	2.45	0.0020	74
20	23	2.3	0.0230	29.8	2.98	0.0012	85
40	22	2.2	0.0110	27.3	2.73	0.0006	96

conc. of Zr-TiO ₂ [mg/L]	between 0-5 min			between 60-180 min			final abatement [%]
	rel. A [%]	abs. A [mg/L]	r [min ⁻¹]	rel. A [%]	abs. A [mg/L]	r [min ⁻¹]	
ibuprofen							
10	5	0.5	0.0100	38	3.8	0.0032	56
20	6	0.6	0.0060	40	4.0	0.0017	71
40	11	1.1	0.0055	29	2.9	0.0006	89
tetracycline							
10	4	0.4	0.0080	20	2.0	0.0017	37
20	5	0.5	0.0050	27	2.7	0.0011	55
40	8	0.6	0.0030	30	3.0	0.0006	70

conc. of ZnO _e [mg/L]	between 0-5 min			between 60-180 min			final abatement [%]
	rel. A [%]	abs. A [mg/L]	r [min ⁻¹]	rel. A [%]	abs. A [mg/L]	r [min ⁻¹]	
ibuprofen							
10	3.3	0.33	0.0066	21.7	2.17	0.0018	31
20	4.9	0.49	0.0049	18.9	1.89	0.0008	50
40	5.5	0.55	0.0028	32.2	3.22	0.0007	71
tetracycline							
10	1.6	0.16	0.0032	25	2.5	0.0021	55
20	1.6	0.16	0.0016	19.6	1.96	0.0008	65
40	6.5	0.65	0.0033	19.2	1.92	0.0004	74

conc. of ZnO _w [mg/L]	between 0-5 min			between 60-180 min			final abatement [%]
	rel. A [%]	abs. A [mg/L]	r [min ⁻¹]	rel. A [%]	abs. A [mg/L]	r [min ⁻¹]	
ibuprofen							
10	5.5	0.55	0.0110	11.1	1.11	0.0009	19
20	4.2	0.42	0.0042	11.9	1.19	0.0005	27
40	6.3	0.63	0.0032	35.6	3.56	0.0007	60
tetracycline							
10	0.9	0.09	0.0018	25	2.50	0.0021	50
20	1.1	0.11	0.0011	25.3	2.53	0.0011	57
40	6	0.60	0.0030	23.5	2.35	0.0005	64

Table 15. Data of the relative absorption of ibuprofen and tetracycline (10 ppm) in water during photocatalytic treatment over titania, Zr-TiO₂ and ZnO photocatalysts (cat conc.: 40 and 100 mg/L). Catalysts loading calculated after 30, 60 and 120 min.

ibuprofen	10 ppm of IBP 100 mg/L of cat				10 ppm of IBP 40 mg/L of cat			
	TiO ₂		Zr-TiO ₂		ZnO _e		ZnO _w	
Time [min]	rel. Ads [%]	loading [mg/mg]	rel. Ads [%]	loading [mg/mg]	rel. Ads [%]	loading [mg/mg]	rel. Ads [%]	loading [mg/mg]
30	1.4	0.0014	18	0.0180	12	0.0300	7	0.0175
60	5	0.0050	19	0.0190	15	0.0375	11	0.0275
120	4.3	0.0043	17	0.0170	16	0.0400	13	0.0325

tetracycline	10 ppm of TC 40 mg/L of cat				10 ppm of TC 40 mg/L of cat			
	TiO ₂		Zr-TiO ₂		ZnO _e		ZnO _w	
Time [min]	rel. Ads [%]	loading [mg/mg]	rel. Ads [%]	loading [mg/mg]	rel. Ads [%]	loading [mg/mg]	rel. Ads [%]	loading [mg/mg]
30	0	0	5	0.0125	16	0.0400	12	0.0300
60	0	0	13	0.0325	21	0.0525	15	0.0375
120	0	0	0	0	22	0.0550	16	0.0400

It is finally concluded (Tab. 16) that:

- 1) Titania shows the best photocatalytic performance with very high final abatement.
- 2) In tendency, higher IBP abatement over titania and lower over ZnO is observed. This is related to the different adsorption behaviors of these materials.

Adsorption data show that titania has very low adsorption in the order:

adsorption of IBP > adsorption of TC

and ZnO has very high adsorption in the order:

adsorption of TC > adsorption of IBP.

The high onset activity of titania is assigned to the presence of highly reactive electron holes species (of high oxidation power) and titania redox ($\text{Ti}^{3+}/\text{Ti}^{4+}$) pairs on the titania surface, compensating the lower adsorption and medium activity. Obviously, the deactivation is faster with titania, due to its high reactivity.

- 3) The doping of titania markedly decreases the onset activity. The onset with Zr-TiO₂ is nearly diminished what leads to lower abatement. The photocatalytic activity is partially compensated by the improved adsorption and slowly catalyst deactivation (high reaction rates).
- 4) Lower photocatalytic activity is observed with ZnO nanoparticles. However, ZnO photocatalyst is known in the literature as a material producing the hydroxyl radicals with high oxidation power.
- 5) Comparison between photocatalysts shows that the best photocatalytic performances are achieved by the presence of high reactive oxidation species (with titania) or by high loading (with ZnO_e).
- 6) The detailed inspections of abatement (at cat-to-sub ration of 1) and adsorption data show that:

ZnO has higher adsorption affinity toward drugs compared to titania based photocatalysts. Adsorption is maintained in the tendency:

$\text{ZnO} > \text{TiO}_2$

This compensates in part lower onset activity of ZnO (less reactive electron holes (h^+) sites), but further medium abatement, which might be also attributed to higher \cdot OH radicals productivity.

Finally, titania posses highly reactive electron holes and high redox potential (due to presence of Ti^{3+}/Ti^{4+} pairs) used for direct oxidation of organics, whereas ZnO has higher efficiency for hydroxyl radicals production. The final photocatalytic abatement can be summarized by order:



- 7) Porous materials like titania/MOF composites and titania nanotubes show very high adsorption, but low onset activity and medium abatement. The deactivation is slower what can be the main advantage for long-term use.

Table 16. The final summary of the photocatalytic and adsorption properties of novel titania and ZnO photocatalysts in the water remediation.

photocatalysts	adsorption	onset activity	2 nd stage activity	final abatement	deactivation
titania	very low	very high	medium	very high	fast
Zr-TiO ₂	medium	low	high	high	slow
ZnO _e	very high	medium	high	medium	medium
ZnO _w	high	low	high	low	fast
porous materials	very high	low	low	medium	slow

List of appendixes

Appendix 1	A 1: Experimental details
Appendix 2	A 2: References
Appendix 3	A 3: Academic achievements

Appendix 1: Experimental details

A 1.1. Photocatalytic materials preparation and characterization

The photocatalytic abatement of two model water pollutants, pharmaceuticals ibuprofen and tetracycline, have been investigated over different types of highly active photocatalytic materials. Titania doped materials as well as porous titania based photocatalysts and zinc oxides have been synthesised and supplied by co-workers of the Vietnamese Academy of Science and Technology in Hanoi in Vietnam (VAST) and of the King Abdulaziz City for Science and Technology (KACST), Riyadh, in Saudi Arabia. All followed photocatalytic materials have been characterized by XRD, N₂ adsorption-desorption isotherms and TEM images.

Titanium dioxide (TiO₂)

The titania TiO₂ can exist in three different phases: anatase, rutile and brookite. These phases have the same fundamental structural octahedron unit (TiO₆) but differ in the arrangement.^[1] In anatase and rutile, the crystal structure consists of an oxygen octahedron frame. The basic building block consists of a titanium atom in the lattice surrounded octahedrally by six oxygen atoms and each oxygen atom is surrounded by three titanium atoms in trigonal arrangement (Fig. 1). Each octahedron in the rutile structure is surrounded by ten neighbouring octahedra (two sharing the edge of octahedron and eight sharing the corner of the octahedron). In the anatase structure, each octahedron is in contact with eight octahedra (four sharing the edge and four sharing the corner). The experimental lattice parameters: for anatase: a=b=3.7842 Å; c=9.5146 Å and for rutile: a=b=4.5937 Å; c=2.9581 Å.^[2] Density of anatase: 3.84 and rutile: 4.26 g/cm³.^[3] Brookite, which has an orthorhombic crystal structure, is usually found in minerals and has no practical importance due to its low stability (structure not shown).^[4]

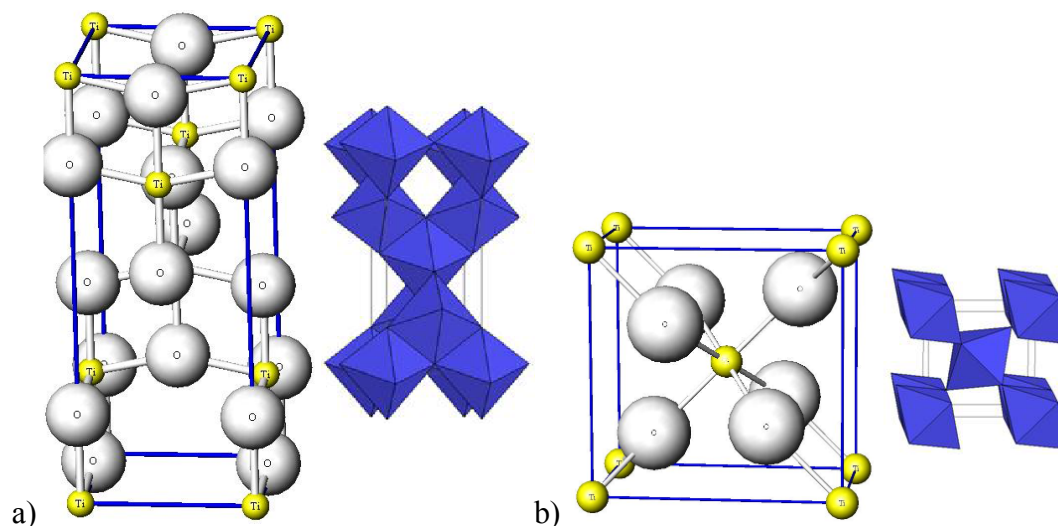


Figure 1. The main crystallographic forms for the TiO₂ phases (left): a) anatase (tetragonal) and b) rutile (tetragonal); Ti (yellow); O (grey); and (right) octahedral structures of different TiO₂ polymorphs.^[5]

The fundamental differences of these two crystalline structures (anatase and rutile) will end up with different properties. They differ in optical properties, band gap values and carrier transport. Rutile, which is the most thermodynamically stable one, has the highest density and the most compact atomic structure.^[6] While, anatase is a metastable phase and it shows superior photocatalytic performance because of fast carrier transport and less electron-hole pairs recombination. The energies of the band gaps of anatase and rutile are 3.2 eV (384 nm)^[7,8] and 3.02 eV (411 nm),^[9,10] respectively. It has been found that in many cases, the anatase phase is photocatalytically more active due to generation of highly energetic holes at the interface, which are strong oxidants. The metastable anatase transforms into the rutile phase irreversibly at the temperature of 700°C~1000°C. This transformation is determined by several factors including crystallite size and impurity levels.^[11,12]

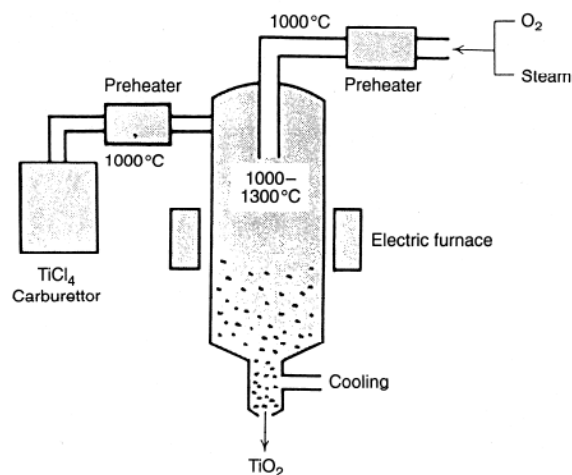
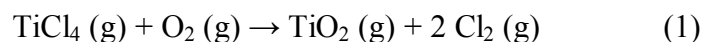


Figure 2. Apparatus for the flame pyrolysis process used for the synthesis of titania P25 (Degussa, Germany).

The main process used in the industrial production of titania P25 is the flame pyrolysis process, also known as the Aerosil® process.^[13] The overall reaction of the process is given in Equation 1.



The method was first employed by Degussa in 1942. The precursor is introduced into hydrogen-oxygen diffusion flame forming molecular or cluster compounds in the gas phase. The particle formation process in the flame pyrolysis is shown in Figure 2. As the aerosol stream leaves the hot temperature zone and cools down, particles are formed through homogeneous nucleation from supersaturated vapor. On the way to the collection zone, particles continuously grow through condensation, surface reactions, and coagulation and aggregation mechanisms. Post-processing like the calcination stage is performed before product collection due to chlorine gas absorption by titania. Finally, particles are collected in a bag house filter, electrostatic precipitator or cyclone separator. Serious operational problems can exist during transport: for example, the particles can be removed from the process stream by diffusion to the reactor walls.^[14] The flame synthesis normally results in micron sized particles, thus careful control and post treatments are required to get nanoparticles.

The resulting titania P25 product is 99.5 % pure and has a composition ratio of 80 to 20 of anatase to rutile.^[15]

The XRD patterns show the pure crystalline anatase and rutile compared with titania P25 (Fig. 3). The titania P25 sample consists of a mixture of anatase with a minor amount of rutile.

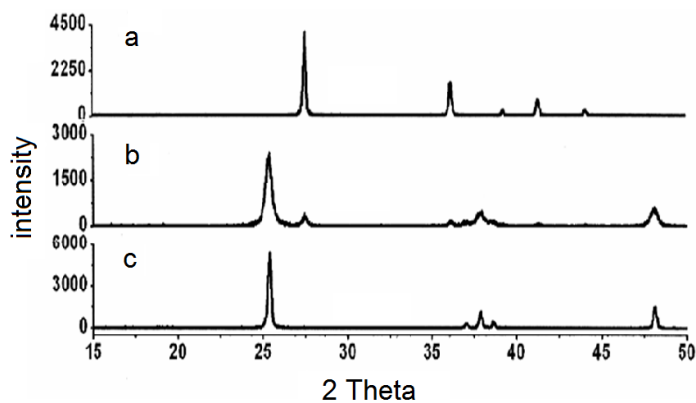


Figure 3. XRD patterns of rutile (a), titania P25 (b) and anatase (c).^[16]

The titania P25 sample consists of agglomerated, round shaped nanoparticles with an average size of 20 nm, confirmed by TEM and SEM images (Fig. 4).

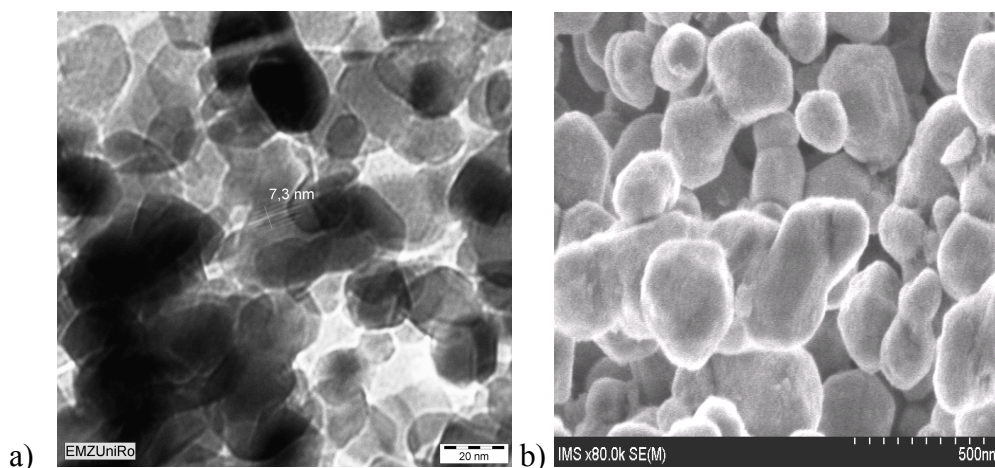


Figure 4. TEM (a) and SEM (b) images of titania P25 photocatalyst.

Figure 5 shows the N₂ adsorption - desorption isotherms of titania displayed adsorption - desorption isotherms characteristic of non - microporous materials with the presence of both meso- and macroporosity (uptake $p/p_0 > 0.8$). The specific surface area amounts *ca.* 55 m²/g.^[17] It contains a very low specific pore volume the pore size distribution showing a maximum at *ca.* 15 nm, probably corresponding to the inter - particle mesoporosity of particle agglomerates. This is consistent with other studies reporting 10 nm pore size mesopores with 200 - 215 nm size agglomerates.^[18]

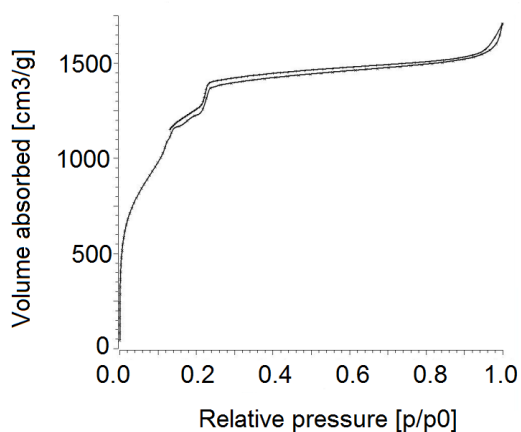


Figure 5. The N₂ adsorption - desorption isotherms of titania P25 (Degussa).^[19]

Doped titania photocatalysts

The zirconium (Zr), iron (Fe) and nitrogen (N) doped TiO₂ materials have been prepared by sol-gel synthesis combined with hydrothermal treatment and finally treated by chemical vapour deposition (CVD) method. All doped titania materials have been provided by the Vietnamese Academy of Science and Technology in Hanoi, Vietnam. The powdered titania precursor, further used for modifications, has been prepared in the following way:

A determined amount of TiCl₄ was added drop wise into *i*-propanol. The resulting solution was introduced into distilled water in an ice-water bath with vigorously magnetic stirring. After that, the pH value of this acidic solution was adjusted to 7 by adding an aqueous ammonia solution to form a white gel. The resulting gel was aged for 24 h at room temperature under stirring condition. The obtained white precipitate was filtered and washed repeatedly with distilled water until complete removal of chloride ions.

Thereafter, the precipitate was well-dispersed by treating in an ultrasonic bath. Then, 30 % H_2O_2 was added drop wise into this mixture under stirring. The resulting yellow transparent solution was poured into an autoclave and heated at 100°C for 20 h. After the hydrothermal treatment, the formed precipitate was washed and dried at 100°C . As a result, a highly disperse TiO_2 powder was obtained, which was further exposed to doping modifications. The N-doped TiO_2 has been prepared by adding the urea solution into sol-gel solution. In case of Zr and Fe doped TiO_2 materials the doping procedure was carried out by chemical vapour deposition (CVD) using zirconyl chloride (ZrOCl_2) and FeCl_3 solutions. This procedure is explained below. The titania precursor was placed into a quartz tube reactor of 2 cm x 25 cm size. Prior to heating, the reaction system was purged with dry nitrogen. Then the TiO_2 precursor was contacted with a nitrogen stream flowing through the vessel containing the ZrOCl_2 or FeCl_3 solution and heated to 350°C . In case of N - doping, the precursor (already treated with urea) was placed in the apparatus and treated with nitrogen stream. After completing deposition, the materials were heated up to 500°C . The resulting doped TiO_2 photocatalysts were washed and calcined in air before photocatalytic testing. The experimental set up is shown in Figure 6.

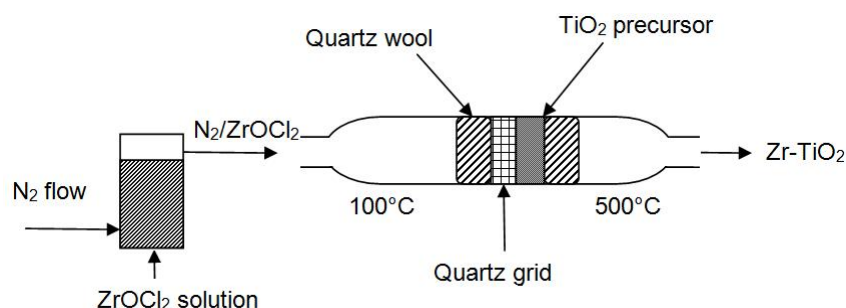


Figure 6. Scheme of Zr-doping of TiO_2 by chemical vapour deposition (CVD) method.

The obtained Zr-doped titania photocatalyst contained *ca.* 5 mol % of zirconium. The XDR pattern (Fig. 7) confirms that the sol-gel derivatives titania indicates the anatase crystal structure (after calcinations at 500°C) with increased crystallinity (narrow peaks).

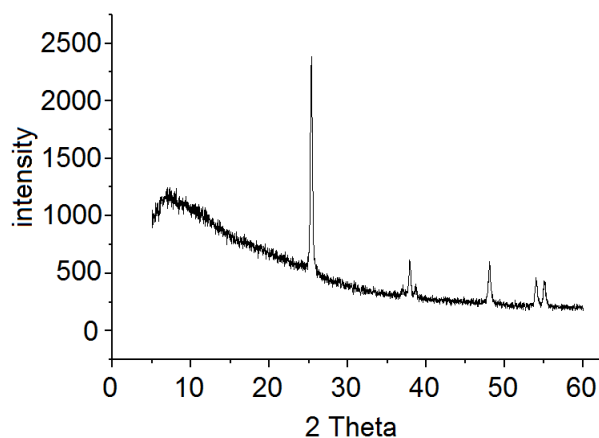


Figure 7. XRD pattern of sol-gel titania after hydrothermal treatment at 500°C.

The prepared 5 % Zr-doped titania adopts an anatase structure. Low concentration of dopant does not change significant the XRD patterns and no additional crystalline phases appear in the sample. Doping with N and Fe elements did not markedly influence the crystal structure and texture, which may be due to low concentration used, what was also observed by Lukáč et al.^[20]

The TEM image shows that the Zr-doped TiO₂ material consists of inter - grown nanoparticles. The particles are compact and with regular shapes, 10 - 15 nm small and agglomerated (Fig. 8). The agglomerates contain mesopores between the Zr-TiO₂ crystals.

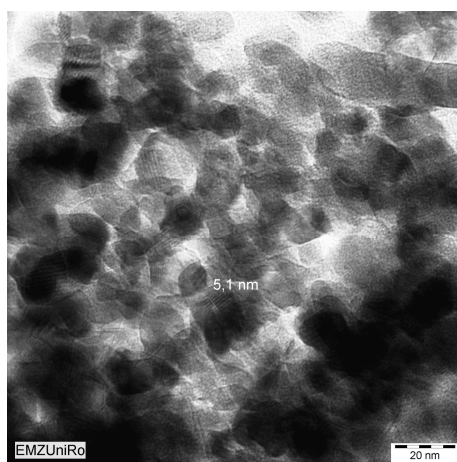


Figure 8. TEM image of Zr-TiO₂ photocatalyst.

The BET surface area of Zr-TiO₂ amounts to 100 m²/g. The nitrogen adsorption-desorption isotherms of Zr-TiO₂ shows an additional adsorption step with a slight

hysteresis at relative nitrogen pressure (p/p_0) of 0.7 - 0.9 due to the presence of mesopores (Fig. 9). The mesopore volume of Zr-TiO₂ amounts to 0.25 cm³/g. The BJH desorption analysis shows uni-modal mesopores with relative narrow size distribution having the pore size maximum at *ca.* 8-9 nm.

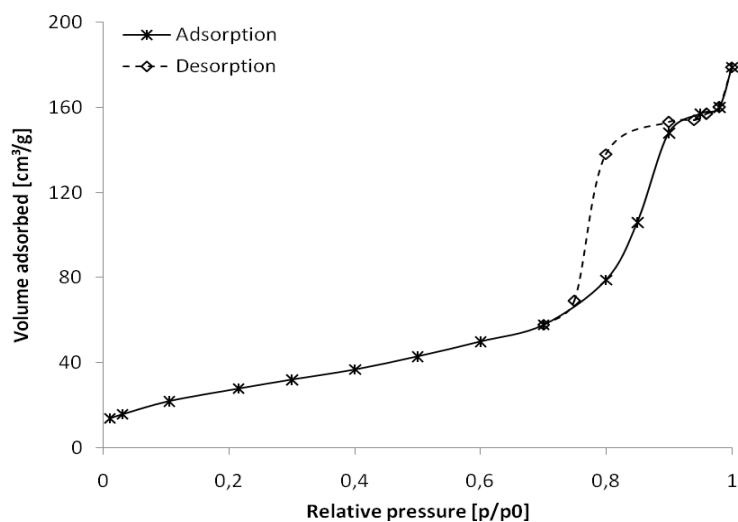


Figure 9. Nitrogen adsorption-desorption isotherms of Zr-TiO₂ photocatalyst.

Titania nanotubes (TNs)

Titania nanotubes are low crystalline titania materials with tubular (needle-like) shape containing one-dimensional round pores of uniform size ranging usually from *ca.* 5 - 30 nm. TN particles are obtained by hydrothermal treatment of titania. These structures are composed of TiO₆ octahedron sheets connected by edges and corners. The TiO₆ octahedron in titania nanotubes and its comparison with TiO₆ octahedron of rutile is presented in Figure 10.

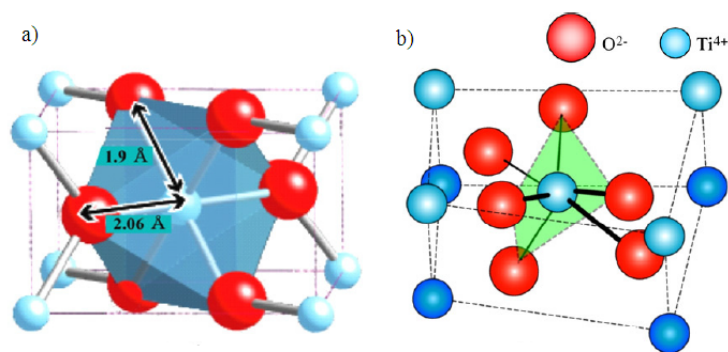


Figure 10. Comparison of titania structures: (a) TiO₆ octahedron in rutile TiO₂ and (b) TiO₆ octahedron in titania nanotubes (TNs).^[21]

However, in the literature there is lack of comprehensive understanding of the building blocks of titania nanotubes, the proposed structure of the anatase unit cell in titania nanotubes is shown in Figure 11. The unit cell of anatase is cleaved in the [001] direction with a spacing of 8.7 Å and give a possible delaminated form of anatase. Titania nanotubes are composed of delaminated anatase, where these layers are located in [001] direction.

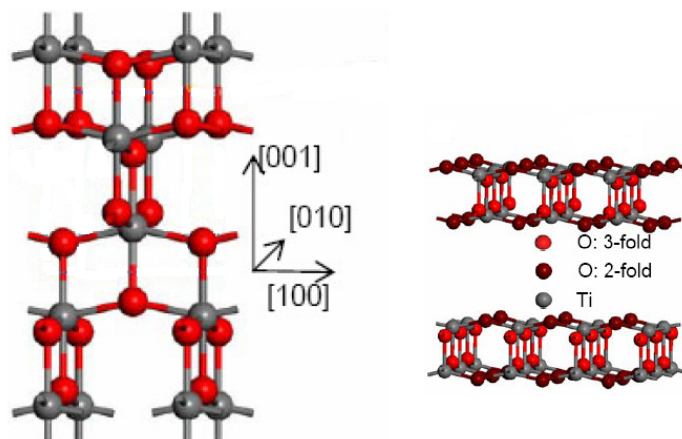


Figure 11. Comparison of the unit cells of (left) anatase and (right) sheets of titania nanotubes made of delaminated anatase.^[22]

The crystalline raw material is first converted to an amorphous product through alkali treatment, and subsequently, titania nanotubes are formed after treatment with distilled water and HCl aqueous solution.

The formation and transformation of nanotubes prepared by the NaOH treatment and post-treatment washing is summarized in Figure 12.

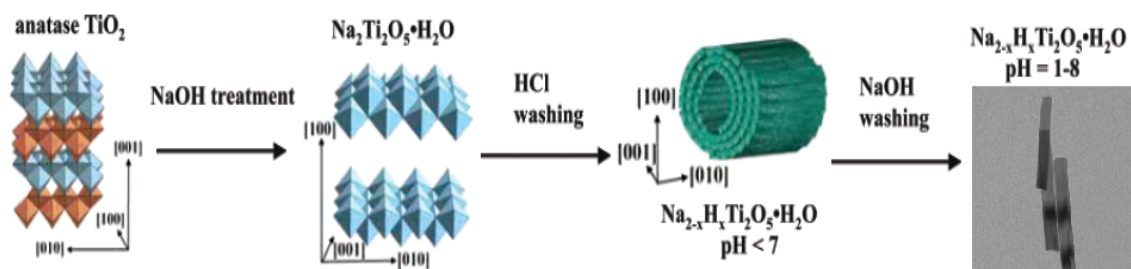


Figure 12. Overall scheme for the formation and transformation of nanotubes induced by the NaOH treatment and the post-treatment washing.^[23]

During NaOH treatment, some of the Ti-O-Ti bonds are broken, forming an intermediate containing Ti-O-Na and Ti-OH. These intermediates would proceed with rearrangement to form sheets of edge sharing TiO_6 octahedra with Na^+ and OH^- intercalated between the sheets. The formed structure is $\text{Na}_2\text{Ti}_2\text{O}_5 \cdot \text{H}_2\text{O}$ (i.e. $\text{Na}_2\text{Ti}_2\text{O}_4(\text{OH})_2$). The sodium titanate exhibits layers of the TiO_6 octahedra edge shown in a zigzag configuration (Figure 12 b) which is unit layer of the anatase TiO_2 projected along [101] (Figure 12 a). If the two longer Ti-O bonds in the TiO_6 octahedra are broken, the anatase TiO_2 would transform into the layered titanate. The formed $\text{Na}_2\text{Ti}_2\text{O}_5 \cdot \text{H}_2\text{O}$ can exchange ions Na^+ with H^+ in the post-treatment acid washing. The exchange would result in a variation of the surface charge, leading to a peeling-off of the individual layers of the titanate and subsequent scrolling of the layers into nanotubes (Figure 12 c). The x value of the nanotube structure, $\text{Na}_{2-x}\text{H}_x\text{Ti}_2\text{O}_5 \cdot \text{H}_2\text{O}$, would increase with the acidity of the post-treatment. During this transformation, the titanate framework would shrink by reducing the interlayer distance and can then transform into titanate nanotubes (Figure 12 d) via a soft-chemical route, i.e. by backwashing with NaOH. Further increase the pH value in the backwashing to above pH of 8, would form crystalline titania plates.

In our laboratory the synthesis of titania nanotubes were carried out by hydrothermal treatment as follow:

A 1 g of titania (Degussa P25) was introduced into a Teflon autoclave (80 mL) containing 60 mL 10 M NaOH.

The suspension was stirred for 1 h and then ultrasonically treated for 1 h in order to receive a sufficient dispersion of titania particles in the reaction mixture. Then, the autoclave was heated up constantly to 150°C for 24. After hydrothermal treatment the NaOH solution was decanted and the precipitate was dispersed in 0.01M HCl and washed until neutral. Finally, the precipitate was dried in air for 48 h (as-synthesized TN) and calcined at 700°C for 1h (sample denoted as TN_700).

Figure 13 shows the XRD patterns of titania nanotubes. As it was former observed, the starting material titania is composed of the anatase co - existing with rutile phases (compare Fig. 3). After chemical treatment the TiO_2 nanoparticles were transformed into tubular morphology (titania nanotubes). The XRD pattern shows the typical

reflections observed with as-synthesized TiO₂ nanotubes (Fig. 13 left).^[24] The peaks are broadened and of low intensity indicating the low crystallinity of the material. However three reflections located at 2 Theta at 24, 28 and 48° have been assigned to titanates such as A₂Ti₂O₅·H₂O (A indicates Na⁺ or H⁺ ions).^[25-27] These results are in line with other study.^[28]

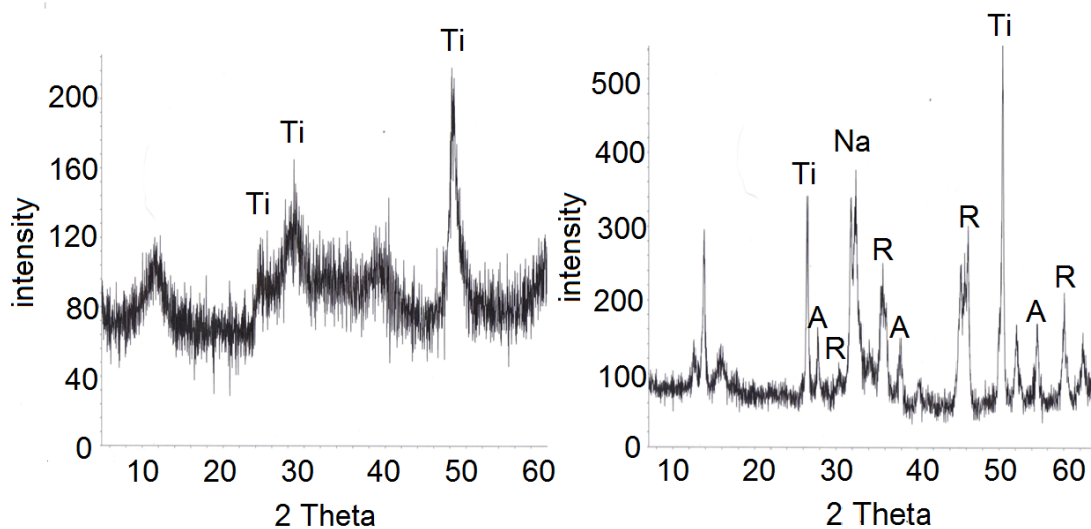


Figure 13. XRD patterns of titania nanotubes (left) as-synthesized (TN) and (right) calcined at 700°C (TN_700); fraction of Ti-titanates, A - anatase, R - rutile phases and Na - sodium hexatitanate.

The further thermal treatment (calcination) of titania nanotubes changes the structure of the material, indicating limited thermal stability. After calcination at 700°C, the crystallinity of TiO₂ nanotubes increases, but still is low what is confirmed by low intensities of X-ray reflections. This observation is in good agreement with other studies.^[29] The tubular elongated structures are changed to different shaped particles as seen with TEM (Fig. 14). Besides of some titanates, indicated by X-ray reflections at 2 Theta at 24 and 48°,^[30] also sodium hexatitanate is found in the material giving rise to a peak of high intensity at 2 Theta at 30°.^[31] Also some anatase (A) and rutile (R) is present in the calcined TN^[32] (Fig. 13 right). The crystallinity of the material is still low (amorphous-like).

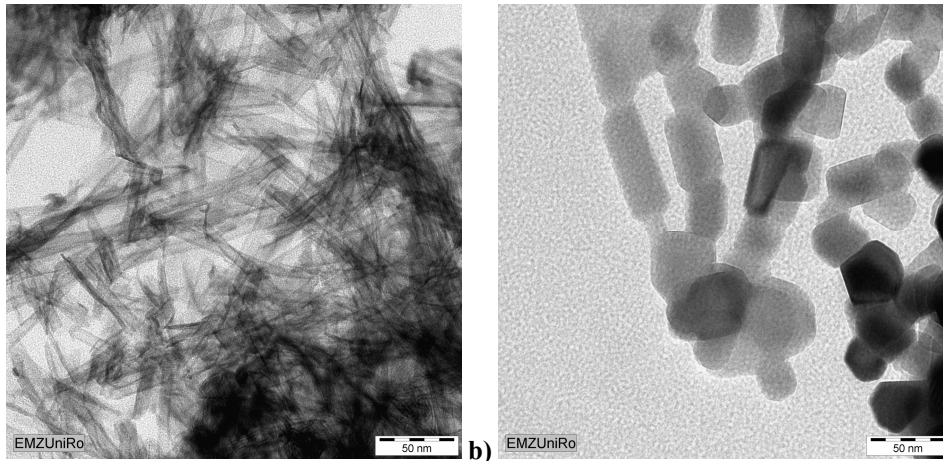


Figure 14. TEM images of titania nanotubes (a) as-synthesized (TN) and (b) calcined at 700°C (TN_700).

The TEM images show titania nanotubes obtained by a hydrothermal treatment (Fig. 14). The as-synthesized titania nanotubes are uniform along their length (inner and outer diameters) and have diameters of *ca.* 10 nm and lengths of hundreds of nanometers (Fig. 14 a). Further calcination at 700°C shows the changing in the titania structure by forming spherical particles of *ca.* 20 to 50 nm size (Fig. 14 b).

The nitrogen adsorption-desorption isotherms of titania nanotubes are shown in Figure 15.

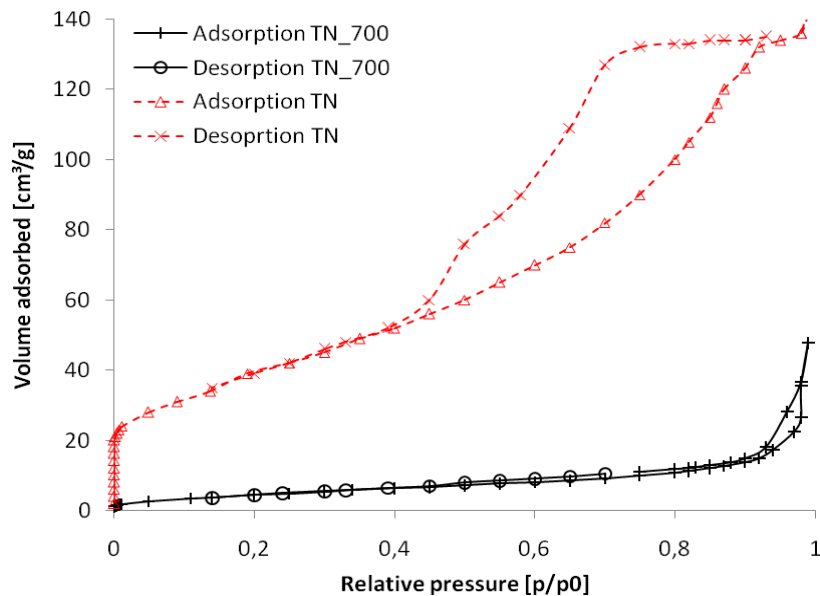


Figure 15. Nitrogen adsorption-desorption isotherms of titania nanotubes.

The hollow tubular structures of as-synthesised titania nanotubes have a specific surface area of 105 m²/g. The adsorption isotherm shows an additional adsorption step

with a slight hysteresis at relative nitrogen pressure (p/p_0) of 0.4 - 0.8 (desorption branch). This indicates that the product is mesoporous (2 - 50 nm) in contrast to the starting material titania P25. The mesopore volume of as-synthesized TN amounts to $0.216 \text{ cm}^3/\text{g}$ having the pore size maximum of *ca.* 4.3 nm. Whereas the BET surface area of titania nanotubes calcined at 700°C is markedly decreased to $14 \text{ m}^2/\text{g}$. At the same time the specific pore volume is decreased from 0.216 and $0.06 \text{ cm}^3/\text{g}$. This finding is confirmed by other studies; where calcination markedly influenced the specific surface areas of TNs decreasing the specific surface area from 225 to $18 \text{ m}^2/\text{g}$ after calcination at 700°C .^[33] The high surface area of the as-synthesized TN and nanotubular structure has been found to be maintained up to *ca.* 400°C . At 450°C a sudden decrease to $100 \text{ m}^2/\text{g}$ occurs.^[34]

In conclusion, the calcination of nanotubes and formation of titania particles at 700°C is accompanied by markedly loss of porosity and decrease of specific surface area, suggesting the collapse the tube structure.

Titania/MIL-101 composite and MIL-125 photocatalyst

Chromium-titania composites Ti/MIL-101 based on metal organic framework possess the chromium sites in the MOF structure. TiO_2 was inserted by depositions of hydrolysed titania tetrachloride. The structure of as-synthesized MIL-101 is given in Figure 16.

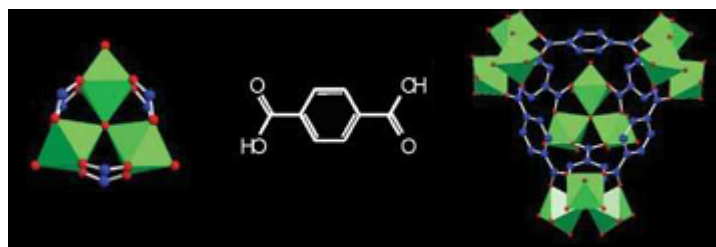


Figure 16. Representative MIL-101 structures consisted of tetrahedron building units (ST) shows the trimeric building block chelated by three carboxylic functions (left). The ST was constructed with (middle) terephthalic acid, which lies (right) on the edges of the ST. Chromium octahedra, oxygen, fluorine and carbon atoms are in green, red, and blue, respectively.^[35]

In detail, the MIL-101 precursor, used further for the preparation of Ti/MIL-101 is composed of inorganic trimeric octahedral chromium metal building blocks and alternative arranged organic 1,4-benzene dicarboxylate (BDC) linker as primary units.

They form so-called supertetrahedral secondary units (ST) building up the ordered and highly porous crystalline framework of the chemical composition $[(Cr_3X(H_2O)_2O(O_2C-C_6H_4-CO_2))]_3 \cdot 25H_2O$, with $X = F, OH$. The pore system of MIL-101 consists of two different sized extra-large cages. The smaller one is accessible via pentagonal windows of *ca.* 12 Å size. The larger cage has both pentagonal (12 Å) and hexagonal windows of *ca.* 14.5 × 16 Å size. The two large cages are delimited by 20 and 28 ST units, respectively. The ST units are microporous with trigonal pore openings of *ca.* 8.6 Å and can be considered as “side pockets” of the walls of the large cavities.^[35] MIL-101 material was typically synthesized in the following way:

A solution containing chromium(III) nitrate 16 g $Cr(NO_3)_3 \cdot 9H_2O$ + 192 ml H_2O was added 8 ml hydrofluoric acid (5M) and 6,56 g 1,4-benzene dicarboxylic acid (H_2BDC) under stirring in 2 hours. The mixture was put into the autoclave and heated at 220°C for 9 h. To eliminate most of the carboxylic acid, the mixture was filtered first using a large pore (Attman n°2) paper filter (n°2); the water and the fresh MIL-101 powder passes through the filter while the free acid stays inside the glass filter. Then, the MIL-101 powder is separated from the solution using a small pores (n°5) paper filter. To remove H_2BDC in MIL-101 pore, the obtained powder was treated in ethanol at 100°C in 22 hours, then filtered, washed and dried (Fig. 17 left).

Preparation of Ti/MIL-101 was carried out as followed:

100 ml solution of TBOT in *i*-PrOH (0.25 M) was added to 2 g of activated MIL-101 under vigorous stirring at room temperature during 20 hours. The resulting solid, MIL-101 was washed by *i*-PrOH to remove excess of TBOT before treated in hydrothermal condition at 220°C in 4 hours. Finally, the powder was filtered, washed and dried at 110°C in 2 hours (Fig. 17 right). The titanium content was determined by EDX. Obtained composite samples are denoted Ti/MIL-101 containing 6.6 and 10.94 Ti (wt.%). The

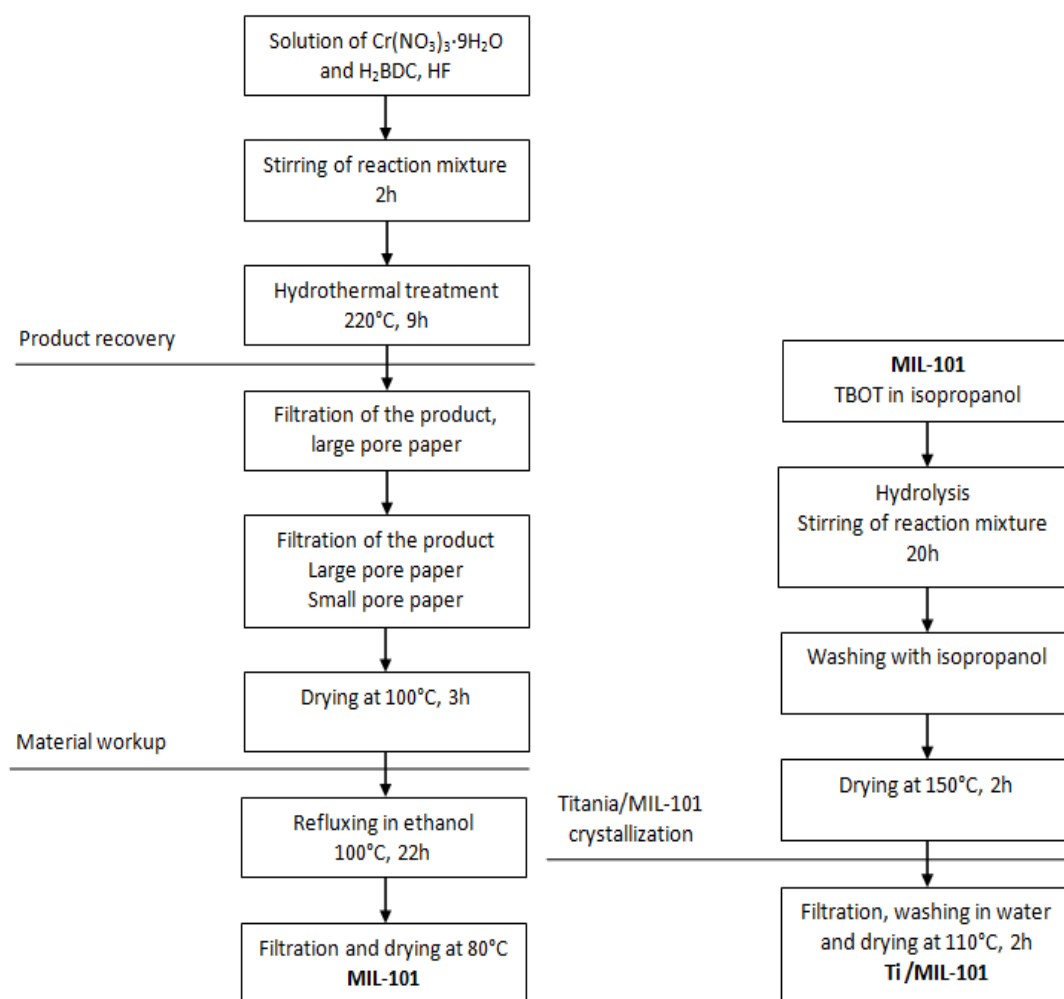


Figure 17. Synthesis scheme of the precursor MIL-101 (left) and Ti/MIL-101 composite (right).

XRD pattern of Ti/MIL-101 is given in Figure 18. The obtained diffraction pattern is in agreement with the simulated one confirming the formation of the MIL-101 structure.^[35,36] The diffractogram shows resolved and narrow reflections indicating a well-crystallized MIL-101 material with the characteristic peaks at the 2 Theta of 1,9°, 2,8°, 4,9° and 9°.^[37] It was proved that the MIL-101 structure was not broken by loading of TiO₂. The modification of MIL-101 with titania does not change markedly the crystallinity of MOF material. In addition, X-ray diffraction of TiO₂ loaded MIL-101 materials shows a broadened peak at 2 Theta of 25° belonging to anatase evidencing that the obtained materials is an anatase/MIL-101 composite.

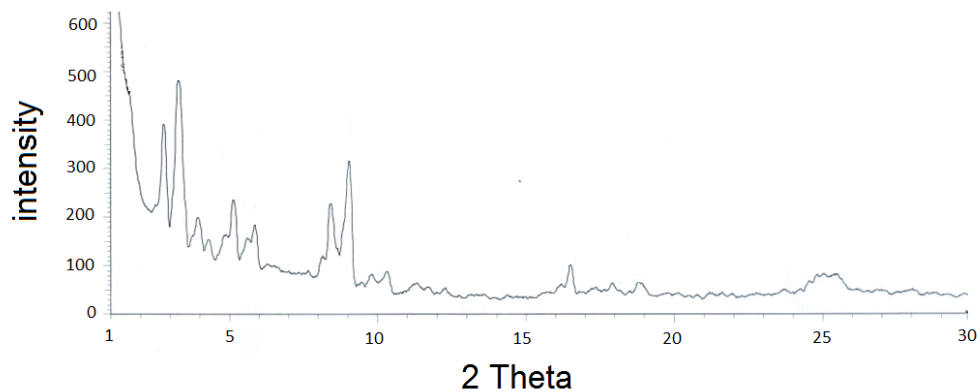


Figure 18. XRD pattern of Ti/MIL-101 composite.

TEM and SEM images show highly agglomerated particles of Ti/MIL-101. The particles of titania is < 10 nm. They form clumps of particles (Fig. 19 and 20).

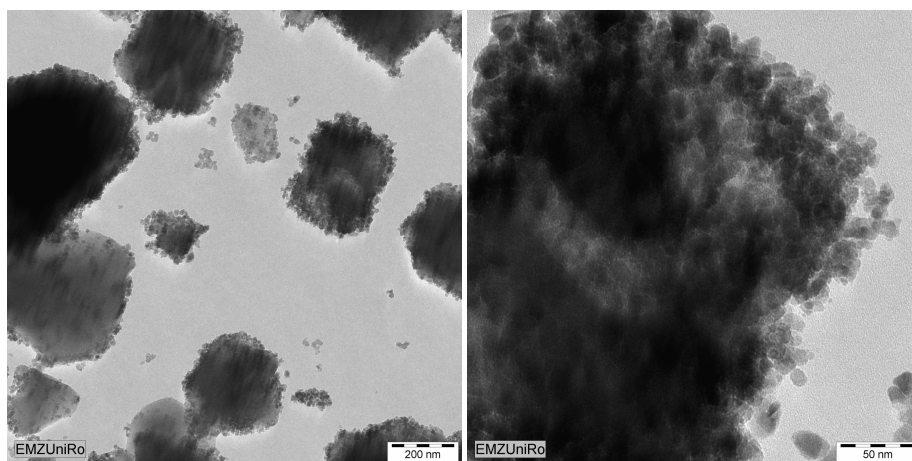


Figure 19. TEM images of Ti/MIL-101 at different magnifications; Ti content of 10.94 Ti (wt%).

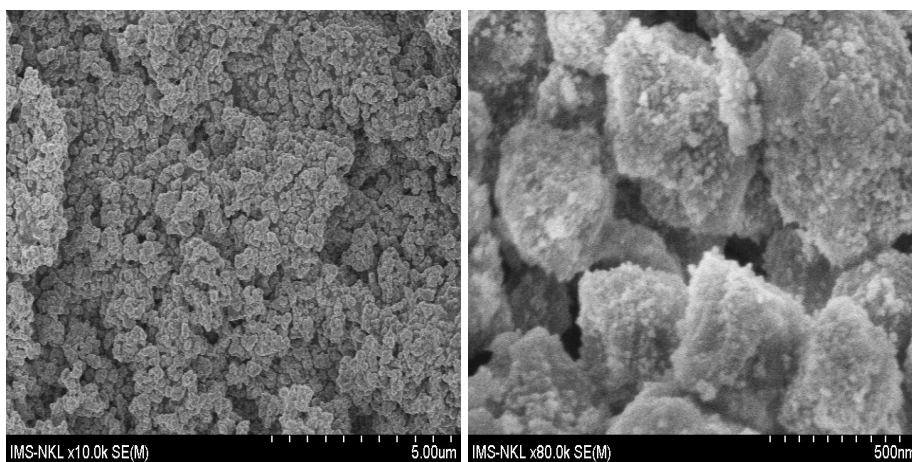


Figure 20. SEM images of Ti/MIL-101 at different magnifications.

The nitrogen adsorption-desorption isotherms of the sample is shown in Figure 21. The adsorption isotherm shows three distinct adsorption steps. At a very low relative pressure up to p/p_0 of 0.01, the uptake curve shows a very steep increase. It is assigned to the filling of micropores. Between the relative pressure of p/p_0 of 0.01-0.2, the slope of the adsorption isotherm decreases. This second step is related to the filling of small mesopores followed by a third step near p/p_0 of 0.25 of final pore filling. Further nitrogen uptake at the high relative pressure above p/p_0 of 0.8 is due to textural porosity. The similar, characteristic adsorption isotherms are former reported in studies.^[38] The well resolved adsorption steps of the isotherm and the high uptake confirms the formation of the well crystallized MIL-101. The BET area of the prepared MIL-101 is of very high value and amounts 4703 m^2/g .

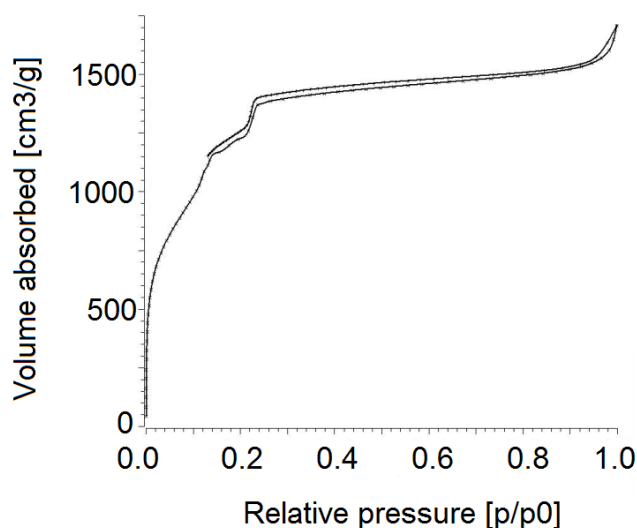


Figure 21. N_2 adsorption and desorption isotherm of the MIL-101 measured at -196°C .

The photocatalytic activity of Ti/MIL-101 has been compared with the metal organic framework MIL-125. Both materials possess the terephthalic acid linker. MIL-125 (Ti) or $\text{Ti}_8\text{O}_8(\text{OH})_4[\text{O}_2\text{C}-\text{C}_6\text{H}_4-\text{CO}_2]_6$ material possess the titania (Ti) isolated sites in the MOF framework (titania octahedron rings as metalsites) (Fig. 22). The preparation procedure is presented in the literature.^[39] MIL-125, the first example of a highly porous and crystalline titanium (IV) dicarboxylate MIL material shows a high thermal stability and photochemical properties. Its structure is built up from a pseudo cubic arrangement of octameric wheels, built up from edge- or corner-sharing titanium

octahedra, and terephthalate dianions leading to a three-dimensional periodic array of two types of hybrid cages with accessible pore diameters of 6.13 Å and 12.55 Å.

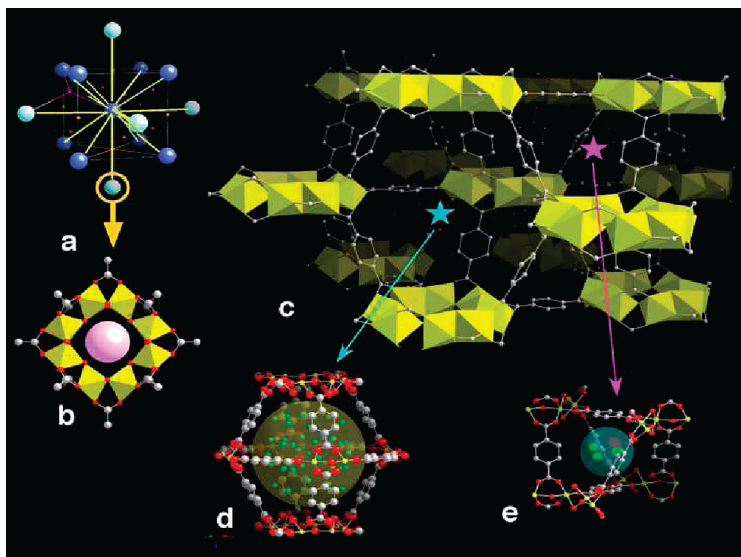


Figure 22. (a) Perspective view of a centered cubic (cc) arrangement; the 12-fold coordination is evidenced by yellow lines. Purple and orange dots indicate the positions of the centers of the tetrahedral and octahedral vacancies. (b) View of the perforated cyclic octamer with edge- and corner sharing Ti octahedra; it corresponds to the atom with an orange circle of the classical cc packing through the SBU augmentation. (c) Perspective view of MIL 125 with the central octamer surrounded by 12 others; the pink and blue stars indicate the centers of the tetrahedral and octahedral vacancies in MIL 125. (d) Ball and stick representation of the octahedral vacancy, filled by water molecules (in green); the large yellow sphere represents the effective accessible volume of the cage. (e) The tetrahedral vacancy; in (d) and (e) the color code is as follows: carbon, gray; oxygen, red; water, green; titanium, yellow.^[39]

TEM images shows that the MIL-125 material consists of agglomerated small nanocrystals (Fig. 23). The particles have a size of *ca.* 100 nm. A high textural porosity of the MIL-125 is observed with combined micro - meso - macro pore system (isotherms not shown). Nitrogen sorption measurements gave a BET surface area of 1360 m²/g. Further characterization is given in literature.^[39]

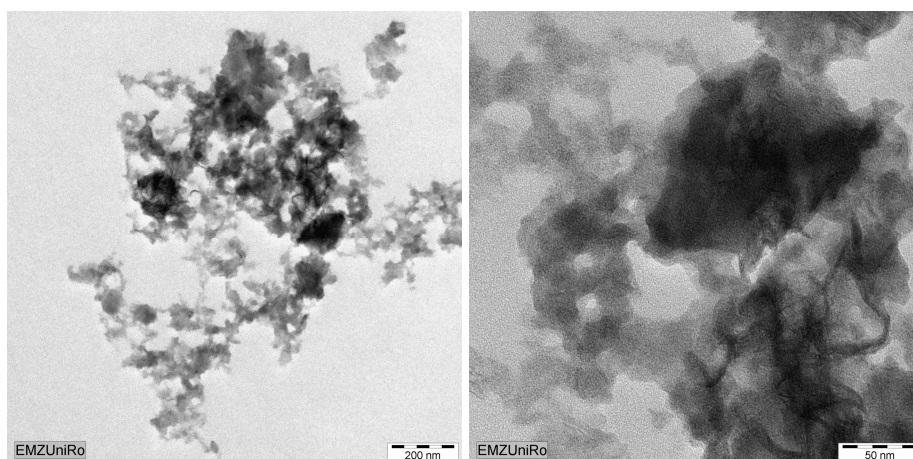


Figure 23. TEM images of MIL-125 photocatalyst at different magnifications.

Zinc oxide nanoparticles (ZnO)

Zinc oxide crystallizes in the hexagonal wurtzite structure type. The crystal structure of zinc oxide is given in Figure 24. ZnO exhibits similar oxidation properties to TiO₂, including the formation of [•]OH radicals and the direct oxidation by photogenerated holes.^[40] ZnO is reported to be as reactive as TiO₂ under concentrated sunlight, as the band gap energy of ZnO is almost equal to that of TiO₂ (i.e., 3.1 - 3.2 eV).^[41] Also a larger band gap of 3.37 eV^[42] has been reported for pure ZnO. The density of ZnO is 5.6 g/cm³.^[43]

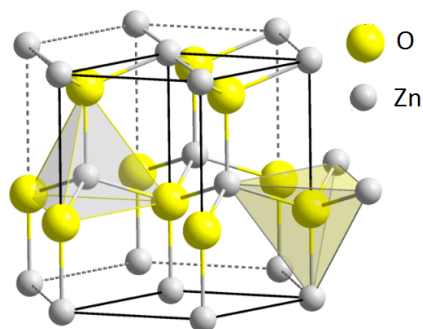


Figure 24. The structure of ZnO (source: www.en.wikipedia.org).

Depending on the solvent, precipitation either in water (ZnO_w) or in ethanol (ZnO_e), two types of ZnO of different size were prepared. The ZnO nanoparticles have been synthesized by a soft precipitation performed in the following way. *Ca.* 30 mmol of zinc nitrate hexahydrate were dissolved in 60 mL of H₂O at room temperature under

continuous magnetic stirring. In a separate beaker, 60 mmol of CHA were dissolved in 20 mL of water at room temperature. The CHA solution was poured into the zinc solution. A white precipitate was formed upon magnetic stirring. An extra amount of 80 mL of water was added to the reaction mixture, which was left stirring for four days. The precipitate was filtered off through an F-size fritted filter, and then washed with 100 mL of H₂O. The precipitate was dried under vacuum for one day. Thereafter, it was suspended in 300 mL of water and magnetically stirred for one day, then filtered off and dried. Alternatively the synthesis was carried out in the same way in EtOH to obtain smaller ZnO nanoparticles (ZnO_e). All samples were calcined at 500°C for photocatalytic use.

Figure 25 shows the XRD patterns of two nanosized zinc oxides prepared from aqueous and ethanolic solutions. The reflections of as-prepared materials are broader indicating some structural disorder or formation of small crystallites in the as-prepared samples, especially in case of precipitation from ethanol. Calcination of the samples increased the crystallinity of materials. Both materials show similar crystallite sizes of average size of *ca.* 29 nm.

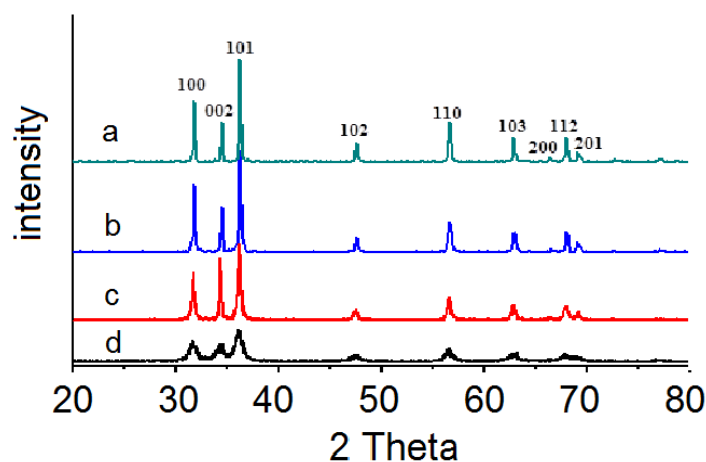


Figure 25. XRD patterns of nanosized zinc oxides prepared by precipitation from aqueous (ZnO_w) and ethanolic (ZnO_e) solutions. From top to bottom: a) ZnO_w calcined at 500°C, b) ZnO_e calcined at 500°C, c) as-prepared ZnO_w and d) as-prepared ZnO_e.

The TEM images confirm the crystallization of zinc oxide nanoparticles (Fig. 26). The particle obtained with H₂O are larger (*ca.* 100 nm) than those obtained from EtOH solution (*ca.* 15 - 30 nm). ZnO_e nanoparticles are uniform shaped and

agglomerated. The replacement of ethanol by water leads to rapid precipitation of ZnO and formation of the large non-uniform nanoparticles.

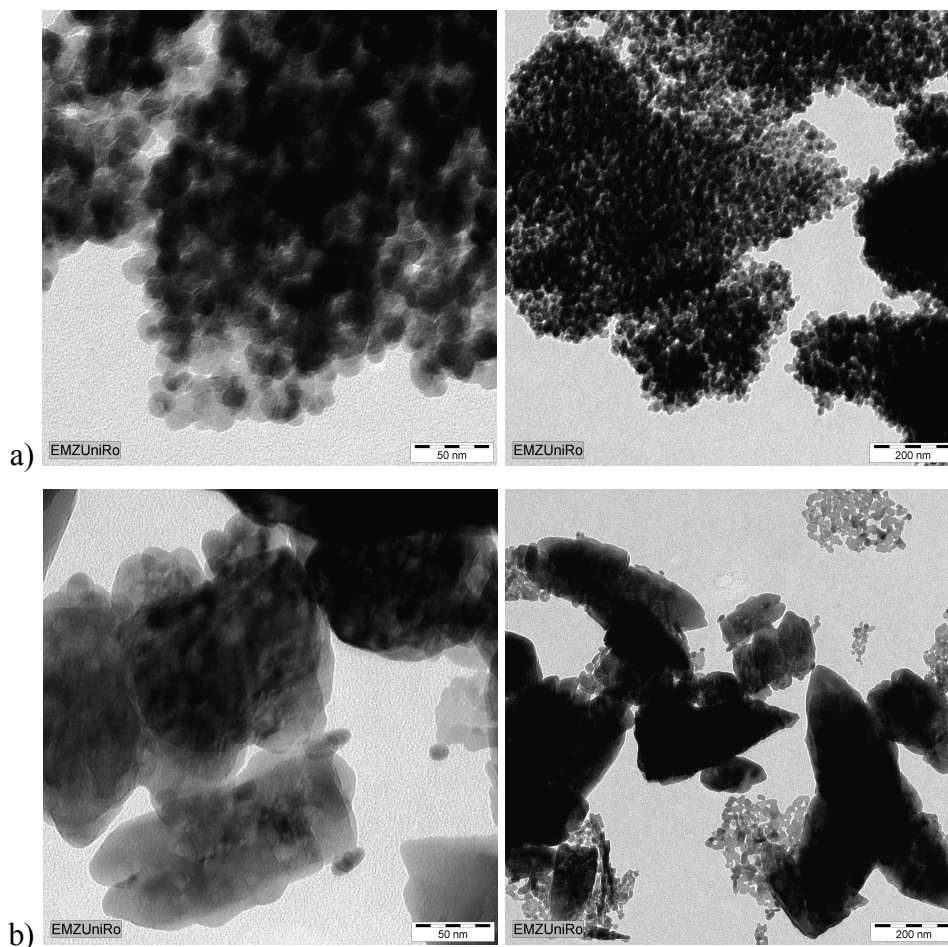


Figure 26. TEM images of ZnO nanoparticles precipitated from a) ethanol (ZnO_e) and b) water (ZnO_w).

The nitrogen adsorption isotherms are shown in Figure 27. They show a low nitrogen uptake at low pressure. In case of ZnO_e an additional increase of the isotherm at $p/p_0 > 0.8$ indicates the presence of nanoporosity. The specific surface areas are *ca.* 8 m²/g for the zinc oxide derived from aqueous solution (ZnO_w) and *ca.* 40 m²/g for the material obtained in ethanol (ZnO_e), reflecting the different nanoparticle sizes (compare Fig. 26).

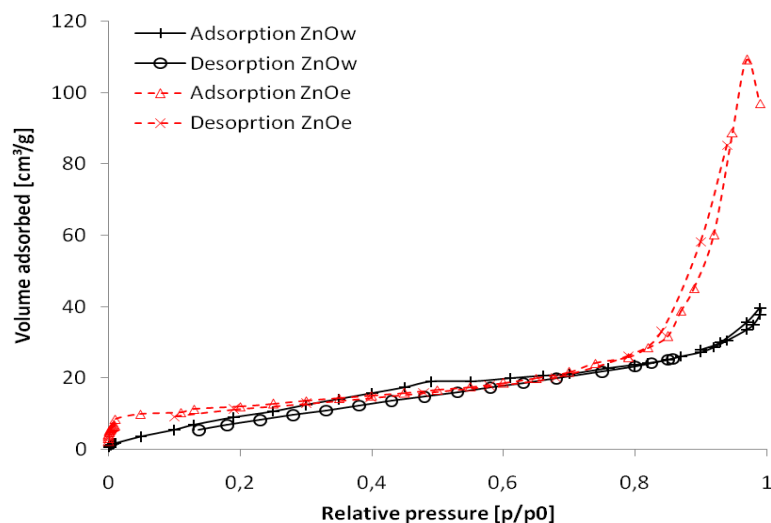


Figure 27. Nitrogen adsorption-desorption isotherms of zinc oxide photocatalysts.

A 1.2. Photocatalytic testing and experimental procedure

Materials

Two model pharmaceuticals have been chosen as new emerging water pollutants i.e. an antibiotic tetracycline and a non-steroidal anti-inflammatory drug ibuprofen. Tetracycline chloride (TC) 95% ($C_{22}H_{24}N_2O_8 \cdot HCl$) was purchased from Sigma (Fig. 28 a). Ibuprofen sodium salt (IBP) 98 % ($C_{13}H_{17}O_2Na$) was supplied by Sigma-Aldrich (Fig. 28 b).

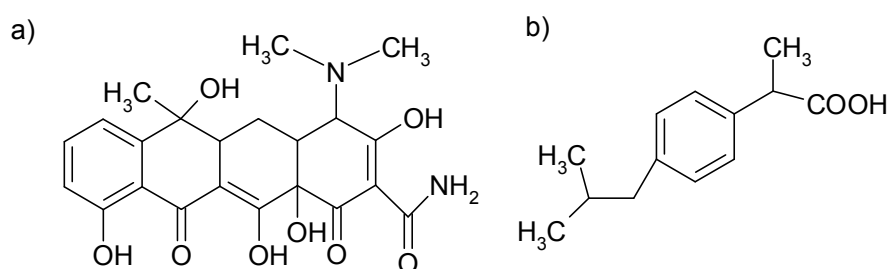


Figure 28. Structures of a) tetracycline and b) ibuprofen.

Ibuprofen is an organic compound belonging to the class of propionic acid derivatives. Ibuprofen as a non-steroidal anti-inflammatory drugs (NSAID's) is used to treat mild pain and lower fevers. It is a stable white crystalline powder slightly soluble in water. Ibuprofen is a weak acid ($pK_a = 4.4$).^[44]

Tetracycline consists of four six - membered rings usually denoted as A, B, C and D.^[45] The stereochemistry is very complex since carbon atoms 4, 4 a, 5, 5 a, 6 and 12 a can, in principle, be asymmetrically substituted. Depending on the pH of the solution, tetracycline is presented in different protonated states (Fig. 29). In aqueous solution, the first deprotonation of the fully protonated species, termed ab^+c occurs at $pK_a = 3.1 - 3.5$. This step leads immediately to the zwitterionic form of the neutral compound a^-b^+c , which represents a non-ionised form (abc). In case of large difference of $pK_{a2} = 7.2 - 8.5$ and $pK_{a3} = 9 - 10.9$, there is no doubt about the complete deprotonation.

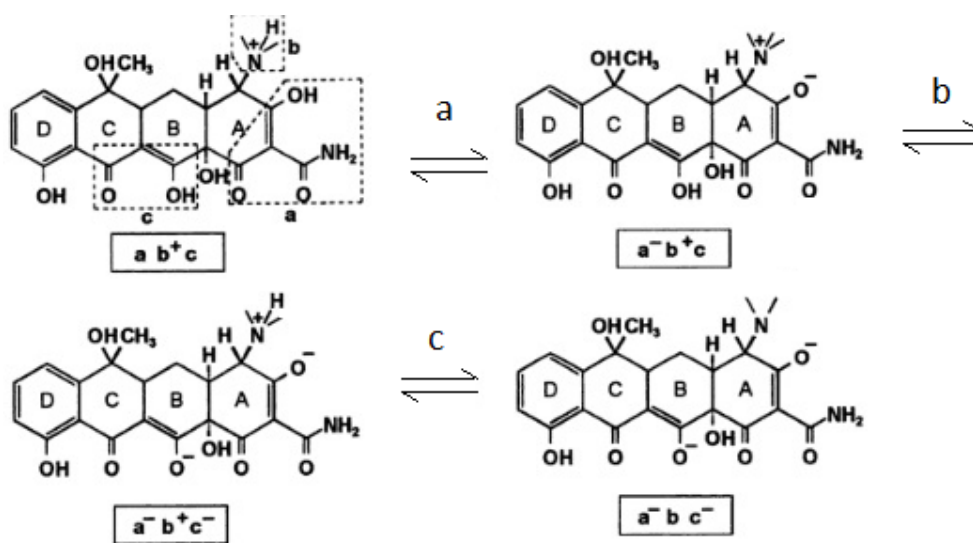


Figure 29. Acid-base equilibria and ionization states of tetracycline (a) $pK_a=3.3$, (b) $pK_{a2}=7.5$ (c) $pK_{a3}=9.4$.^[46]

The relative amount of occurring species of TC is shown in Figure 30. Between *ca.* pH 4.2 and pH 7.2, the zwitterionic species a^-b^+c are the dominant ones. Around pH 9 about 80 % of the molecules are presented as anionic species $a^-b^+c^-$.^[47]

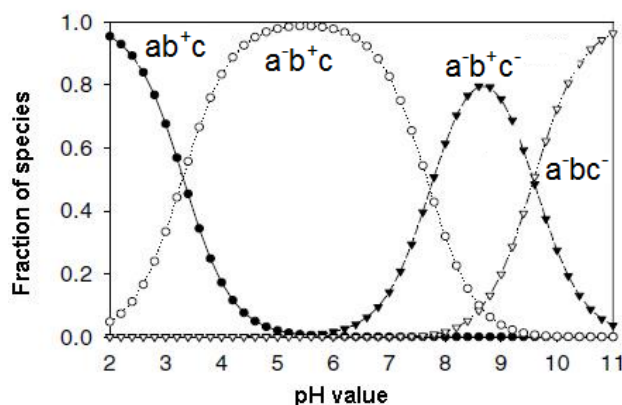


Figure 30. The influence of the pH value on the distribution of tetracycline species in aqueous solution.^[48]

The zwitterionic character of the TC molecule is influenced by change of pH value. At acidic, neutral and alkaline conditions different deprotonated states of TC occur. In acidic solution, after adding the strong acid, fully protonated (cationic) states is observed (b^+). By adding the strong base, the TC states are changing. The hydroxyl group is deprotonated forming the (a^-) anionic state of TC. With increasing pH value, next protons are removed from the OH groups. Finally, the complete deprotonation of TC molecule is achieved at pH of 9 - 10.9, forming the anionic TC species ($a^- b c^-$).

Photocatalytic performances

The photocatalytic abatement of two model pharmaceuticals: tetracycline and ibuprofen was carried out under reliable conditions. A 1 L glass baker (a batch reactor) was placed into a closed aluminum box equipped with four UV-Vis solarium lamps and irradiated from the top with a total power of 60 W (4 lamps x 15 W, Phillips). The irradiation intensity of the experimental setup was 3.2 mW/cm^2 . These lamps mainly simulate the UV part of sun light between 320 nm and 400 nm besides of additional emission lines in the visible light range. The irradiation intensity was similar to sun light radiation at the Baltic Sea, Rostock, on a clouded day and measured using an UV light meter. The distance between applied lamps and the surface of pollutant solution was 15 cm (Fig. 31).

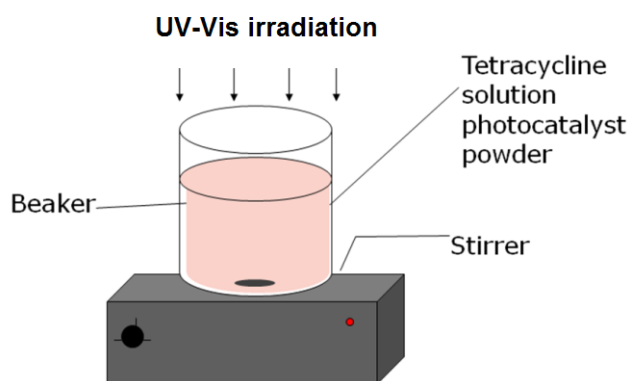


Figure 31. Scheme of the photocatalytic batch reactor.

Appropriate amount of photocatalysts were added into pollutants solution. The solution was further mixed magnetically during the adsorption and photocatalytic experiments. The photocatalysts were separated from the aliquots by using a 0.45 μm PTFE filter and then taken for further quantitative analysis. Additionally, adsorption measurements were carried out in the same way; in the closed aluminum box, without any irradiation (experiments in the dark). The quantitative progress of the oxidative photocatalytic abatement of ibuprofen and tetracycline was estimated using the calibration data. The concentration of high concentrated ibuprofen and tetracycline solutions (ppm range) was monitored by UV - Vis spectrometer (Varian, Cary WinUV). While for the determination of low concentrated tetracycline solutions (ppb range) a new measurement procedure has been developed based on voltammetry.

Reaction intermediates

The quantitative abatement of the pharmaceuticals was followed by the disappearance of the band corresponding to ibuprofen and tetracycline at 222 and 360 nm, respectively (Fig 32 and 33).

The IBP absorbance intensity at 222 nm markedly decreases with treatment time. Additionally, a second absorbance at 262 nm appears during the course of the treatment, what is attributed to the formation of temporary products of ibuprofen in the solution (Fig. 32 arrow).

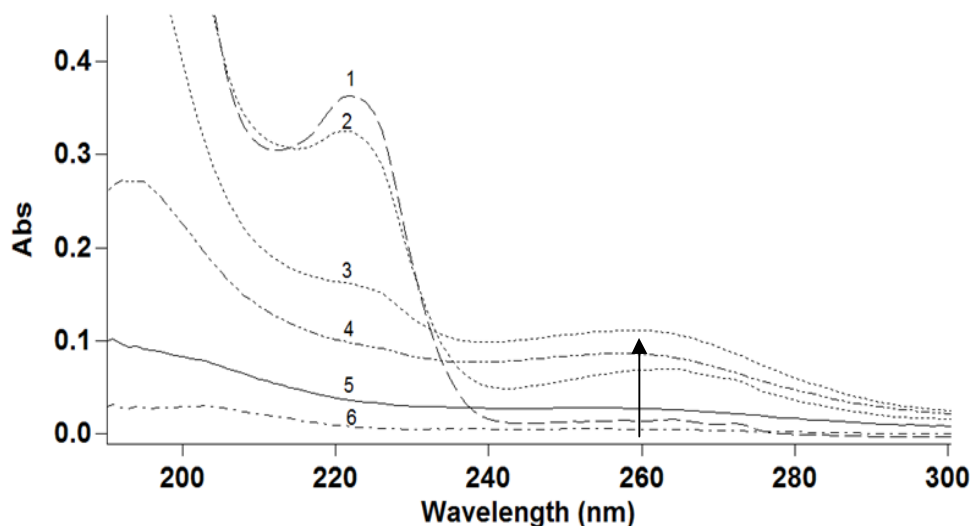


Figure 32. UV-Vis spectra of an aqueous ibuprofen solution after photocatalytic treatment over titania 25 photocatalyst under UV-Vis irradiation: (1) starting IBP solution (10 ppm) and after (2) 5 min, (3) 30 min, (4) 60 min, (5) 120 min, (6) 180 minutes of photocatalytic treatment. Concentration of ibuprofen determined based on the absorbance at 222 nm. Experimental conditions: IBP conc.: 10 ppm, cat conc.: 20 mg/L, cat-to-sub ratio of 2:1, pH=7.

In case of tetracycline, the concentration was determined based on the absorption band at 360 nm. During the course of abatement no other bands appear which could be used to check the appearance of intermediates as is was with IBP (Fig. 32).

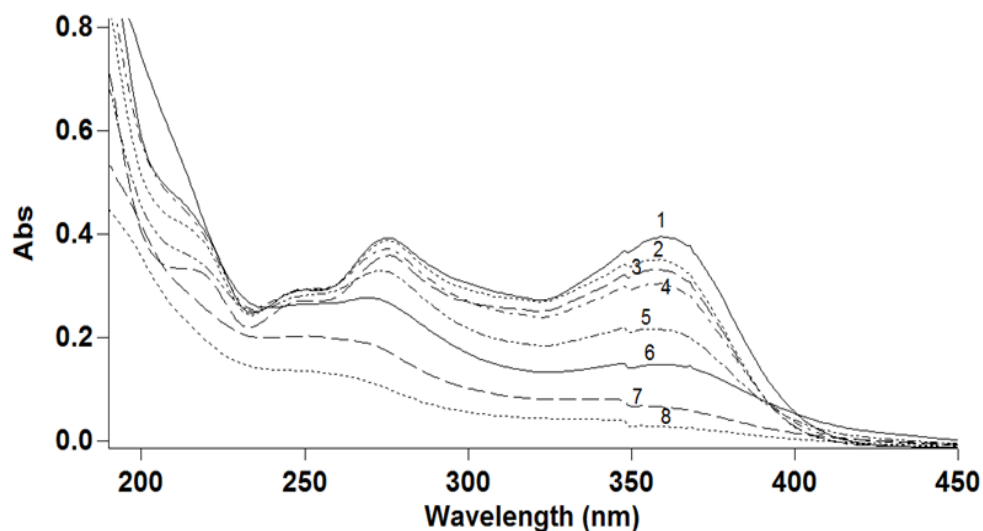


Figure 33. UV-Vis spectra of an aqueous tetracycline solution after photocatalytic treatment over titania 25 photocatalyst under UV-Vis irradiation: (1) starting TC solution (10 ppm) and after (2) 5 min, (3) 10 min, (4) 30 min, (5) 60 min, (6) 120 min, (7) 180 min, (8) 240 minutes of photocatalytic treatment. Concentration of ibuprofen determined based on the absorbance at 362 nm. Experimental conditions: TC conc.: 10 ppm, cat conc.: 10 mg/L, cat-to-sub ratio of 1:1, pH=7.

ESI-TOF-MS/HPLC

The ibuprofen and tetracycline intermediates formed during photocatalytic treatment were qualitatively investigated and determined by ESI-TOF-MS measurements using an electrospray ionization mass spectrometer HPLC System 1200/ESI-TOF-MS 6210 (Agilent). The ESI-TOF-MS uses a “soft” ionisation method to obtain positively or negatively charged molecule ions by adding or removal the protons from the molecule. The deprotonated molecular ion of the formula $[M-H]^-$ formed in the negative ionisation mode gives the signals, which are plotted as mass-to-charge (m/z) peaks vs. counts (intensities). They allow for a qualitative determination of IBP and TC and its decomposition products in the aqueous solution.

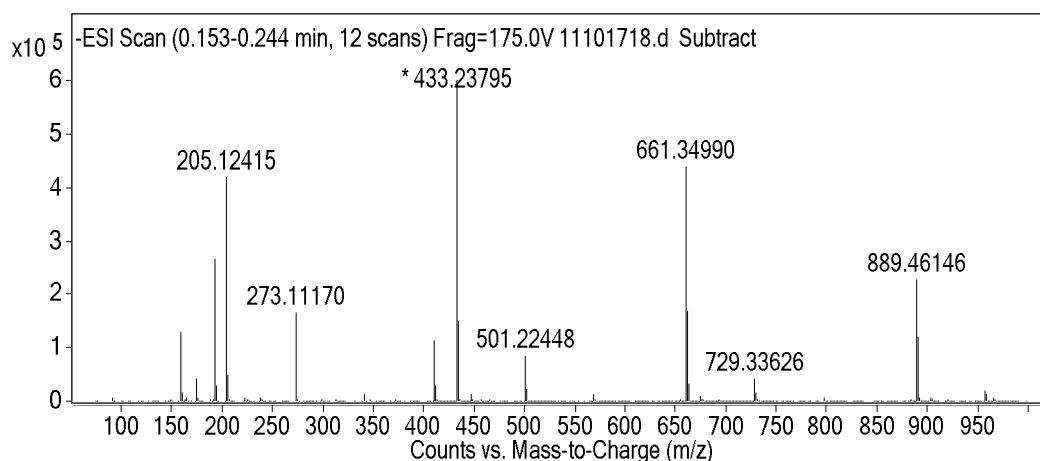


Figure 34. Negative ESI-TOF-MS of starting aqueous solution of ibuprofen 20 ppm.

The negative ESI-TOF-MS spectrum shows the intensity vs. mass-to-charge (m/z) peaks of the starting ibuprofen solution (Fig. 34). Beside the molecular peak at m/z 205 attributed to the ibuprofen anion, higher mass-to-charge peaks are observed at m/z 433, 661 and 889. The mass signals at m/z 205 and m/z 433, 661 and 889 indicates some impurities in the sample. The peaks arising at m/z 501 and 729 are belonging to formed molecular self - aggregates of ibuprofen sodium salt.

Voltammetry

The polarographic method voltammetry has been developed for the detection of tetracycline at very low concentration (ppb range).^[49] For this purpose the measurement conditions of used modes have been optimized by lengths. The

optimization included, e.g. the type of the buffer, the pH value of the solution as well as the accumulation time, deposition potential and modes. This way the detection limit of tetracycline could be extended to 1 ppb and lower. The limit of detection of tetracycline was further extended down to 45 ppt based on square wave voltammetry (SWV) (Fig. 35). This novel procedure enables to determine TC contaminations down to the low ppt- ppb-level using the popular hanging mercury electrode (HMDE).

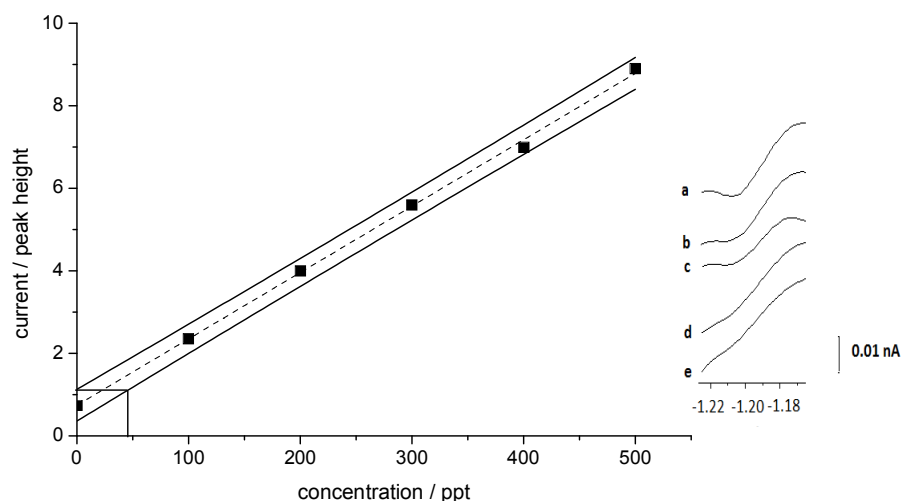


Figure 35. Calibration curves of tetracycline based on SWV representative peaks shown in inset. The limit of detection (LOD) was found at *ca.* 45 ng/L using the prediction bands of the calibration data set.

The deeply development of this sensitive electroanalytical method allowed to determine the photocatalytic abatement of low tetracycline concentrations of 200, 500 and 1000 ppb in aqueous solution. The changes of TC concentrations have been monitored by adsorptive stripping voltammetry (AdSV) using the Polarograph 797 VA Metrohm AG, (Herisau, Switzerland).

The electrochemical cell has been equipped with the hanging mercury drop electrode a working electrode and with a reference electrode in a supporting electrolyte e.g. boric acid solution. All solutions were prepared using ultrapure water ($> 18 \text{ M}\Omega \text{ TOC} < 2 \text{ ppb}$). The stock solution containing 100 ppm of tetracycline in water was prepared daily. The buffer solution: a 0.025 M boric acid aqueous solution was adjusted to pH 7 and used as supporting electrolyte. For analysis 10 mL aliquots of the reaction solution containing tetracycline (taken after photocatalytic treatment) were pipetted into the electrochemical cell containing 10 mL of buffer and was deoxygenated by purging with nitrogen for 300 seconds. Each measurement was repeated three times

including intermediate purging for 30 sec. The stirring (2000 rpm) was kept constant during the deposition at the hanging mercury drop electrode, by using the fresh mercury drop. The deposition time was 200 sec. The voltammograms were recorded over the range of -0.60 V to -1.60 V, where the height of the reduction peak at -1.2 V, corresponding to TC peak, was taken to determine the calibration curve (Fig. 36). All data were obtained at room temperature.

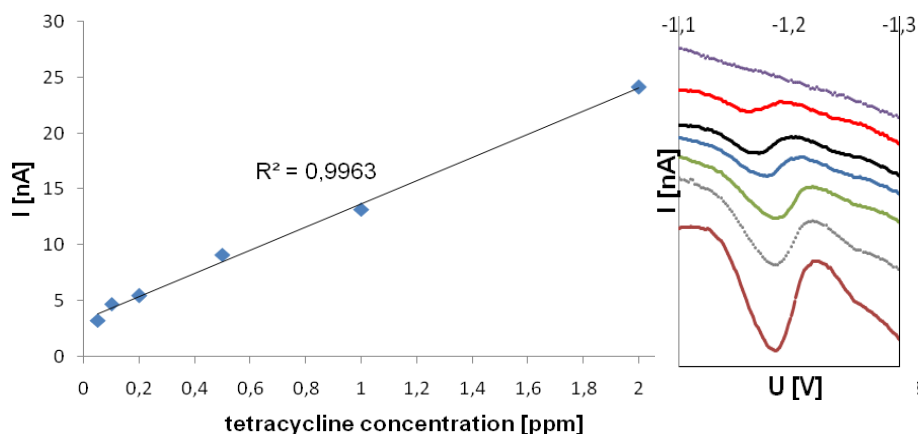


Figure 36. The calibration plot and adsorptive stripping voltammetric response (inset) of 0, 0.05, 0.1, 0.2, 0.5, 1 and 2 ppm (from top to bottom) in 25 mM boric acid solution (pH 5.5) detection limit *ca.* 10 ppb.

Finally, this work deals with the preparation of new active photocatalytic materials and development of the analytical procedures for the detection of pharmaceuticals at low ppm-ppb scale. A couple of photocatalytic materials which differ in the nature and structure have been prepared and characterized regarding crystallinity, morphology and texture, mainly by XRD, TEM and N_2 adsorption measurements (Tab. 1). List of the prepared active photocatalytic materials is given below:

- Commercial TiO_2 - mixture of rutile and anatase.
- Nitrogen (N), iron (Fe) and zirconium (Zr) doped titania.
- Titania nanotubes (TNs) - titania composed of (TiO_6) octahedron sheets.
- Ti/MIL-101, titania/MOF composites incorporated with chromium and titanium.
- MIL-125 structures.
- Two different sized zinc oxide (ZnO) nanoparticles.

Table 1. Comparison of the morphological properties of used photocatalysts.

Photocatalysts	Structure type	Specific surface area [m ² /g]	Bang gap [eV]	Particle size [nm]
Titania P25	anatase/ rutile	55	3.2	10-30
Zr-TiO ₂	anatase	100	2.9	10-15
as-synthesized TN	TiO ₆ rings	220	-	10x100-200
TN calcined	transformed to antase	105		20-50
Ti/MIL-101	MOF	3488	-	-
MIL-125	MOF	1360	-	-
ZnO _e	wurtzite	8	3.17	100
ZnO _w	wurtzite	40	3.16	15-30

The electrochemical method like voltammetry has been chosen for the development of determination of the test molecule tetracycline at low concentration (ppb range). By standardization of the experimental parameters like: buffer, pH value of solution, the deposition time and potential, the detection limit was successfully decreased to low 1 ppb range. The influence of tap water matrix on the presence of tetracycline has been also checked (water matrix similar to waste and surface waters) but so far, not applied in the photocatalytic course of abatement.

References

- [1] Y. Lan, Y. Lu, Z. Ren, *Nano Energy* **2**, **2013**, *5*, 1031 - 1045.
- [2] U. Diebold, *Surf. Sci. Rep.* **2003**, *48*, 533 - 229.
- [3] B. S. Richards, N. T. P. Huong, A. Crosky, *J. Electrochem. Soc.* **2005**, *152*, F71 - F74.
- [4] J. Xie, X. Lü, J. Liu, H. Shu, *Pure Appl. Chem.* **2009**, *81*, 2407 - 2415.
- [5] M. Landmann, E. Rauls, W.G. Schmidt, *J. Phys. Condensed Matter* **2012**, *24*, 195503.
- [6] A. K. Ray, S. M. Tracey, B. McQuillin, S. N. B. Hodgson, *IEEE Proc. Sc. Meas. Technol.* **2000**, *147*, 301 - 305.
- [7] L. Kavan, M. Grätzel, S. E. Gilbert, C. Klemenz, H. J. Scheel, *J. Am. Chem. Soc.* **1996**, *118*, 6716 - 6723.
- [8] H. Tang, F. Lévy, H. Berger, P. E. Schmid, *Phys. Rev. B* **1995**, *52*, 7771 - 7774.
- [9] J. Pascual, J. Camassel, H. Mathieu, *Phys. Rev. B* **1978**, *18*, 5606 - 5614.
- [10] A. Amtout, R. Leonelli, *Phys. Rev. B* **1995**, *51*, 6842 - 6851.
- [11] N. T. Nolan, M. K. Seery, S. C. Pillai, *J. Phys. Chem. C* **2009**, *113*, 16151-16157.
- [12] B. Choudhury, A. Choudhury, *Int. Nano Lett.* **2013**, *3*, 1 - 9.
- [13] H. Kloepfer, Patent No. DE-PS 870 242.Germany, **1953**.
- [14] S. Pratsinis, *Prog. Energ. Combust. Sci.* **1998**, *24*, 192 - 219.
- [15] D. A. H. Hanaor, C. C. Sorrell, *J. Mater. Sci.* **2011**, *46*, 855 - 874.
- [16] K. J. A. Raj, B. Viswanathan, *Indian Journal of Chemistry* **2009**, *48*, 1378 - 1382.
- [17] S.-J. Kim, J.-K. Lee, E. G. Lee, H.-G. Lee, S.-J. Kim, K. S. Lee, *J. Mater. Res.* **2003**, *18*, 729 - 732.
- [18] V. Nguyen, R. Amal, D. Beydoun, *Chem. Eng. Sci.* **2005**, *60*, 5759 - 5769.
- [19] A. Alonso - Tellez, R. Masson, D. Robert, N. Keller, V. Keller, *J. Photochem. Photobiol. A* **2012**, *250*, 58 - 65.
- [20] M. Lukáč, P. Klementová, S. Bezdička, S. Bakardjieva, J. Šubrt, L. Szatmáry, Z. Bastl, J. Jirkovsky, *Appl. Catal. B* **2007**, *74*, 83 - 91.

- [21] L. Miao, S. Tanemura, T. Jiang, M. Tanemura, K. Yoshida, N. Tanaka, G. Xu, *Superlattices Microst.* **2009**, *46*, 357 - 364.
- [22] G. Mogilevsky, Q. Chen, H. Kulkarni, A. Kleinhammes, W. M. Mullins, Y. Wu, *J. Phys. Chem. C* **2008**, *112*, 3239 - 3246.
- [23] C.-C. Tsai, H. Teng, *Chem. Mater.* **2006**, *18*, 367 - 373.
- [24] J. Yu, H. Yu, B. Cheng, C. Trapalis, *J. Mol. Catal. A* **2006**, *249*, 135 - 142.
- [25] H. H. Ou, S.-L. Lo, *Sep. Purif. Technol.* **2007**, *58*, 179 - 191.
- [26] C.-C. Tsai, H. Teng, *Chem. Mater.* **2006**, *18*, 367 - 373.
- [27] M. Zhang, J. Zhensheng, J. Zhang, X. Guo, J. Yang, W. Li, X. Wang, Z. Zhang, *J. Mol. Catal. A* **2004**, *217*, 203 - 210.
- [28] S. Mozia, *Catal. Today* **2010**, *156*, 198 - 207.
- [29] W. Liu, J. Gao, F. Zhang, G. Zhang, *Mater. T.* **2007**, *48*, 2464 - 2466.
- [30] L. B. Fen, T. K. Han, N. M. Nee, B. C. Ang, M. R. Johan, *Appl. Surf. Sci.* **2011**, *258*, 431 - 435.
- [31] C.-K. Lee, C.-C. Wang, M.-D. Lyu, L.-C. Juang, S.-S. Liu, S.-H. Hung, *J. Coll. Inter. Sci.* **2007**, *316*, 562 - 569.
- [32] C. C. Tsai, H. Teng, *Chem. Mater.* **2004**, *16*, 4352 - 4358.
- [33] A. Turki, H. Kochkar, C. Guillard, G. Berhault, A. Ghorbel, *Appl. Catal. B* **2013**, *138-139*, 401 - 415.
- [34] T. Sekino, *Inorganic and Metallic Nanotubular Materials, Topics in Applied Physics* **2010**, *117*, 17 - 32.
- [35] G. Férey, C. Mellot-Draznieks, C. Serre, F. Millange, J. Dutour, S. Surblé, I. Margiolaki, *Science* **2005**, *309*, 2040 - 2042.
- [36] J. Yang, Q. Zhao, J. Li, J. Dong, *Micropor. Mesopor. Mater.* **2010**, *130*, 174 - 179.
- [37] T. V. Vu, H. Kosslick, A. Schulz, J. Harloff, E. Paetzold, M. Schneider, J. Radnik, N. Steinfeldt, G. Fulda, U. Kragl, *Appl. Catal. A* **2013**, *468*, 410 - 417.
- [38] D.-Y. Hong, Y. K. Hwang, C. Serre, G. Férey, J.-S. Chang, *Adv. Funct. Mater.* **2009**, *19*, 1537 - 1552.
- [39] M. Dan-Hardi, C. Serre, T. Frot, L. Rozes, G. Maurin, C. Sanchez, G. Férey, J. *Am. Chem. Soc.* **2009**, *131*, 10857 - 10859.

- [40] N. Daneshvar, D. Salari, A. R. Khataee, *J. Photochem. Photobiol. A: Chem.* **2004**, *162*, 317 - 322.
- [41] L. Bahadur, M. Hamdani, J.F. Koenig, P. Chartier, *Sol. Energ. Mat.* **1986**, *14*, 107 - 120.
- [42] A. Srivastava, N. Kumar, S. Khare, *Opt. Electron.* **2014**, *22*, 68 - 76.
- [43] G.-D. Liang, T.-T. Liu, W.-P. Qin, F.-M. Zhu, Q. Wu, *Polym. Eng. Sci.* **2012**, *52*, 1250 - 1257.
- [44] P. Rajanikant, P. Nirav, N. M. Patel, M. M. Patel, P. Rajanikant, *Int. J. Res. Pharm. Sci.* **2010**, *1*, 57 - 64.
- [45] S. S. Kadam, K. R. Mahadik, K. G. Bothara, Principles of Medicinal Chemistry, Richmond, TX, U.S.A. Vol. I, **2006**
- [46] M. Nelson, W. Hillen, R. A. Greenwald, Tetracyclines in Biology, Chemistry and Medicine, Birkhäuser Basel, **2001**, p.336.
- [47] R. B. Martin, Tetracycline and Daunorubicin. In: anitibiotics and their complexes. Marcel Dekker, New York, **1985**, *19*, 19 - 52.
- [48] Y. Zhao, J. Geng, X. Wang, X. Gu, S. Gao, *Ecotoxicology* **2011**, *20*, 1141 - 1147.
- [49] J. Choina, H. Duwensee, G.-U. Flechsig, H. Kosslick, A. W. Morawski, V. A. Tuan, A. Schulz, *Cent. Eur. J. Chem.* **2010**, *8*, 1288 - 1297.

A 2. References

- [1] D. Barcelo, *Trends Anal. Chem.* **2003**, *22*, 725 - 733.
- [2] A. Azzouz, E. Ballesteros, *Chemosphere* **2013**, *93*, 2046 - 2054.
- [3] A. Pal, K. Y.-H. Gin, A. Yu-Chen Lin, M. Reinhard, *Sci. Total Environ.* **2010**, *408*, 6062 - 6069.
- [4] C. G. Daughton, *Comprehensive Analytical Chemistry* **2013**, *62*, 37 - 69.
- [5] A. M. Vajda, L. B. Barber, J. L. Gray, E. M. Lopez, J. D. Woodline, D. O. Norris, *Environ. Sci. Technol.* **2008**, *42*, 3407 - 3414.
- [6] L. C. Xu, S. Hong, J. F. Chen, Q. Bian, J. Song, X. R. Wang, *Toxicology* **2005**, *616*, 197 - 203.
- [7] D. D. Richardson, M. J. Plewa, E. D. Wagner, R. Schoeny, D. M. De Marini, *Mutat. Res.* **2007**, *636*, 178 - 242.
- [8] M. Ghisari, E. C. Bonfeld-Jorgensen, *Mol. Cell Endocrinol.* **2005**, *244*, 31 - 41.
- [9] S. Biau, S. Bayle, P. de Santa Barbara, B. Roig, *Analyt. Bioanalyt. Chem.* **2007**, *387*, 1397 - 1403.
- [10] B. Roig, *Pharmaceuticals in the Environment: Current Knowledge and Need Assessment to Reduce Presence and Impact*, IWA Publishing, **2010**, p.198.
- [11] S. Öllers, H. P. Singer, P. Fässler, S. R. Müller, *J. Chromat. A* **2001**, *911*, 225 - 234.
- [12] H. Sanderson, B. Laird, L. Pope, R. Brain, C. Wilson, D. Johnson, G. Bryning, A. S. Peregrine, A. Boxall, K. Solomon, *Aquat. Toxicol.* **2007**, *85*, 229 - 240.
- [13] J. M. Conley, S. J. Symes, S. A. Kindelberger, S. M. Richards, *J. Chromat. A* **2008**, *1185*, 206 - 215.
- [14] T. A. Ternes, *Trends Anal. Chem.* **2001**, *20*, 419 - 434.
- [15] V. L. Trudeau, C. D. Metcalfe, C. Mimeault, T. W. Moon, *Biochem. Mol. Biol.* **2005**, *6*, 475 - 493.
- [16] B. D. Blair, J. P. Crago, C. J. Hedman, R. D. Klaper, *Chemosphere* **2013**, *93*, 2116 - 2123.
- [17] T.-H. Fang, F.-H. Nan, T.-S. Chin, H.-M. Feng, *Mar. Pollut. Bull.* **2012**, *64*, 1435 - 1444.

- [18] A. Nikolaou, S. Meric, D. Fatta, *Analyt. Bioanalyt. Chem.* **2007**, *387*, 1225 - 1234.
- [19] D. M. Cuong, K.-W. Kim, T. Q. Toan, T. D. Phu, *Geosystem Engineering* **2011**, *14*, 35 - 42.
- [20] T. Colborn, F. S. vom Saal, A. M. Soto, *Environ. Health Perspect.* **1993**, *101*, 378 - 384.
- [21] N.W.T. Quinn, International Perspectives on Water Quality Management and Pollutant Control, Publisher: InTech, **2013**, p.121.
- [22] B. Halling-Sorensen, S. Nors Nielsen, P. F. Lanzky, F. Ingerslev, H. C. Holten Liitzhofl, S. E. Jorgensen, *Chemosphere* **1998**, *36*, 357 - 393.
- [23] K. Kümmerer, *Chemosphere* **2001**, *45*, 957 - 969.
- [24] K. S. Le Corre, C. Ort, D. Kateley, B. Allen, B. I. Escher, J. Keller, *Environ. Int.* **2012**, *45*, 99 - 111.
- [25] D. J. Lapworth, N. Baran, M. E. Stuart, R. S. Ward, *Environ. Poll.* **2012**, *163*, 287 - 303.
- [26] A. Ziylan, N. H. Ince, *J. Hazard. Mater.* **2011**, *187*, 24 - 36.
- [27] D. W. Kolpin, E. T. Furlong, M. T. Meyer, E. M. Thurman, S. D. Zaugg, L. B. Barber, H. T. Buxton, *Environ. Sci. Technol.* **2002**, *36*, 2002 - 1211.
- [28] O. Cardoso, J.-M. Porcher, W. Sanchez, *Chemosphere*, **2014**, <http://dx.doi.org/10.1016/j.chemosphere.2014.02.004>
- [29] M. Boroski, A. C. Rodrigues, J. C. Garcia, L. C. Sampaio, J. Nozaki, N. Hioka, *J. Hazard. Mater.* **2009**, *162*, 448 - 454.
- [30] J. P. Bound, K. Kitsou, N. Voulvoulis, *Environ. Toxicol. and Pharmacol.* **2006**, *21*, 301 - 307.
- [31] V. Matamoros, C. Arias, H. Brix, J. M. Bayona, *Water Res.* **2009**, *43*, 55 - 62.
- [32] T. Sweeney, *Domest. Anim. Endocrin.* **2002**, *23*, 203 - 209.
- [33] Y. Matsui, T. Ozu, T. Inoue, T. Matsushita, *Desalination* **2008**, *226*, 215 - 221.
- [34] R. Merle, P. Hajek, A. Käsbohrer, C. Hegger-Gravenhorst, Y. Mollenhauer, M. Robanus, F.-R. Ungemach, L. Kreienbrock, *Prev. Vet. Med.* **2012**, *104*, 34 - 43.

- [35] G. Hamscher, H. T. Pawelzick, S. Sczesny, H. Nau, J. Hartung, *Environ. Health Persp.* **2003**, *111*, 1590 - 1594.
- [36] G. Rigos, I. Nengas, M. Alexis, G. M. Troisi, *Aquat. Toxicol.* **2004**, *69*, 281 - 288.
- [37] M. Hatha, A. A. Vivekanandhan, G. J. Joice, *Int. J. Food Microbiol.* **2005**, *98*, 131 - 134.
- [38] R. S. S. Wu, *Mar. Poll. Bull.* **1995**, *31*, 159 - 166.
- [39] T. Heberer, *Toxicol. Lett.* **2002**, *131*, 5 - 17.
- [40] E. R. Cooper, T. C. Siewicki, K. Phillips, *Sci. Total Environ.* **2008**, *398*, 26 - 33.
- [41] F. Pomati, C. Orlandi, M. Clerici, F. Luciani, E. Zuccato, *Toxicol. Sci.* **2008**, *102*, 129 - 137.
- [42] CHMP, Guideline on the environmental risk assessment of medicinal products for human use. Committee for Human Use Medicinal Products, European Medicines Agency (EMA), London, UK, **2006** (www.emea.europa.eu/pdfs/human/swp/444700_en.pdf).
- [43] European Commission, 2003, Technical guidance document on risk assessment in support of Commission Directive 93/67/EEC on risk assessment for new notified substances, Commission Regulation (EC) No 1488/94 on Risk assessment for existing substances, Directive 98/8/EC of the European Parliament and of the Council concerning the placing of biocidal products on the market, <http://jrc.ecb.eu.it/>
- [44] C. G. Daughton, T. A. Ternes, *Environ. Health Perspect.* **1999**, *107*, 907 - 938.
- [45] <https://www.consumerreports.org/health/resources/pdf/best-buy-drugs/Nsaids2.pdf>
- [46] S. Loaiza-Ambuludi, M. Panizza, N. Oturan, M. A. Oturan, *Catal. Today* **2014**, *224*, 29 - 33.
- [47] R. Rodil, J. B. Quintana, E. Concha-Graña, P. López-Mahía, S. Muniategui-Lorenzo, D. Prada-Rodríguez, *Chemosphere* **2012**, *86*, 1040 - 1049.
- [48] K. Press-Kristensen, A. Ledin, J. E. Schmidt, M. Henze, *Sci. Total Environ.* **2007**, *373*, 122 - 130.

- [49] D. S. Maycock, C. D. Watts, Pharmaceuticals in Drinking Water, *Encyclopedia of Environmental Health*, **2011**, 472 - 484.
- [50] O. A. Jones, J. N. Lester, N. Voulvoulis, *Trends Biotechnol.* **2005**, *23*, 163 - 167.
- [51] M. S. Fram, K. Belitz, *Sci. Total Environ.* **2011**, *409*, 3409 - 3417.
- [52] A. Azzouz, E. Ballesteros, *Chemosphere* **2013**, *93*, 2046 - 2054.
- [53] D. Gerrity, B. D. Stanford, R. A. Trenholm, S. A. Snyder, *Water Res.* **2010**, *44*, 493 - 504.
- [54] C. Köhler, S. Venditti, E. Igos, K. Klepiszewski, E. Benetto, A. Cornelissen, *J. Hazard. Mater.* **2012**, *239*, 70 - 77.
- [55] D. P. Mohapatra, S. K. Brar, R. D. Tyagi, P. Picard, R. Y. Surampalli, *Sci. Total Environ.* **2014**, *470-471*, 58 - 75.
- [56] M. Horáková, Š. Klementová, P. Kříž, S. K. Balakrishna, P. Špatenka, O. Golovko, P. Hájková, P. Exnar, *Surf. Coat. Technol.* **2014**, *241*, 154 - 158.
- [57] K. Nakata, A. Fujishima, *J. Photochem. Photobiol. C* **2012**, *13*, 169 - 189.
- [58] K. Nakata, T. Ochiai, T. Murakami, A. Fujishima, *Electrochim. Acta* **2012**, *84*, 103 - 111.
- [59] D. Robert, S. Malato, *Sci. Total Environ.* **2002**, *291*, 85 - 97.
- [60] D. Ljubas, *Energy* **2005**, *30*, 1699 - 1710.
- [61] N. Mehrdadi, S. G. Joshi, T. Nasrabadi, H. Hoveidi, *Int. J. Environ. Res.* **2007**, *1*, 42 - 48.
- [62] J. Choi, H. Lee, Y. Choi, S. Kim, Se. Lee, S. Lee, W. Choi, J. Lee, *Appl. Catal. B: Environ.* **2014**, *147*, 8 - 16.
- [63] E. M. Rodríguez, G. Márquez, E. A. León, P. M. Álvarez, A. M. Amat, F. J. Beltrán, *J. Environ. Manage.* **2013**, *127*, 114 - 124.
- [64] S. Esplugas, D. M. Bila, L. G. T. Krause, M. Dezotti, *J. Hazard. Mater.* **2007**, *149*, 631 - 642.
- [65] M. Ibáñez, E. Gracia-Lor, L. Bijlsma, E. Morales, L. Pastor, F. Hernández, *J. Hazard. Mater.* **2013**, *260*, 389 - 398.
- [66] J. L. Acero, F. J. Benitez, F. J. Real, G. Roldan, *Water Res.* **2010**, *44*, 4158 - 4170.

- [67] J. B. Quintana, R. Rodil, P. López-Mahía, S. Muniategui-Lorenzo, D. Prada-Rodríguez, *Water Res.* **2010**, *44*, 243 - 255.
- [68] B. A. Wols, C. H. M. Hofman-Caris, D. J. H. Harmsen, E. F. Beerendonk, *Water Res.* **2013**, *47*, 5876 - 5888.
- [69] A. Lopez, A. Bozzi, G. Mascolo, J. Kiwi, *J. Photochem. Photobiol. A* **2003**, *156*, 121 - 126.
- [70] I. Kim, N. Yamashita, H. Tanaka, *Chemosphere* **2009**, *77*, 518 - 525.
- [71] M. G. Maniero, D. M. Bila, M. Dezotti, *Sci. Total Environ.* **2008**, 407, 105 - 115.
- [72] E. S. Elmolla, M. Chaudhuri, *Desalination* **2010**, *252*, 46 - 52.
- [73] R. Nageswara Rao, N. Venkateswarlu, *Dyes Pigments* **2008**, *77*, 590 - 597.
- [74] Z. Pengyi, L. Fuyan, Y. Gang, C. Qing, Z. Wanpeng, *J. Photochem. Photobio. A* **2003**, *156*, 189 - 194.
- [75] Y. Yalcin Gurkan, N. Turkten, A. Hatipoglu, Z. Cinar, *Chem. Eng. Journal* **2012**, *184*, 113 - 124.
- [76] P. Wang, T. Zhou, R. Wang, T.-T. Lim, *Water Res.* **2011**, *45*, 5015 - 5026.
- [77] C. J. Lin, Y. H. Liou, Y. Zhang, C. L. Chen, Ch.-L. Dong, S.-Y. Chen, G. D. Stucky, *Appl. Catal. B* **2012**, *127*, 175 - 181.
- [78] D. Avisar, I. Horovitz, L. Lozzi, F. Ruggieri, M. Baker, M.-L. Abel, H. Mamane, *J. Hazard. Mater.* **2013**, *244-245*, 463 - 471.
- [79] P. Wang, P.-S. Yap, T.-T. Lim, *Appl. Catal. A* **2011**, *399*, 252 - 261.
- [80] C.-J. Lin, W.-T. Yang, *Chem. Eng. Journal* **2014**, *237*, 131 - 137.
- [81] P. M. Álvarez, J. Jaramillo, F. López-Piñero, P. K. Plucinski, *Appl. Catal. B* **2010**, *100*, 338 - 345.
- [82] W. Alahmad, M. A. Alawi, *J. J. Pharm. Sci.* **2010**, *39*, 121 - 136.
- [83] J. Madhavan, P. S. S. Kumar, S. Anandan, M. Zhou, F. Grieser, M. Ashokkumar, *Chemosphere* **2010**, *80*, 747 - 752.
- [84] H. S. Hilal, G. Y. M. Al-Nour, A. Zyoud, M. H. Helal, I. Saadeddin, *Solid State Sci.* **2010**, *12*, 578 - 586.
- [85] M. El-Kemary, H. El-Shamy, I. El-Mehasseb, *J. Lumin.* **2010**, *130*, 2327 - 2331.
- [86] E. S. Elmolla, M. Chaudhuri, *J. Hazard. Mater.* **2010**, *173*, 445 - 449.

- [87] A. Chatzitakis, C. Berberidou, I. Paspaltsis, G. Kyriakou, T. Sklaviadis, I. Poullos, *Water Res.* **2008**, *42*, 386 - 394.
- [88] R. A. Palominos, M. A. Mondaca, A. Giraldo, G. Peñuela, M. Pérez-Moya, H. D. Mansilla, *Catal. Today* **2009**, *144*, 100 - 105.
- [89] S. Kaniou, K. Pitarakis, I. Barlagianni, I. Poullos, *Chemosphere* **2005**, *60*, 372 - 380.
- [90] T. B. Ivetić, M. R. Dimitrievska, N. L. Finčur, Lj. R. Đaćanin, I. O. Gúth, B. F. Abramović, S. R. Lukić-Petrović, *Ceram. Int.* **2014**, *40*, 1545 - 1552.
- [91] A. Hu, X. Zhang, K. D. Oakes, P. Peng, Y. N. Zhou, M. R. Servos, *J. Hazard. Mater.* **2011**, *189*, 278 - 285.
- [92] G. Laera, Bo Jin, H. Zhu, A. Lopez, *Catal. Today* **2011**, *161*, 147 - 152.
- [93] L. M. Pastrana-Martínez, S. Morales-Torres, S. K. Papageorgiou, F. K. Katsaros, G. E. Romanos, J. L. Figueiredo, J. L. Faria, P. Falaras, A. M.T. Silva, *Appl. Catal. B* **2013**, *142-143*, 101 - 111.
- [94] L. M. Pastrana-Martínez, S. Morales-Torres, V. Likodimos, J. L. Figueiredo, J. L. Faria, P. Falaras, A. M.T. Silva, *Appl. Catal. B* **2012**, *123-124*, 241 - 256.
- [95] X. Zhang, F. Wu, N. Deng, *Catal. Commun.* **2010**, *11*, 422 - 425.
- [96] S. Murphy, C. Saurel, A. Morrissey, J. Tobin, Mi. Oelgemöller, K. Nolan, *Appl. Catal. B* **2012**, *119-120*, 156 - 165.
- [97] P. Huo, Z. Lu, X. Liu, X. Gao, J. Pan, D. Wu, J. Ying, H. Li, Y. Yan, *Chem. Eng. Journal* **2012**, *198-199*, 73 - 80.
- [98] B. Ohtani, *J. Photochem. Photobiol. C* **2010**, *11*, 157 - 178.
- [99] M. A. Henderson, *Surf. Sci. Rep.* **2011**, *66*, 185 - 297.
- [100] A. Y. C. Tong, R. Braund, D. Warre, B. Peake, *Cent. Eur. J. Chem.* **2012**, *10*, 989 - 1027.
- [101] A. Fujishima, T. N. Rao, D. A. Tryk, *J. Photochem. Photobiol. C* **2000**, *1*, 1 - 21.
- [102] R. Vinu, G. Madras, *J. Indian Instit. Sci.* **2010**, *90*, 189 - 230.
- [103] M. Schiavello, *Electrochim. Acta* **1993**, *38*, 11 - 14.
- [104] B. Ohtani, *Chem. Lett.* **2008**, *37*, 216 - 229.
- [105] J. Winkler, Titanium dioxide, Hannover Vincentz, European Coating Literature, **2003**, p. 128.

- [106] C. S. Turchi, D. F. Ollis, *J. Catal.* **1990**, *122*, 178 - 192.
- [107] J. Jing, M. Liu, V. L. Colvin, W. Li, W. W. Yu, *J. Mol. Catal. A* **2011**, *351*, 17 - 28.
- [108] U. I. Gaya, A. H. Abdullah, *J. Photochem. Photobiol. C* **2008**, *9*, 1 - 12.
- [109] E. Grabowska, J. Reszczyńska, A. Zaleska, *Water Res.* **2012**, *46*, 5453 - 5471.
- [110] O. Carp, C. L. Huisman, A. Reller, *Prog. Solid State Chem.* **2004**, *32*, 33 - 177.
- [111] X. B. Chen, S. S. Mao, *Chem. Rev.* **2007**, *107*, 2891 - 2959.
- [112] K. Hashimoto, H. Irie, A. Fujishima, *Japn. J. Appl. Phys.* **2005**, *44*, 8269 - 8285.
- [113] A. Mills, S. Le Hunte, *J. Photochem. Photobiol. A* **1997**, *108*, 1 - 35.
- [114] I. K. Konstantinou, T. A. Albanis, *Appl. Catal. B* **2004**, *49*, 1 - 14.
- [115] V. Augugliaro, M. Bellardita, V. Loddo, G. Palmisano, L. Palmisano, S. Yurdakal, *J. Photochem. Photobiol. C* **2012**, *13*, 224 - 245.
- [116] M. A. Lazar, S. Varghese, S. S. Nair, *Catalysts* **2012**, *2*, 572 - 601.
- [117] Y. Nosaka, S. Komori, K. Yawata, T. Hirakawa, A. Y. Nosaka, *Phys. Chem. Chem. Phys.* **2003**, *5*, 4731 - 4735.
- [118] P. Schwarz, N. J. Turro, S. H. Bossmann, A. M. Braun, A. A. Abel Wahab, H. Dürr, *J. Phys. Chem. B* **1997**, *101*, 7127 - 7134.
- [119] Q. Xiang, J. Yu, P. K. Wong, *J. Coll. Inter. Sci.* **2011**, *357*, 163 - 167.
- [120] D. Zhang, R. Qiu, L. Song, B. Eric, Y. Mo, X. Huang, *J. Hazard. Mater.* **2009**, *163*, 843 - 847.
- [121] M. Panizza, G. Cerisola, D. V. Zinger, In *Advances in Chemistry Research*, Nova Science Publishers, New York, vol. 2, **2006**.
- [122] C. Comninellis, A. Kapalka, S. Malato, S. A. Parsons, I. Poullos, D. Mantzavinos, *J. Chem. Technol. Biotechnol.* **2008**, *83*, 769 - 776.
- [123] M. Ni, M. K. H. Leung, D. Y. C. Leung, K. Sumathy, *Renew. Sust. Energ. Rev.* **2007**, *11*, 401 - 425.
- [124] K. A. Miseki, *Chem. Soc. Rev.* **2009**, *38*, 253 - 278.
- [125] G. Palmisano, V. Augugliaro, M. Pagliaro, L. Palmisano, *Chem. Commun.* **2007**, *193*, 3425 - 3437.
- [126] Y. Wada, H. Yin, S. Yanagida, *Catal. Sur. Japan* **2002**, *5*, 127 - 138.

- [127] C.-H. Liao, C.-W. Huang, J. C. S. Wu, *Catalysts* **2012**, *2*, 490 - 516.
- [128] J. R. Swierk, T. E. Mallouk, *Chem. Soc. Rev.* **2013**, *42*, 2357 - 2387.
- [129] R. van de Krol, Y. Liang, J. Schoonman, *J. Mater. Chem.* **2008**, *18*, 2311 - 2320.
- [130] A. Zaleska, *Recent Pat. Eng.* **2008**, *2*, 157 - 164.
- [131] M. Pelaez, N. T. Nolan, S. C. Pillai, M. K. Seery, P. Falaras, A. G. Kontosd, P. S. M. Dunlop, J. W. J. Hamilton, J. A. Byrne, K. O'Shea, M. H. Entezari, D. D. Dionysiou, *Appl. Catal. B* **2012**, *125*, 331 - 349.
- [132] Y. Niu, M. Xing, B. Tian, J. Zhang, *Appl. Catal. B* **2012**, *115–116*, 253-260.
- [133] U. G. Akpan, B. H. Hameed, *Appl. Catal. A* **2010**, *375*, 1 - 11.
- [134] M. V. Dozzi, E. Selli, *J. Photochem. Photobiol. C* **2013**, *14*, 13 - 28.
- [135] M. A. Malati, W. K. Wong, *Surf. Technol.* **1984**, *22*, 305 - 322.
- [136] N. Patel, R. Jaiswal, T. Warang, G. Scarduelli, Alpa Dashora, B.L. Ahuja, D.C. Kothari, A. Miotello, *Appl. Catal. B* **2014**, *150-151*, 74 - 81.
- [137] H. Park, Y. Park, W. Kim, W. Choi, *J. Photochem. Photobiol. C* **2013**, *15*, 1 - 20.
- [138] A. O. Ibhaddon, P. Fitzpatrick, *Catalysts* **2013**, *3*, 1 - 29.
- [139] M. Anpo, *Pure Appl. Chem.* **2000**, *72*, 1787 - 1792.
- [140] M. D. H. A. Fuerte, A. J. Maira, A. Martinez-Arias, M. Fernandez-Garcia, J. C. Conesa, J. Soria, *Chem. Commun.* **2001**, *24*, 2718 - 2719.
- [141] S. N. R. Inturi, T. Boningari, M. Suidan, P. G. Smirniotis, *Appl. Catal. B* **2014**, *144*, 333 - 342.
- [142] J. Lim, D. Monllor-Satoca, J. S. Jang, S. Lee, W. Choi, *Appl. Catal. B* **2014**, *152–153*, 233 - 240.
- [143] L. G. Devi, R. Kavitha, *Appl. Catal. B* **2013**, *140–141*, 559 - 587.
- [144] S. Anandan, K. Kathiravan, V. Murugesan, Y. Ikuma, *Catal. Commun.* **2009**, *10*, 1014-1019.
- [145] C. Di Valentin, G. Pacchioni, *Catal. Today* **2013**, *206*, 12 - 18.
- [146] C. M. Teh, A. R. Mohamed, *J. Alloys Compd.* **2011**, *509*, 1648 - 1660.
- [147] R. Asahi, T. Morikawa, T. Ohwaki, K. Aoki, Y. Taga, *Science* **2001**, *293*, 269 - 271.

- [148] H. Lin, A. K. Rumaiz, M. Schulz, C. P. Huang, S. I. Shah, *J. Appl. Phys.* **2010**, *107*, 124305, 1 – 7.
- [149] H. Fakhouri, J. Pulpytel, W. Smith, A. Zolfaghari, H. R. Mortahe, F. Meshkini, R. Jafari, E. Sutter, F. Arefi-Khonsari, *Appl. Catal. B* **2014**, *144*, 12- 21.
- [150] M. Zhou, J. Yu, B. Cheng, H. Yu, *Mater. Chem. Phys.* **2005**, *93*, 159 - 163.
- [151] W. Hung, S. Fu, J. Tseng, H. Chu, T. Ko, *Chemosphere* **2007**, *66*, 2142 - 2151.
- [152] J. Zhu, W. Zheng, B. He, J. Zhang, M. Anpo, *J. Mol. Catal. A* **2004**, *216*, 35 - 43.
- [153] X. Zhang, M. Zhou, L. Lei, *Catal. Commun.* **2006**, *7*, 427 - 431.
- [154] X. Vargas, E. Tauchert, J.-M. Marin, G. Restrepo, R. Dillert, D. Bahnemann, *J. Photochem. Photobiol. A* **2012**, *243*, 17 - 22.
- [155] E. Piera, M. I. Tejedor, M. Zorn, M. Anderson, *Appl. Catal. B* **2003**, *46*, 671 - 685.
- [156] P. Bouras, E. Stathatos, P. Lianos, *Appl. Catal. B* **2007**, *73*, 51 - 59.
- [157] M. R. Hoffmann, S. T. Martin, W. Choi, D. W. Bahnemann, *Chem. Rev.* **1995**, *95*, 69 -96.
- [158] U. G. Akpan, B. H. Hameed, *J. Hazard. Mater.* **2009**, *170*, 520 - 529.
- [159] A. R. Khataee, M. B. Kasiri, *J. Mol. Catal. A* **2010**, *328*, 8 - 26.
- [160] M. A. Rauf, M. A. Meetani, S. Hisaindee, *Desalination*, **2011**, *276*, 13 - 27.
- [161] F. Han, V. Subba R. Kambala, M. Srinivasan, D. Rajarathnam, R. Naidu, *Appl. Catal. A* **2009**, *359*, 25 - 40.
- [162] V. Maroga Mboula, V. Hequet, Y. Gru, R. Colin, Y. Andres, *J. Hazard. Mater.* **2012**, *209-210*, 355 - 364.
- [163] S. Yurdakal, V. Loddo, V. Augugliaro, H. Berber, G. Palmisano, L. Palmisano, *Catal. Today* **2007**, *129*, 9 - 15.
- [164] R. Molinari, A. Caruso, P. Argurio, T. Poerio, *J. Membrane Sci.* **2008**, *319*, 54 - 63.
- [165] M. A. Sousa, C. Gonçalves, V. J. P. Vilar, R. A. R. Boaventura, M. F. Alpendurada, *Chem. Eng. Journal* **2012**, *198-199*, 301 - 309.

- [166] A. Bernabeu, R. F. Vercher, L. Santos-Juanes, P. J. Simón, C. Lardín, M. A. Martínez, J. A. Vicente, R. González, C. Llosá, A. Arques, A. M. Amat, *Catal. Today* **2011**, *161*, 235 - 240.
- [167] I. Muñoz, J. Peral, J. A. Ayllón, S. Malato, P. Passarinho, X. Domènech, *Water Res.* **2006**, *40*, 3533 - 3540.
- [168] R. R. Giri, H. Ozaki, S. Ota, R. Takanami, S. Taniguchi, *Int. J. Environ. Sci. Tech.* **2010**, *7*, 251 - 260.
- [169] C.-H. Chiou, C.-Y. Wu, R.-S. Juang, *Chem. Eng. Journal* **2008**, *139*, 322 - 329.
- [170] P. Meunprasertdee, S. Chotisuwan, *Suranaree J. Sci. Technol.* **2010**, *17*, 203 - 210.
- [171] S. Ahmed, M. G. Rasul, W. N. Martens, R. Brown, M. A. Hashib, *Desalination* **2010**, *261*, 3 - 18.
- [172] W. Y. Wang, Y. Ku, *Colloids Surf. A: Physicochem. Eng. Aspects* **2007**, *302*, 261 - 268.
- [173] V. A. Sakkas, P. Calza, C. Medana, A. E. Villioti, C. Baiocchi, E. Pelizzetti, T. Albanis, *Appl. Catal. B* **2007**, *77*, 135 - 144.
- [174] K. Suttiponparnit, J. Jiang, M. Sahu, S. Suvachittanont, T. Charinpanitkul, P. Biswas, *Nanoscale Res. Lett.* **2011**, *6*, 1 - 8.
- [175] S. A. Abo-Farha, *Researcher* **2010**, *2*, 52 - 71.
- [176] S. Jiao, S. Zheng, D. Yin, L. Wang, L. Chen, *Chemosphere* **2008**, *73*, 377 - 382.
- [177] X.-D. Zhu, Y.-J. Wang, R.-J. Sun, Do.-M. Zhou, *Chemosphere* **2013**, *92*, 925 - 932.
- [178] M. H. Khana, H. Baea, J.-Y. Jung, *J. Hazard. Mater.* **2010**, *181*, 659 - 665.
- [179] Y. Wang, H. Zhang, L. Chen, S. Wang, D. Zhang, *Sep. Purif. Technol.* **2012**, *84*, 138 - 146.
- [180] Y. Wang, H. Zhang, J. Zhang, C. Lu, Q. Huang, J. Wu, F. Liu, *J. Hazard. Mater.* **2011**, *192*, 35 - 43.
- [181] Y. Liang, M. B. Denton, R. B. Bates, *J. Chromatogr. A* **1998**, *827*, 45 - 55.
- [182] F. Méndez-Arriaga, S. Esplugas, J. Giménez, *Water Res.* **2008**, *42*, 585 - 594.
- [183] F. Méndez-Arriaga, S. Esplugas, J. Giménez, *Water Res.* **2010**, *44*, 589 - 595.

- [184] G. Caviglioli, P. Valeria, P. Brunella, C. Sergio, A. Attilia, B. Gaetano, *J. Pharm. Biomed. Anal.* **2002**, *30*, 499 - 509.
- [185] A. D. Coelho, C. Sans, A. Agüera, M. J. Gómez, S. Espugas, M. Dezotti, *Sci. Total Environ.* **2009**, *407*, 3572 - 3578.
- [186] J. Choina, Ch. Fischer, G.-U. Flechsig, H. Kosslick, V. A. Tuan, N. D. Tuyen, N.A. Tuyen, A. Schulz, *J. Photochem. Photobiol. A* **2014**, *274*, 108 - 116.
- [187] J. Madhavan, F. Grieser, M. Ashokkumar, *J. Hazard. Mater.* **2010**, *178*, 202 - 208.
- [188] T. J. Collins, C. Walter, *Sci. Am.* **2006**, *294*, 82 - 90.
- [189] H. J. Kim, H. S. Kim, 2010 International Conference on Biology, Environment and Chemistry, IPCBEE, vol. 1, Singapore, **2011**, 105 - 108.
- [190] H. Higashimura, K. Fujisawa, M. Kubota, S. Kobayashi, *J. Polym. Sci., Part A: Polym. Chem.* **2005**, *43*, 1955 - 1962.
- [191] J. Choina, H. Kosslick, C. Fischer, G.-U. Flechsig, L. Frunza, A. Schulz, *Appl. Catal. B* **2013**, *129*, 589 - 598.
- [192] H. Oka, Y. Ikai, N. Kawamura, M. Yamada, K. Harada, S. Ito, M. Suzuki, *J. Agric. Food Chem.* **1989**, *37*, 226 - 231.
- [193] J. Niu, S. Ding, L. Zhang, J. Zhao, C. Feng, *Chemosphere* **2013**, *93*, 1 - 8.
- [194] J. Wu, H. Zhang, N. Oturan, Y. Wang, L. Chen, M. A. Oturan, *Chemosphere* **2012**, *87*, 614 - 620.
- [195] W.-R. Chen, C.-H. Huang, *Environ. Poll.* **2011**, *159*, 1092 - 1100.
- [196] L. V. Dmitrenko, E. B. Vulikh, G. V. Samsonov, *Bulletin of the Academy of Sciences of the USSR, Division of Chemical Science* **1972**, *21*, 702 - 704.
- [197] S. Gangula, S.-Y. Suen, E. D. Conte, *Microchem. Journal* **2010**, *95*, 2 - 4.
- [198] A. Akyol, H. C. Yatmaz, M. Bayramoglu, *Appl. Catal. B.* **2004**, *54*, 19 - 24.
- [199] D. Mijin, M. Savić, P. Snežana, A. Smiljanić, O. Glavaški, M. Jovanović, S. Petrović, *Desalination* **2009**, *249*, 286 - 292.
- [200] M. H. Khan, H. Bae, J.-Y. Jung, *J. Hazard. Mater.* **2010**, *181*, 659 - 665.

A 3: Academic achievements

List of papers

- 1) Study of nitrogen-modified titanium dioxide as an adsorbent for azo dyes
M. Janus, J. Choina, E. Kusiak, A. W. Morawski,
Adsorption Science and Technology, **26**, **7** (2008) **501-513**
- 2) TiO₂ modified by ammonia as a long lifetime photocatalyst for dyes decomposition
J. Choina, D. Dolat, E. Kusiak, M. Janus, A.W. Morawski,
Polish Journal of Chemical Technology **11,4** (2009) **1-6**
- 3) Azo dyes decomposition on new nitrogen-modified anatase TiO₂ with high adsorptivity
M. Janus, J. Choina, A.W. Morawski,
Journal of Hazardous Materials, **166**, **1** (2009) **1-5**
- 4) Lifetime of Carbon-Modified TiO₂ Photocatalysts under UV Light Irradiation
M. Janus, E. Kusiak, J. Choina, A. W. Morawski,
Catalysis Letters, **131**, **3-4** (2009) **606-611**
- 5) Enhanced adsorption of two azo dyes produced by carbon modification of TiO₂
M. Janus, E. Kusiak, J. Choina, J. Ziebro, A. W. Morawski,
Desalination, **249**, **1** (2009) **359-363**
- 6) Studies on nitrogen modified TiO₂ photocatalyst prepared in different conditions
K. Bubacz, J. Choina, D. Dolat, E. Borowiak-Paleń, D. Moszyński, A.W. Morawski,
Materials Research Bulletin, **45**, **9** (2010) **1085-1091**
- 7) Methylene blue and phenol photocatalytic degradation on nanoparticles of anatase TiO₂
K. Bubacz, J. Choina, D. Dolat, A.W. Morawski,
Polish Journal of Environmental Studies **19**, **4** (2010) **685-691**
- 8) Removal of hazardous pharmaceutical from water by photocatalytic treatment
J. Choina, H. Duwensee, G.-U. Flechsig, H. Kosslick, A.W. Morawski, V.A. Tuan, A. Schulz,
Central European Journal of Chemistry **6** (2010) **1288-1297**
- 9) Photocatalytic decomposition of pharmaceutical ibuprofen pollutions in water over titania catalyst

J. Choina, H. Kosslick, Ch. Fischer, G.-U. Flechsig, L. Frunza, A. Schulz,

Applied Catalysis B: Environmental, 129, 17 (2013) 589-598

10) Photocatalytic properties of Zr-doped titania in the degradation of the pharmaceutical ibuprofen

J. Choina, Ch. Fischer, G.-U. Flechsig, H. Kosslick, V.A. Tuan, N. D. Tuyen, N.A. Tuyen, A. Schulz,

Journal of Photochemistry and Photobiology A: Chemistry, 274 (2014) 108-116

11) The textural properties of ZnO nanoparticles and the influence on adsorption and photocatalytic remediation of water from pharmaceuticals

J. Choina, A. Bagabas, Ch. Fischer, G.-U. Flechsig, H. Kosslick, A. Alshammari, A. Schulz,

Catalysis Today (2014) accepted

List of conference abstracts

1) Catalysis for Society- XL Annual Polish Conference on Catalysis

11- 15.05, 2008 Kraków, Poland,

„New nitrogen modified anatase TiO₂ (TiO₂/N) with high photocatalytic activity under UV and visible light irradiation”

J. Choina, M. Janus, A.W. Morawski

Poster presentation

2) The 17th International Conference on Photochemical Conversion and Storage of Solar Energy

27.07-01.08, 2008 Sydney, Australia,

“New method for receiving active N-doped TiO₂ photocatalyst by modification under elevated pressure”

J. Choina, M. Janus, A.W. Morawski

Oral presentation

3) YoungChem, International Congress of Young Students

15-19.10, 2008 Krakow, Poland,

“Influence of pH on adsorption and photocatalytic decomposition of azo dyes on TiO₂ - nitrogen modified”

J. Choina, D. Dolat, M. Janus, A.W. Morawski

Poster presentation

4) 6th World Congress on Oxidation Catalysis

5-10.06, 2009 Lille, France,

“Deactivation of photocatalytic activity of TiO₂”

D. Dolat, J. Choina, B. Tryba, A. W. Morawski

Poster presentation

5) EuropaCat IX Congress

30.08-04.09, 2009 Salamanca, Spain,

“Nitrogen modified TiO₂ photocatalyst as a effective azo dye adsorbent in various pH values”

J. Choina, M. Janus, A.W. Morawski

Oral presentation

6) European Symposium on Photocatalysis JEP 2009

21-22.09, 2009 Cité Mondiale- Bordeaux, France,

“pH influence on adsorption and photocatalytic decomposition of Methylene Blue on TiO₂ surface”

D. Dolat, K. Bubacz, J. Choina, M. Janus, A.W. Morawski

Poster presentation

7) 6th European Meeting on Solar Chemistry and Photocatalysis: Environmental Applications (SPEA 6)

13-16.06, 2010 Prague, Czech Republic,

“The adsorption contribution of tetracycline abatement assisted by photocatalysis”

J. Choina, H. Duwensee, G.-U. Flechsig, H. Kosslick, A.W. Morawski, V.A. Tuan, A. Schulz

Poster presentation

8) Nanoporous Materials VI

21-24.08, 2011 Banff, Canada,

“Removal of Hazardous Pharmaceuticals from Water by Photocatalytic Treatment using Nanostructured Titania”

H. Kosslick, J. Choina, G.-U. Flechsig, J. Harloff, V.A. Tuan, N.D. Tuyen, T.L.H. Pham, A. Schulz

Oral presentation

9) The second Indo-German Catalysis Conference

19-22.06, 2011 Rostock, Germany,

“New materials for photocatalytic water treatment”

J.Choina, G.-U.Flehsig, H.Kosslick, A.Schulz

Oral presentation

10) The 2nd Saudi International Nanotechnology Conference

11-13.11, 2012 Riyadh, Saudi Arabia,

“Application of Zinc Oxide Nanoparticles in the Photocatalytic Degradation of Cyanide and Tetracycline in Water”

J. Choina, A. Bagabas, R. M. Mohamed, M. F. Aboud, A. Alshammari, H. Kosslick, A. Schulz, Z. Al- Othman

Poster presentation

11) 4th International Conference on Semiconductor Photochemistry (SP4)

23-27.06,2013 Prague, Czech Republic

“Photocatalytic degradation of pharmaceuticals over zinc oxide”

H. Kosslick, J. Choina, A. Bagabas, Ch. Fischer, G.-U. Flehsig , A. Alshammari and A. Schulz

Oral and poster presentation

12) XIth European Congress on Catalysis

1-6.09, 2013, Lyon, France

“Application of ZnO nanoparticles for decomposition of tetracycline and ibuprofen in photocatalytic treatment”

J. Choina, A. Bagabas, C. Fischer, G.-U. Flehsig, H. Kosslick, A. Alshammari, A. Schulz

Oral and poster presentation